

JOHANNES GUTENBERG
UNIVERSITÄT MAINZ



MAX PLANCK INSTITUTE
FOR POLYMER RESEARCH

BACHELOR THESIS

Department of Chemistry
Johannes Gutenberg University Mainz

Comparison of different Activation Mechanisms to form Self-assembling Peptides

Nelly Haasch

Born on 29.03.2000 in Darmstadt

1st Reviewer: Prof. Dr. Tanja Weil

2nd Reviewer: Prof Dr. Andreas Walther

07.11.2022

This thesis was written between 08.08.2022 and 07.11.2022 at the Max Planck Institute for Polymer Research in the group of Prof. Dr. Tanja Weil (subgroup of Dr. David Ng).

Eigenständigkeitserklärung

Ich, Nelly Haasch, Matrikelnummer 2756767 versichere, dass ich meine Bachelorarbeit selbstständig verfasst und keine anderen als die angegebenen schriftlichen und elektronischen Quellen sowie andere Hilfsmittel benutzt habe. Alle Ausführungen, die anderen Schriften wörtlich oder sinngemäß entnommen wurden, habe ich kenntlich gemacht.

Mainz, 07.11.2022

(Ort, Datum)

Nelly Haasch

(Unterschrift)

Contents

Abbreviations	VII
List of Figures	IX
List of Schemes	XI
List of Tables	XIII
1 Introduction	1
1.1 Aim of the Project.....	2
2 Theory	4
2.1 Peptides.....	4
2.1.1 Depsipeptides.....	6
2.2 Peptide Synthesis.....	7
2.2.1 Solid Phase Peptide Synthesis.....	7
2.2.2 Click Reactions.....	12
2.3 Application.....	14
2.3.1 Cell Uptake.....	14
2.3.2 Cleavage.....	15
2.3.3 Self-assembly.....	17
3 Results and Discussion	18
3.1 Synthesis of Linkers.....	18
3.1.1 H ₂ O ₂ sensitive Linker.....	18
3.1.2 GSH sensitive Linker.....	23
3.2 Synthesis of Peptides.....	24
3.2.1 H ₂ O ₂ sensitive Peptides.....	24
3.2.2 GSH sensitive Peptides.....	27
3.3 Morphology.....	28
3.3.1 H ₂ O ₂ sensitive Peptides.....	28
3.3.2 GSH sensitive Peptides.....	33
3.4 Kinetic studies.....	36
3.4.1 H ₂ O ₂ sensitive Peptides.....	36

3.4.2	GSH sensitive Peptides.....	40
4	Experimental Part	43
4.1	Methods	43
4.1.1	Column Chromatography	43
4.1.2	High Performance Liquid Chromatography.....	43
4.1.3	Kinetic studies	44
4.1.4	Mass Spectrometry	44
4.1.5	Nuclear Magnetic Resonance Spectroscopy	45
4.1.6	Solid Phase Peptide Synthesis.....	45
4.1.7	Thin Layer Chromatography.....	46
4.1.8	Transmission Electron Microscopy	46
4.2	Synthesis	47
4.2.1	4-Nitrophenyl (4-(4,4,5,5-tetramethyl-1,3,2-dioxaborolan-2-yl)benzyl) carbonate 47	
4.2.2	4-Azidosalicylic acid	47
4.2.3	<i>N</i> -trityloxyamine	48
4.2.4	4-Azido-2-hydroxy- <i>N</i> -(trityloxy)benzamide.....	49
4.2.5	SHA-TAT.....	49
4.2.6	BA-Depsi-ISA	51
4.2.7	BA-KFKFQF	53
4.2.8	4-Nitrophenyl(2-(pyridine-2-yl)disulfaneyl) ethyl carbonate.....	55
4.2.9	TAT-SS-Depsi-ISA	56
4.2.10	TAT-SS-KFKFQF	59
5	Summary	63
6	Zusammenfassung	65
	Acknowledgements	69
	References	70
	Appendix	73

Abbreviations

ACN	Acetonitrile
BA	Boronic acid linker
Boc	<i>Tert</i> -butoxycarbonyl
CPP	Cell penetrating peptide
CuACC	Copper-catalyzed azide-alkyne cycloaddition
DCM	Dichloromethane
DCC	<i>N,N'</i> -Dicyclohexylcarbodiimid
Depsi	Depsipeptide
DIC	<i>N,N'</i> -Diisopropylcarbodiimid
DIPEA	<i>N,N</i> -Diisopropylethylamine
DMAP	4-Dimethylaminopyridine
DMF	Dimethylformamide
DMSO	Dimethyl sulfoxide
DNA	Desoxyribonucleic acid
E1cB	Elimination unimolecular conjugate base
EDC	1-Ethyl-3-(3-dimethylaminopropyl)carbodiimide
ESI-MS	Electron spray ionization – mass spectrometry
Fmoc	Fluoren-9-ylmethoxycarbonyl
GSH	Glutathione
HATU	1-[Bis(dimethylamino)methylene]-1H-1,2,3-triazolo[4,5-b]pyridinium 3-oxide hexafluorophosphate
¹H-NMR	Proton nuclear magnetic resonance
HPLC	High performance liquid chromatography
LC-MS	Liquid chromatography – mass spectrometry
MALDI-TOF-MS	Matrix assisted laser desorption ionization - time of flight - mass spectrometry
MMT	Monomethoxy trityl
Oxyma	Ethyl 2-cyano-2-(hydroxyimino)acetate
PBS	Phosphate buffered saline
PyBOP	1-Benzotriazolylxy-tris-pyrrolidinophosphonium hexafluorophosphate
ROS	Reactive oxygen species
SHA	4-Azido-2-hydroxy- <i>N</i> -(trityloxy)benzamide
SPPS	Solid phase peptide synthesis
SS	Disulfide linker
TAT	Transactivator of transcription

Abbreviations

TBTA	Tris[(1-benzyl-4-triazolyl) methyl] amine
TEA	Triethylamine
TEM	Transmission electron microscopy
TFA	Trifluoroacetic acid
THF	Tetrahydrofuran
TIPS	Triisopropyl silane
TLC	Thin Layer Chromatography
Trt	Trityl

List of Figures

Figure 1: Peptides synthesized within the frame of this work: TAT-SHA:BA-Depsi ISA, TAT-SHA:BA-KFKFQF, TAT-SS-Depsi ISA and TAT-SS-KFKFQF.	2
Figure 2: Schematic depiction of primary to quaternary structure of proteins. Figure taken from <i>BioRender.com</i>	6
Figure 3: Structure of TAT sequence.....	15
Figure 4: ¹ H-NMR spectra of 4-azidosalicylic acid (2), in red, and 4-aminosalicylic acid, in turquoise.	20
Figure 5: LC-MS chromatogram of 4-azidosalicylic acid (2) detected at $\lambda = 214$ nm.	20
Figure 6: TLC of test reactions for coupling of <i>N</i> -trityloxyamine (3) with 4-azidosalicylic acid (2) to form 4-azido-2-hydroxy- <i>N</i> -(trityloxy) benzamide (4).....	21
Figure 7: ¹ H-NMR spectrum of 4-azido-2-hydroxy- <i>N</i> -(trityloxy) benzamide (4).....	22
Figure 8: LC-MS chromatogram of 4-azido-2-hydroxy- <i>N</i> -(trityloxy) benzamide (4) detected at $\lambda = 214$ nm.	23
Figure 9: LC-MS chromatogram of BA-Depsi ISA after first purification with preparative HPLC detected at $\lambda = 214$ nm.	25
Figure 10: LC-MS chromatogram of BA-Depsi ISA detected at $\lambda = 214$ nm.	26
Figure 11: LC-MS chromatogram of BA-KFKFQF detected at $\lambda = 214$ nm.....	26
Figure 12: TEM pictures of boronic acid linker peptides with TAT sequence at 1 mM concentration. Scale bar = 500 nm.	28
Figure 13: TEM pictures of TAT-SHA:BA-Depsi ISA and TAT-SHA:BA-KFKFQF incubated with H ₂ O ₂ . Aggregates are framed with blue circles. Scale bar = 500 nm.	29
Figure 14: Closeup of TEM picture of TAT-SHA:BA-Depsi ISA incubated with H ₂ O ₂ . Scale bar = 500 nm. Arrows point to twists in the fibril.....	30
Figure 15: TEM pictures of boronic acid linker peptides without TAT sequence at 10 mM concentration. Scale bar = 500 nm.	30
Figure 16: TEM pictures of BA-KFKFQF incubated with H ₂ O ₂ . Scale bar = 500 nm.....	31
Figure 17: TEM picture of BA-KFKFQF without H ₂ O ₂ . Scale bar = 500 nm.....	32
Figure 18: TEM pictures of disulfide linker peptides at 1 mM concentration. Scale bar = 500 nm.	33
Figure 19: TEM pictures of TAT-SS-KFKFQF with GSH. Scale bar = 500 nm.	34
Figure 20: Closeup of TEM picture of TAT-SS-KFKFQF with GSH. Blue arrows point to tube-like fibrils and red arrows to twisted fibrils. Scale bar = 100 nm.	34
Figure 21: Closeup of TEM picture of TAT-SS-KFKFQF with GSH. Scale bar = 100 nm.	35
Figure 22: Kinetics of BA-KFKFQF incubated with H ₂ O ₂ (10 mM).....	36

Figure 23: MALDI-TOF spectra of the three peaks found in the kinetic studies of BA-KFKFQF (Figure 22).....	38
Figure 24: Kinetics of TAT-SS-KFKFQF incubated with GSH (10 mM).....	40
Figure 25: MALDI-TOF spectra of the four peaks found in the kinetic studies of TAT-SS-KFKFQF (Figure 24).....	41
Figure 26: LC-MS chromatogram of SHA-TAT detected at $\lambda = 214$ nm.	51
Figure 27: LC-MS chromatogram of BA-Depsi ISA detected at $\lambda = 214$ nm.....	53
Figure 28: LC-MS chromatogram of BA-KFKFQF detected at $\lambda = 214$ nm.....	54
Figure 29: LC-MS chromatogram of (Pyr)-SS-Depsi ISA detected at $\lambda = 214$ nm.	57
Figure 30: LC-MS chromatogram of TAT-SS-Depsi ISA detected at $\lambda = 214$ nm.	59
Figure 31: LC-MS chromatogram of (Pyr)-SS-KFKFQF detected at $\lambda = 214$ nm.....	60
Figure 32: LC-MS chromatogram of TAT-SS-KFKFQF detected at $\lambda = 214$ nm.....	62
Figure 33: $^1\text{H-NMR}$ spectrum of 4-nitrophenyl (4-(4,4,5,5-tetramethyl-1,3,2-dioxaborolan-2-yl) benzyl) carbonate.....	73
Figure 34: $^1\text{H-NMR}$ spectrum of 4-azidosalicylic acid.....	74
Figure 35: $^1\text{H-NMR}$ spectrum of <i>N</i> -trityloxyamine.	74
Figure 36: $^1\text{H-NMR}$ spectrum of 4-azido-2-hydroxy- <i>N</i> -(trityloxy)benzamide.....	75
Figure 37: $^1\text{H-NMR}$ spectrum of 4-nitrophenyl(2-(pyridine-2-yl)disulfaneyl) ethyl) carbonate.....	75
Figure 38: MALDI-TOF spectrum of SHA-TAT.....	76
Figure 39: MALDI-TOF spectrum of BA-Depsi ISA.	76
Figure 40: MALDI-TOF spectrum of BA-KFKFQF.....	77
Figure 41: MALDI-TOF spectrum of TAT-SS-Depsi ISA.	77
Figure 42: MALDI-TOF spectrum of TAT-SS-KFKFQF.....	78

List of Schemes

Scheme 1: Formation of peptide bond which is highlighted in blue.	4
Scheme 2: Resonance structures of peptide bond.....	5
Scheme 3: Structures of depsipeptides.	6
Scheme 4: Deprotection mechanism of N-terminus. Fmoc moiety is highlighted in blue.	8
Scheme 5: Deprotection mechanism of trityl protected cysteine and subsequent deactivation of trityl cation with TIPS as scavenger.	10
Scheme 6: Activation mechanism of carboxyl group of amino acid with DIC.	11
Scheme 7: Side reactions with carbodiimide-based activators like DIC. Arrows showing the <i>O,N</i> -acyl shift are orange and arrows showing the overactivation are blue.	11
Scheme 8: Racemization of C-atom as a result of the activation of carboxyl group.	12
Scheme 9: Formation of a less reactive active ester with Oxyma.	12
Scheme 10: Mechanism of CuAAC with terminal alkynes. Scheme taken from [25].	14
Scheme 11: Steps for cleavage of boronic acid linker peptides.	15
Scheme 12: Mechanism of H ₂ O ₂ -induced cleavage of boronic acid linker.....	16
Scheme 13: Cleavage of disulfide linker peptides with GSH.	16
Scheme 14: <i>O,N</i> -acyl shift of depsipeptide to linear peptide.	17
Scheme 15: Reaction scheme of 4-nitrophenyl (4-(4,4,5,5-tetramethyl-1,3,2-dioxaborolan-2-yl) benzyl) carbonate (1) [7].	18
Scheme 16: Synthesis scheme of 4-azido-2-hydroxy- <i>N</i> -(trityloxy) benzamide (4).....	19
Scheme 17: Reaction scheme of 4-nitrophenyl(2-(pyridine-2-yl)disulfaneyl) ethyl) carbonate (5).....	23
Scheme 18: Synthesis routes for SHA-TAT, BA-Depsi ISA and BA-KFKFQF.....	24
Scheme 19: Synthesis routes for TAT-SS-Depsi ISA and TAT-SS-KFKFQF.	27
Scheme 20: H ₂ O ₂ induced cleavage of BA-KFKFQF and postulated subsequent side reaction. The structures are highlighted matching the peaks in Figure 22	39
Scheme 21: GSH induced cleavage of TAT-SS-KFKFQF. The structures are highlighted matching the colors of the peaks in Figure 24	42
Scheme 22: Synthesis of SHA-TAT: (A) SPPS of TAT sequence, (B) modification of N-terminus with 4-pentynoic acid, (C) CuAAC with SHA, (D) cleavage from resin and deprotection.	49
Scheme 23: Synthesis of BA-Depsi-ISA: (A) SPPS of SA sequence, (B) modification of N-terminus with boronic acid ester, (C) esterification of serine with isoleucine, (D) cleavage from resin and deprotection.	51
Scheme 24: Synthesis of BA-KFKFQF: (A) SPPS of KFKFQF sequence, (B) modification of N-terminus with boronic acid ester, (C) cleavage from resin and deprotection.....	53

Scheme 25: Synthesis of TAT-SS-Depsi-ISA: (1A) SPPS of SA sequence, (1B) modification of N-terminus with 4-nitrophenyl(2-(pyridine-2-yl)disulfaneyl) ethyl carbonate, (1C) esterification of serine with isoleucine, (1D) cleavage from resin and deprotection, (2A) SPPS of Cys-TAT, (2B) disulfide exchange, (2C) cleavage from resin and deprotection.56

Scheme 26: Synthesis of TAT-SS-KFKFQF: (1A) SPPS of KFKFQF sequence, (1B) modification of N-terminus with 4-nitrophenyl(2-(pyridine-2-yl)disulfaneyl) ethyl carbonate, (1C) cleavage from resin and deprotection, (2A) SPPS of Cys-TAT, (2B) disulfide exchange, (2C) cleavage from resin and deprotection.59

List of Tables

Table 1: Protecting groups of side chain moieties of different amino acids.....	9
Table 2: Model gradients for semi-preparative and preparative HPLC.	44
Table 3: Concentrations of reagents used for automated SPPS.	45
Table 4: Reagent usage for SPPS of YGRKKRRQRRR sequence (0.10 mmol scale).	50
Table 5: Reagent usage for SPPS of SA sequence (1.00 mmol scale).	52
Table 6: Reagent usage for SPPS of KFKFQF sequence (0.10 mmol scale).	54
Table 7: Reagent usage for SPPS of SA sequence (0.50 mmol scale).	56
Table 8: Reagent usage for SPPS of CYGRKKRRQRRR sequence (0.10 mmol scale).....	58
Table 9: Reagent usage for SPPS of KFKFQF sequence (0.10 mmol scale).	60
Table 10: Reagent usage for SPPS of CYGRKKRRQRRR sequence (0.10 mmol scale).....	61

1 Introduction

Biological systems rely heavily on supramolecular interactions to ensure hierarchical structures, such as proteins or deoxyribonucleic acids (DNA), are correctly assembled and disassembled in a dynamic environment. These structures are involved in a variety of physiological relevant processes and inaccurate self-assemblies of peptides were found to be involved in neurodegenerative diseases such as Alzheimer's disease or Parkinson's disease. Understanding the underlying mechanism of self-assemblies allows for artificial systems, which can self-assemble in a controllable fashion and be potential therapeutics. Especially peptide-based systems have high potential, due to their relatively easy and cost-effective synthesis. [1,2]

Peptide assemblies can be used for nanomaterials for various applications including biomedical applications like drug delivery or tissue regeneration. Peptides can self-assemble through non-covalent inter- and intramolecular interactions like electrostatic bonds, hydrogen bonds, Van der Waals interactions or π - π -stacking. In nature it is these interactions that allow the formation of secondary to quaternary structure of proteins or protein assemblies like the cytoskeleton. In order to mimic these structures knowledge of the basic mechanism of self-assembly is necessary. Advances understanding the mechanism have been accomplished through analyses of natural and synthetic peptides. Nevertheless, prediction of the assembly behavior remains challenging. Further investigations could elucidate this complex process. [1,3–6]

For controlled self-assembly different strategies are investigated. While depsipeptides (Depsi) follow the approach of a pro-assembling motif that linearizes into a self-assembling motif upon cleavage others directly use a self-assembling motif and attach it to a cleavable motif that inhibits self-assembly. In both cases cleavage is induced by a trigger. Peptides that are designed to self-assemble under certain conditions found in cancer cells have great potential for anticancer applications since the mechanical stress resulting from the fiber formation leads to apoptosis. Research regarding the self-assembling motif and the trigger aims to increase efficacy of these systems. [5,7]

1.1 Aim of the Project

During this work four peptides that can self-assemble upon cell uptake were synthesized and their self-assembly abilities were analyzed. The peptide systems are shown in **Figure 1**.

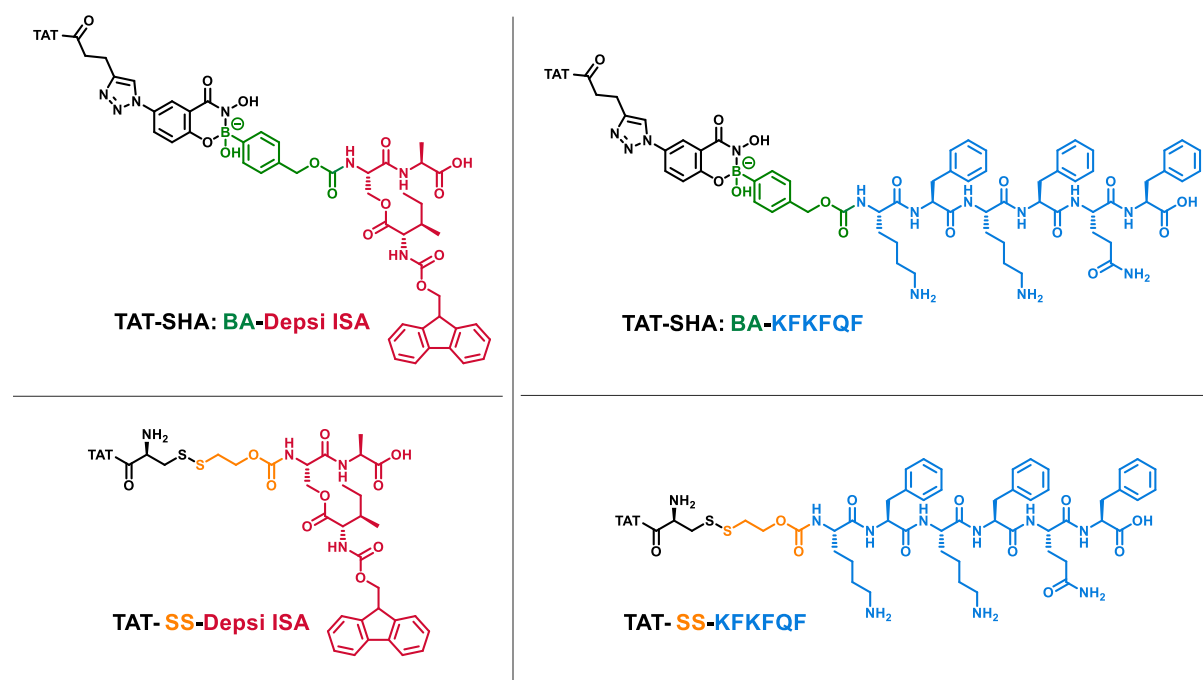


Figure 1: Peptides synthesized within the frame of this work: TAT-SHA:BA-Depsi ISA, TAT-SHA:BA-KFKFQF, TAT-SS-Depsi ISA and TAT-SS-KFKFQF. The boronic acid linker is colored in green and the disulfide linker is colored in orange. The self-assembling sequences Depsi ISA and KFKFQF are colored in red and blue, respectively.

Intracellular self-assembly of peptides for anticancer applications has been investigated by the group of Prof. Dr. T. Weil. Among others systems that respond to hydrogen peroxide (H_2O_2) or glutathione (GSH) were found. Previous work of Pieszka *et al.* [7,8] found a H_2O_2 sensitive linker, the boronic acid linker (BA). S. Chagri adapted a GSH labile linker, the disulfide linker (SS), from Skakuj *et al.* [9] in her yet unpublished work. The Depsi ISA sequence as a pro-assembling motif was described by Pieszka *et al.* [7,8]. Another self-assembling sequence, the KFKFQF sequence derived from the CKFKFQF sequence that was described by Sieste *et al.* [10] was investigated by K. Maxeiner. The transactivator of transcription (TAT) sequence enables cell uptake. [11] In case of the boronic acid linker systems the TAT sequence and the self-assembling sequence are not only connected by the linker but also by 4-Azido-2-hydroxy-*N*-(trityloxy)benzamide (SHA).

This research on different linkers and self-assembling sequences was combined in this work. The aim was to investigate the impact of those on the self-assembly behavior. The comparison of the systems might provide deeper understanding of the influencing factors of self-assembly.

The synthesis part includes the synthesis of the linkers as well as the synthesis of the peptides. For the boronic acid linker systems protocols by Pieszka *et al.* [7,8] and for the disulfide linker protocols by Skakuj *et al.* [9] were followed. Peptides were synthesized in an automated peptide synthesizer. Further modifications were conducted in a Merrifield apparatus.

To investigate the self-assembly behavior of the peptides transmission electron microscopy (TEM) images were recorded. The cleavage from the linkers was analyzed in a kinetic study.

The results obtained in this thesis were compiled as part of Konrad Maxeiner's dissertation.

2 Theory

2.1 Peptides

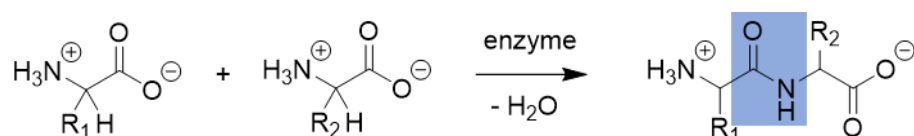
Peptides are essential to biochemical mechanisms and therefore for life. They fulfill duties as energy supplier, catalyst, messenger, mechanical stabilizer and form part of the immune system. [1]

Peptides are composed of amino acids. An α -carbon atom forms the core of the general structure of amino acids. Attached to this C_{α} -atom are a carboxyl group, an amino group, a hydrogen atom and a specific side chain. Due to the four different residues amino acids are chiral, except for the amino acid glycine that has a second hydrogen atom as side chain. In nature mainly *L*-amino acids occur. [1,12,13]

Amino acids have an isoelectric point a pH at which the molecule appears uncharged to the outside. [1,13]

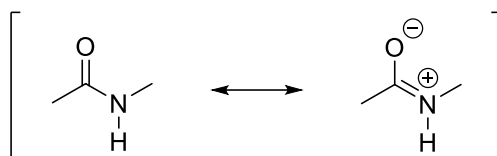
The 20 amino acids that form peptides in nature can be divided into four groups: amino acids with nonpolar, polar uncharged, acidic and basic side chains. [1,13]

Peptides consist of amino acids that are connected by peptide bonds. Peptide bonds are formed via the reaction of the carboxyl group of one amino acid with the amino group of another amino acid. This condensation reaction is shown in **Scheme 1**. [1,13]



Scheme 1: Formation of peptide bond which is highlighted in blue.

Peptide bonds are very stable, due to a partial double bond character. This phenomenon can be explained with the resonance structure of the peptide bond, which is shown in **Scheme 2**. The partial double bond character of this single bond means it behaves like a double bond. This includes: all atoms in the blue-colored field are in one level and rotation around this bond is impossible hence there are cis and trans configurations. The preferred configuration is trans, so that side chains have the most space. The only exception of the 20 proteinogenic amino acids is proline. Between both configurations there is no significant energy difference. Thus, both configurations exist evenly. [1,13]



Scheme 2: Resonance structures of peptide bond.

The primary structure of a peptide is the amino acid sequence, which is always stated from the N-terminus to the C-terminus. The primary structure determines the secondary, tertiary and quaternary structure and thus the function and characteristics, like morphology and surface charge of the protein.

While the primary structure describes the sequence of the covalently linked amino acids, the secondary structure describes the structural motifs of the peptide due to intramolecular interactions of the peptide backbone. Those structures are based on hydrogen bonds between the hydrogen atom of the H-N bond of one peptide bond and the oxygen of the O=C bond of another peptide bond, as shown in **Figure 2**. Two major structures can be found, the α -helix and the β -sheet. α -Helices emerge from hydrogen bridge bonds that are formed between every five amino acids. β -Sheets however form hydrogen bonds between peptide bonds that are much further apart. This is how the respective structures that are depicted in **Figure 2** emerge. [1,13]

β -Sheets can be formed between parallel or anti-parallel orientated peptide strands. The anti-parallel orientation forms more stable β -sheets because the angle between the H-N bond and the O=C bond numbers about 180° which is the optimal angle for hydrogen bonds. β -Sheets mostly contain 5-10 peptide strands. It is known that β -sheets are inclined to fibrillate to so called amyloid structures. In nature these structures play functional and pathological roles. An example for pathological impacts of amyloids is the hypothesis that amyloids cause diseases like Alzheimer's disease. [1,2,10]

α -Helices can exhibit self-assembling properties as well. These structures are called coiled coil, as two α -helices coil themselves around each other. Non-covalent interactions between side chains are the reason for the attachment of the two α -helices. [1,14]

The tertiary structure describes the 3D-folding of the whole protein. Tertiary structures are also based on non-covalent bonds, but this time it is the side chains that interact. The variety of functional groups allows interactions such as disulfide bridges, hydrogen bonds, electrostatic, Van-der-Waals and hydrophobic interactions.

Proteins that consist of more than one peptide have a quaternary structure made of non-covalent intermolecular interactions. [1,13]

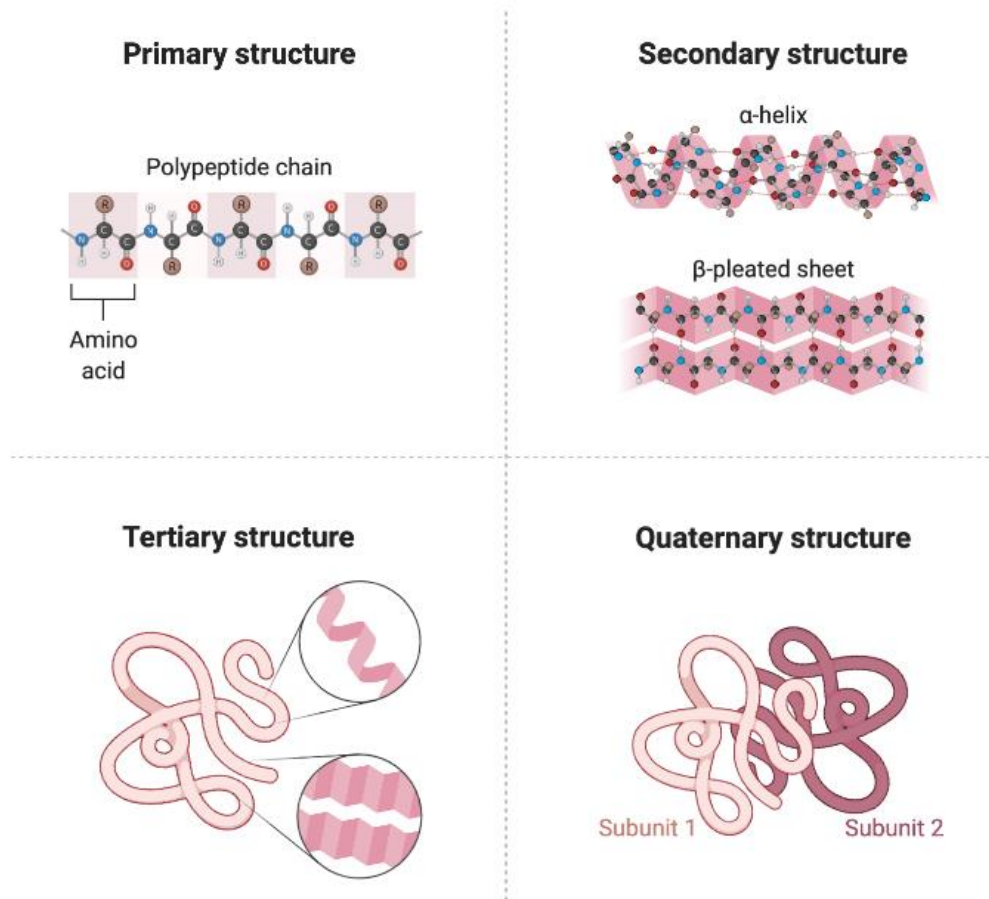
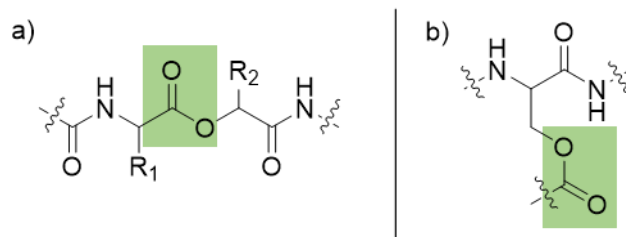


Figure 2: Schematic depiction of primary to quaternary structure of proteins. Figure taken from *BioRender.com*.

2.1.1 Depsipeptides

Peptides that not only contain peptide bonds but also ester bonds are called depsipeptides. These ester bonds can either be formed between an amino acid and an α -hydroxy carboxylic acid or between the C-terminal carboxylic acid and hydroxyl moieties of either serine or tyrosine. [15]



Scheme 3: Structures of depsipeptides. The ester bonds are highlighted in green. Shown are depsipeptides formed between a) an amino acid and an α -hydroxy carboxylic acid and b) an amino acid and the hydroxyl group of serine.

Depsipeptides with a kink in their backbone, as shown in **Scheme 3 b**), next to the N-terminus linearize through a *O,N*-acyl shift due to the higher nucleophilicity of the free amino group. This feature can be used for controlled self-assembly, since the kink inhibits self-assembly through steric hindrance. [7]

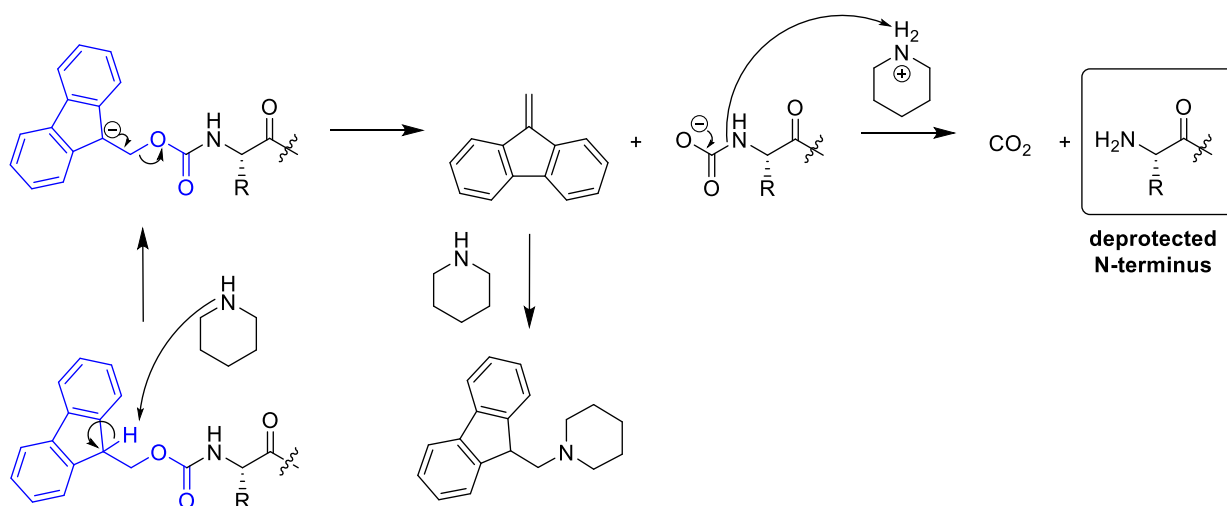
2.2 Peptide Synthesis

2.2.1 Solid Phase Peptide Synthesis

The first solid phase peptide synthesis (SPPS) was introduced by Robert Bruce Merrifield in 1963. To form the desired peptide bond between two amino acids the amino group of the one and the carboxyl group of the other one must be protected. The implementation of SPPS provided a solution by anchoring the peptide on the C-terminus to a resin. Thereby protection of C-terminus was no longer required. Thus, peptide synthesis in laboratory scale and now even automated peptide synthesis is possible. [16]

In principle the SPPS method consists of four repetitive steps in a sequential manner. In the first step the N-terminus of the anchored amino acid is deprotected to allow the third step, the coupling. Before the coupling of the amino acids can take place, a washing step is necessary. Afterwards the N-terminally protected amino acid, as well as the coupling reagents can be added to form the peptide bond. Another washing step is required before the procedure starts all over again for the next amino acid. [16]

While the question how to protect the carboxyl group is resolved, the protection of the amino group remains unresolved. The two mainly used N_α -protecting groups are fluoren-9-ylmethoxycarbonyl (Fmoc) and *tert*-butoxycarbonyl (Boc) group. The main difference between those two protecting groups is the removal. Fmoc can be removed under mild basic conditions with secondary amines like piperidine, whereas Boc needs to be removed under acidic conditions with trifluoroacetic acid (TFA). During this thesis only Fmoc strategy was used, hence only Fmoc-SPPS will be discussed in the following. To deprotect the amino group after each coupling a solution of piperidine in dimethylformamide (DMF) was used. The mechanism of this deprotection step is shown in **Scheme 4**. [16]


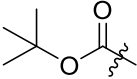
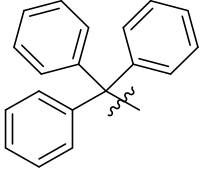
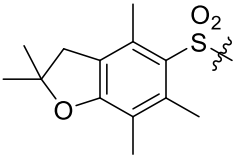


Scheme 4: Deprotection mechanism of N-terminus. Fmoc moiety is highlighted in blue.

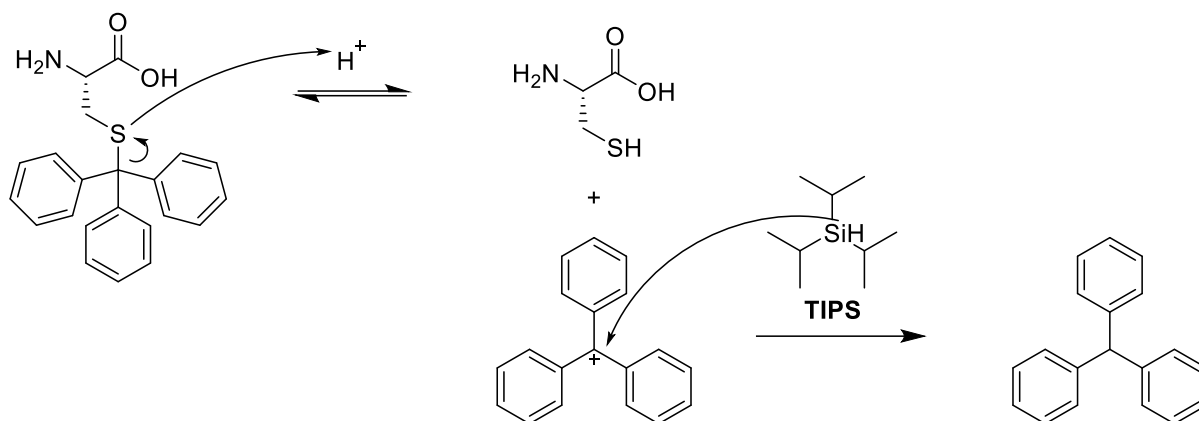
The first step of this mechanism follows an elimination unimolecular conjugate base (E1cB) mechanism, where a base, in this case piperidine, deprotonates the cyclopentyl C-atom and after elimination of a carboxylate residue a new double bond is formed. The carbamate degrades releasing carbon dioxide and the deprotected N-terminus of the peptide. The emerging nucleophilic double bond reacts with the piperidine in an electrophilic addition.

To avoid side reactions with functional groups on side chains of the amino acids, protection of these functional groups is required. Common protecting groups and their corresponding amino acids are listed in **Table 1**. [16]

Table 1: Protecting groups of side chain moieties of different amino acids.

Protecting Group		Amino Acids
tBu		Ser, Thr, Tyr, Asp, Glu
Boc		Lys, Trp
Trt		Cys, His, Asn, Gln
Pbf		Arg

All of those protecting groups shown above are acid labile and can be removed with TFA. As demonstrated exemplary in **Scheme 5** with the Trityl (Trt) protecting group, deprotection of side chains develops different carbocations, which are very reactive due to their electrophilicity. To avoid potential side reactions with nucleophilic moieties of the peptide, reagents that can react and thereby deactivate the carbocations, so called scavengers, are added. Here triisopropyl silane (TIPS) was used. Silanes are suitable for such purposes as they can act as hydride donors even under acidic conditions. Deactivation of trityl carbocation with TIPS is shown in **Scheme 5**. [16]

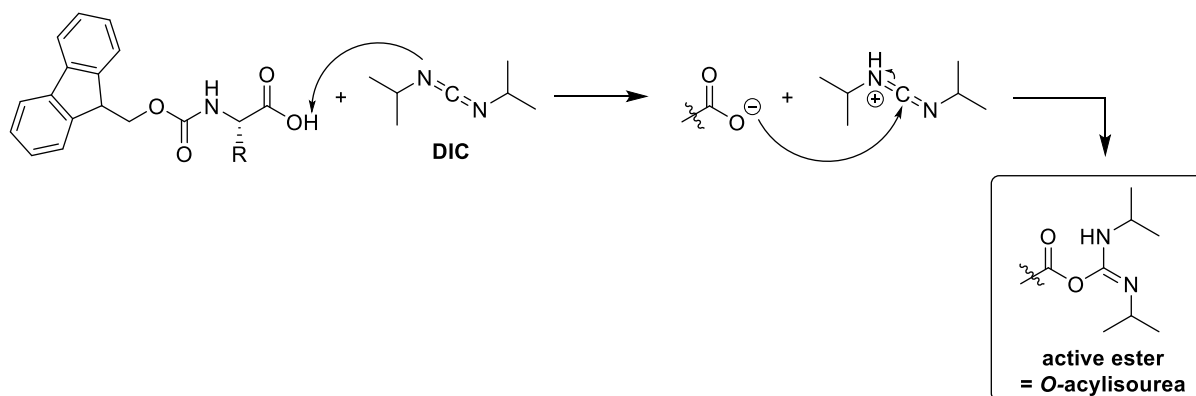


Scheme 5: Deprotection mechanism of trityl protected cysteine and subsequent deactivation of trityl cation with TIPS as scavenger.

Monomethoxy trityl (MMT) moieties are also acid labile protecting groups suitable for amino acids with trityl as their protecting group, however these protecting groups can be cleaved under rather mild acidic conditions. This is due to the electron-donating methoxy group that enhances the electron density at the central carbon atom making the carbon hetero atom bond less polar and thus less stable. The ability of this protecting group to be cleaved under rather mild acidic conditions makes selective deprotection for modification of the peptide at the resin possible. [16]

To initiate the coupling the nucleophilicity of the C-atom of the carboxyl group needs to be increased. In contrast to other carbonyl C-atoms the C-atoms of carboxylic acids are rather unreactive. This is because of the electron-donating +M-effect the hydroxyl moiety has. Commonly used activators are carbodiimide-based activators such as *N,N'*-dicyclohexylcarbodiimide (DCC) and *N,N'*-diisopropylcarbodiimide (DIC) or so called in situ activators like 1-[bis(dimethylamino)methylene]-1H-1,2,3-triazolo[4,5-b]pyridinium 3-oxide hexafluorophosphate (HATU) and 1-benzotriazolyl-oxo-tris-pyrrolidinophosphonium hexafluorophosphate (PyBOP). For SPPS of peptides prepared for this work DIC was used as an activator. [16]

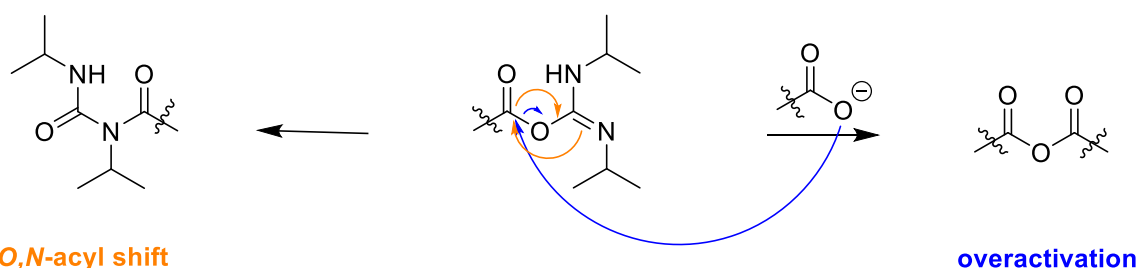
The activation mechanism is shown in **Scheme 6**.



Scheme 6: Activation mechanism of carboxyl group of amino acid with DIC.

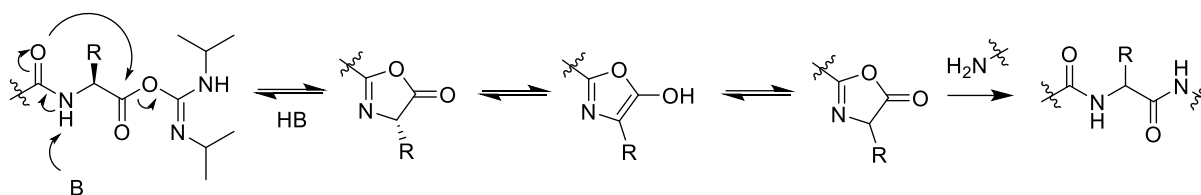
The carboxylic acid is deprotonated by the slightly basic carbodiimide. The nucleophilic carboxylate attacks the carbodiimide C-atom forming the active ester.

Possible side reactions with carbodiimide-based activators are the *O,N*-acyl shift of the *O*-acylisourea intermediate or the overactivation forming an anhydride. [16,17] These side reactions are shown in **Scheme 7**.



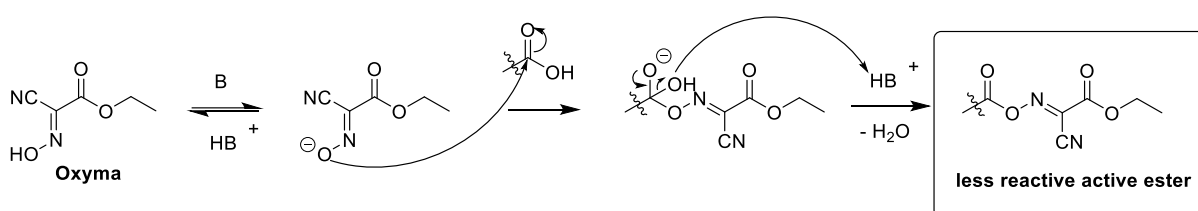
Scheme 7: Side reactions with carbodiimide-based activators like DIC. Arrows showing the *O,N*-acyl shift are orange and arrows showing the overactivation are blue.

Further drawback of carbodiimide-based activators is epimerization of the C_{α} -atom of the amino acid due to the very reactive *O*-acylisourea intermediate. As shown in **Scheme 8** deprotonation of the peptide bond next to the activated carboxyl group can lead to the carbonyl group of this peptide bond attacking the activated carbonyl group. This leads to formation of a lactone. Subsequent tautomerization causes the loss of stereo information. [16]



Scheme 8: Racemization of C-atom as a result of the activation of carboxyl group.

Addition of an activator base can reduce the before mentioned side reactions and prevent racemization. 1-Hydroxybenzotriazole (HOBt) or ethyl 2-cyano-2-(hydroxyimino) acetate (Oxyrna) can be used as activator bases. Oxyrna forms less reactive and thus more stable active esters leading to lower levels of racemization and side reactions. [16,18]



Scheme 9: Formation of a less reactive active ester with Oxyrna.

Scheme 9 shows the mechanism of formation of a less reactive active ester with Oxyrna. Oxyrna competes with the amino acid for the base e.g., DIC. Subsequent to deprotonation of the hydroxyamino moiety of Oxyrna, a nucleophilic substitution at the carbonyl C-atom of the C-terminus of the amino acid takes place.

Commonly used resins for Fmoc-SPPS of shorter sequences are based on polystyrene. Linkers are molecules that connect the resin with the growing peptides. Thus, they need one functional group to bind the resin and one to bind the C-terminus of an amino acid like a side chain protecting group. This allows the cleavage of the peptide from the support under acidic conditions. Cleavage and deprotection of side chains is carried out simultaneously with TFA. [16]

2.2.2 Click Reactions

This year's Nobel Prize in Chemistry was awarded to Carolyn R. Bertozzi, Morten Meldal and K. Barry Sharpless "for the development of click chemistry and bioorthogonal chemistry". [19]

Click reactions allow very easy linkage of two molecules. Therefore, it is used for many applications, also peptide synthesis. Advantages of these reactions are high yields,

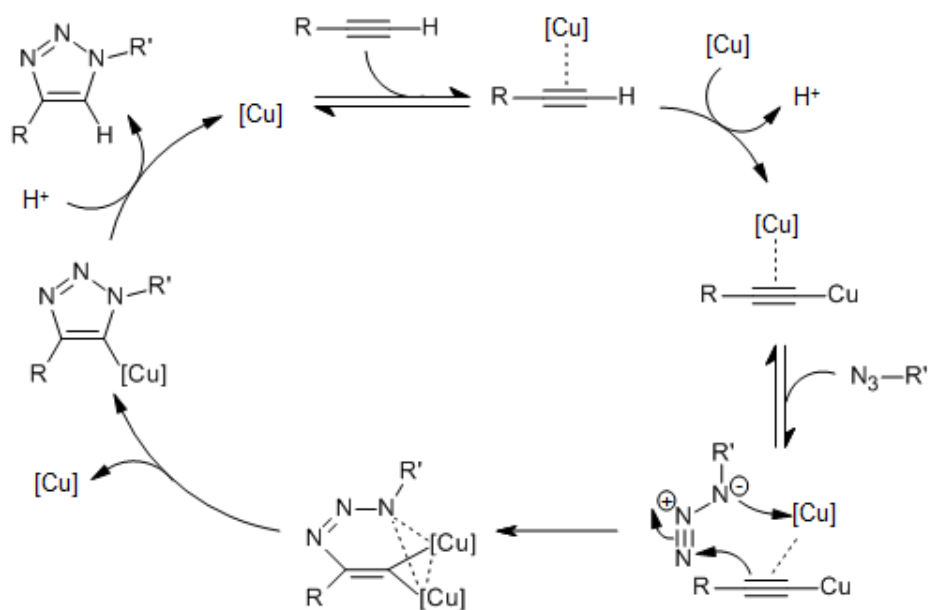
biocompatible conditions are possible and there are limited or no side products, making it possible to run certain click reactions even in living systems. [20,21]

Apart from the originally introduced copper-catalyzed azide-alkyne cycloaddition (CuAAC), other click reactions like strain-promoted azide-alkyne cycloaddition or thiol-ene reaction have emerged. [20,22] Since only CuAAC was used, in the following the focus will lay on CuAAC.

CuAAC is the copper-catalyzed Huisgen 1,3-dipolar cycloaddition to triazoles, which is very slow at room temperature and shows no regioselectivity without catalyzation. CuAAC only produces 1,4-triazoles. [23]

The active copper species is Cu(I) making this click reaction incompatible for usage in biological systems. [20] One can use either Cu(II) salts and reduce them *in situ* or directly use Cu(I) salts. Cu(I) salts like CuBr or CuI have the disadvantage of being instable under aerobic conditions. A possibility to prevent the oxidation of Cu(I) to Cu(II) is working under anaerobic conditions or using a stabilizing ligand. The most common ligand is tris[(1-benzyl-4-triazolyl) methyl] amine (TBTA). TBTA has also shown to accelerate the triazole formation. Cu(II) salts are in need of a reducing agent to produce the Cu(I) species. For aqueous solutions ascorbate and for organic solutions hydrazine are suitable reducing agents. [23]

The mechanism of CuAAC reactions, especially the complexation of Cu(I), remained elusive for about a decade. Worrell *et al.* [24] however could prove that the CuAAC mechanism involves a dinuclear copper intermediate as shown in **Scheme 10**. Coordination of a copper to the alkyne leads to formation of Cu(I) acetylide that coordinates another copper. Subsequently, azide is coordinated to the Cu(I) acetylide. After formation of a bond between the alkyne and the azide the dinuclear copper intermediate evolves. Under release of a copper Cu(I) triazolide is formed. Proteolysis of the Cu(I) triazolide leads to the desired 1,4-triazole under recovery of the catalyst.



Scheme 10: Mechanism of CuAAC with terminal alkynes. Scheme taken from [25].

2.3 Application

Modern peptide design allows controlled intracellular assembly that can be used for anticancer applications among others. Due to mechanistic stress, that the assemblies exert on cells, apoptosis can be caused. Cancer cells typically exhibit specific conditions like a slightly acidic environment (pH 6.70 – 7.10), increased levels of GSH or reactive oxygen species (ROS) and enzymes that are overexpressed. Creating peptides that respond to one of these conditions allows selective self-assembly. [5]

2.3.1 Cell Uptake

To facilitate cellular uptake of the designed peptides cell penetrating peptide (CPP) sequences can be utilized. CPP are short positively charged peptides that can translocate into cells carrying cargos. The first one to be discovered was the TAT sequence. TAT derives from the TAT protein that originates from human immunodeficiency virus type 1 (HIV-1). First TAT protein was found to be taken up by cells and later it was found that the basic domain, the amino acids 47 - 57, is the reason for cell uptake. YGRKKRRQRRR is the TAT sequence, which is depicted in **Figure 3**. [11,26–28]

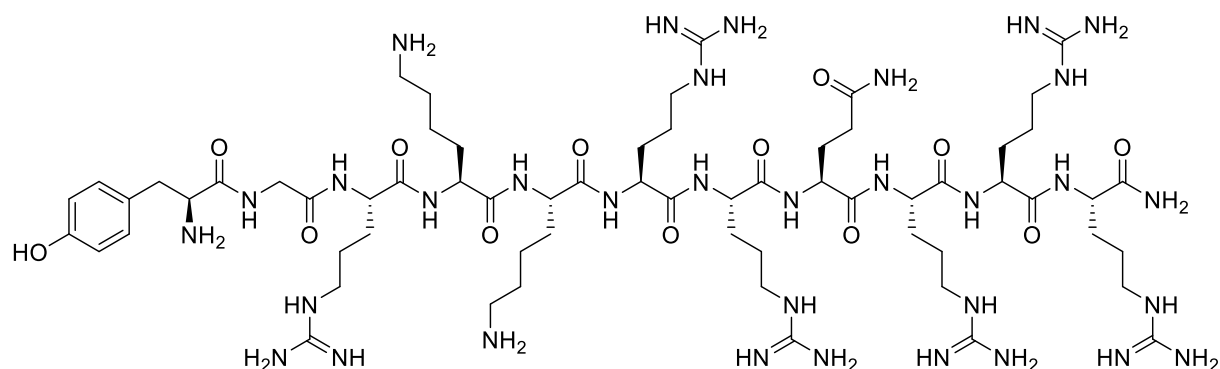


Figure 3: Structure of TAT sequence.

While the mechanism for cell uptake still remains uncertain, it is known that cell uptake with TAT is unspecific. [5]

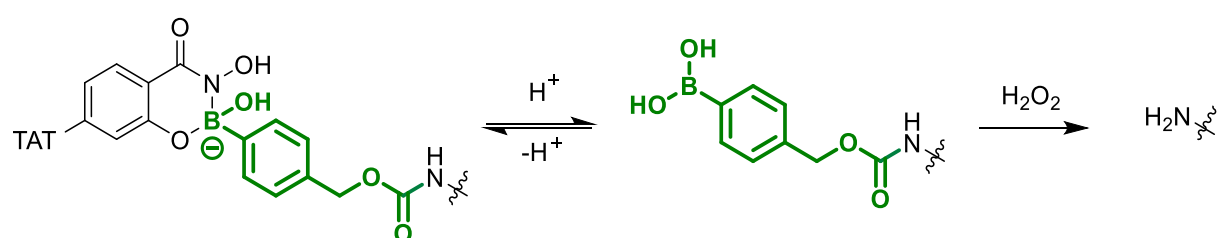
Another effect of the positively charged amino acids is that they repel each other and thereby prevent self-assembly. This is very useful, since only the self-assembling motif is supposed to self-assemble after intracellular cleavage.

2.3.2 Cleavage

Upon cell uptake of the peptides several stimuli can induce the cleavage of the peptides to allow self-assembly. Since increased H_2O_2 and GSH levels are found in many cancer cell lines, these conditions will be described in more detail as potential triggers. [5]

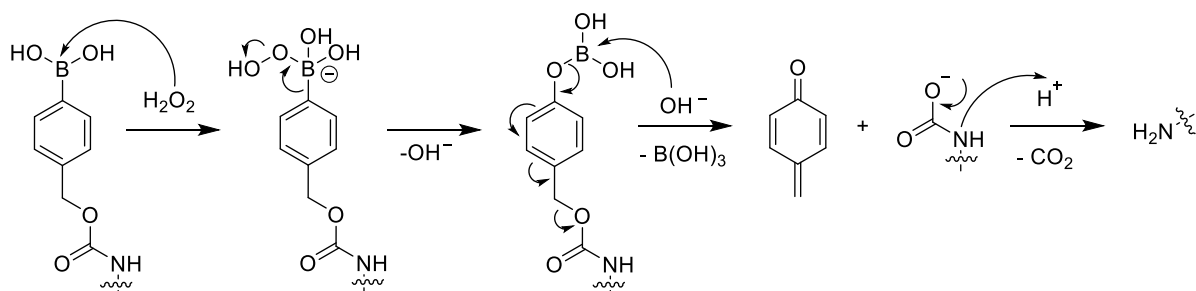
H_2O_2 sensitive Systems

The peptides with the boronic acid linker undergo a two-step cleavage as shown in **Scheme 11**. At first the dynamic covalent bonds of the boronate ester are cleaved by acid catalyzed hydrolysis ($\text{pH} = 5$) inside endosomes. Later cleavage from the boronic acid linker is induced by H_2O_2 . [8]



Scheme 11: Steps for cleavage of boronic acid linker peptides.

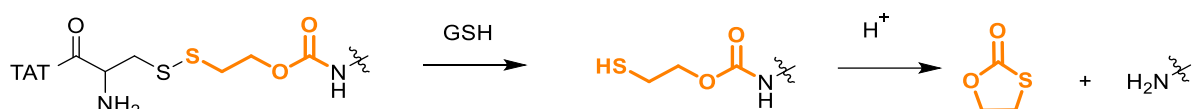
The mechanism of the second step is shown in **Scheme 12**. The first step of this mechanism is the coordination of a hydroperoxide forming a boronate anion. A *B,O*-phenyl-shift with hydroxide leaving is the next step. The boron is attacked by a nucleophilic hydroxide anion and subsequently leaves as boric acid. A quinone and a carbamate emerge. The carbamate immediately degrades to carbon dioxide and an amine. In this case the resulting amines are the cleaved peptides. [8,29]



Scheme 12: Mechanism of H_2O_2 -induced cleavage of boronic acid linker.

GSH sensitive Systems

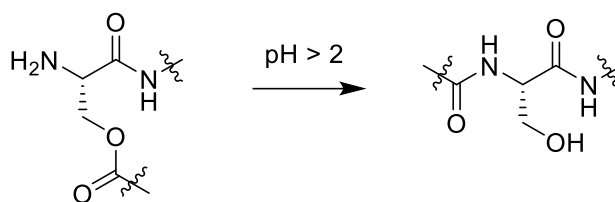
The cleavage of the peptides with disulfide linkers is induced by GSH. GSH is a natural reducing agent consisting of glutamate, cysteine and glycine. The thiol moiety of the cysteine provides the reduction abilities. The reaction scheme is shown in **Scheme 13**. [5]



Scheme 13: Cleavage of disulfide linker peptides with GSH.

First, a disulfide exchange is conducted, and a thiol intermediate is formed. In the second step 2-oxathiolone is released and the N-terminally deprotected peptide remains.

In case of depsipeptides an additional step is carried out before self-assembly is possible. This is due to the kink in the backbone of depsipeptides that sterically hinders self-assembly. The intramolecular *O,N*-acyl shift linearizes the depsipeptide which is shown in **Scheme 14**. [8,30]



Scheme 14: O,N-acyl shift of depsipeptide to linear peptide.

2.3.3 Self-assembly

Self-assembly of peptides is possible through supramolecular interactions. These non-covalent interactions are ion-ion, ion-dipole, hydrogen bond, dipole-dipole, cation- π and π - π , van der Waals and hydrophobic interactions. [31]

The cytoskeleton represents an example for peptide self-assembly found in nature. Its dynamic fibrillar structures are crucial to stabilization and movement of the cell. [4,5]

For self-assembly of artificial peptides there are two strategies that can be followed. One is to utilize self-assembly that can be found in natural peptides, like β -sheets that can fibrillate and α -helices that can form coiled coil structures. The second strategy is to covalently modify the peptide for instance by linking it to an alkyl chain to create a peptide amphiphile or an aromatic group that can cause self-assembly due to π - π interactions. [6]

An example for the second strategy is Fmoc-ISA. It was reported as a self-assembling motif by Pieszka *et al.* [8]. Fmoc-ISA self-assembles due to π - π stacking of the attached Fmoc moiety.

Another self-assembling motif is the CKFKFQF sequence that was found by Sieste *et al.* [10]. It is derived from the peptide enhancing factor-2. Further unpublished work of K. Maxeiner showed that KFKFQF already exhibits self-assembling properties. KFKFQF sequence can self-assemble by forming β -sheets, thus using the first strategy. As Ulijn *et al.* [6] reported alternating hydrophobic and hydrophilic amino acids form the basic motif for a peptide with the ability to form β -sheets. Thereby a hydrophilic side and a hydrophobic side is obtained. In addition to the hydrogen bonds of the β -sheets this enables supramolecular interactions such as hydrophobic and ion-ion interactions. Using phenylalanine as the hydrophobic amino acid enhances supramolecular interactions as π - π stacking is possible. [5,6,10]

3 Results and Discussion

The aim of this work was to synthesize different peptides that self-assemble upon cell uptake and intracellular cleavage from the respective linkers induced by H_2O_2 or GSH. Whether the peptides fulfill the expected properties was examined by analyzing the morphology of the fibrils and kinetics of the cleavage. Both synthesis and analysis of the peptides will be discussed in the following.

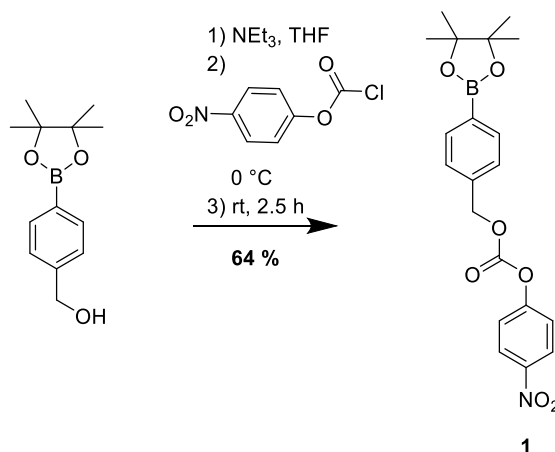
All peptide systems consist of three parts: 1) a TAT sequence, 2) a self-assembling motif and 3) a linker. The TAT sequence serves for cellular uptake and inhibition of self-assembly. Depsi-ISA and KFKFQF sequences were used as self-assembling sequences. Depsi-ISA itself is not able to self-assemble due to a kink in its backbone. Linearization upon cleavage leads to the self-assembling motif Fmoc-ISA. The linkers connect these two sequences, yet certain intracellular stimuli can induce their cleavage. A H_2O_2 sensitive linker, the boronic acid linker, and a GSH sensitive linker, the disulfide linker, were used.

3.1 Synthesis of Linkers

Previous work from the group of Prof. Dr. T. Weil showed that both linkers exhibit cleavage under expected conditions.

3.1.1 H_2O_2 sensitive Linker

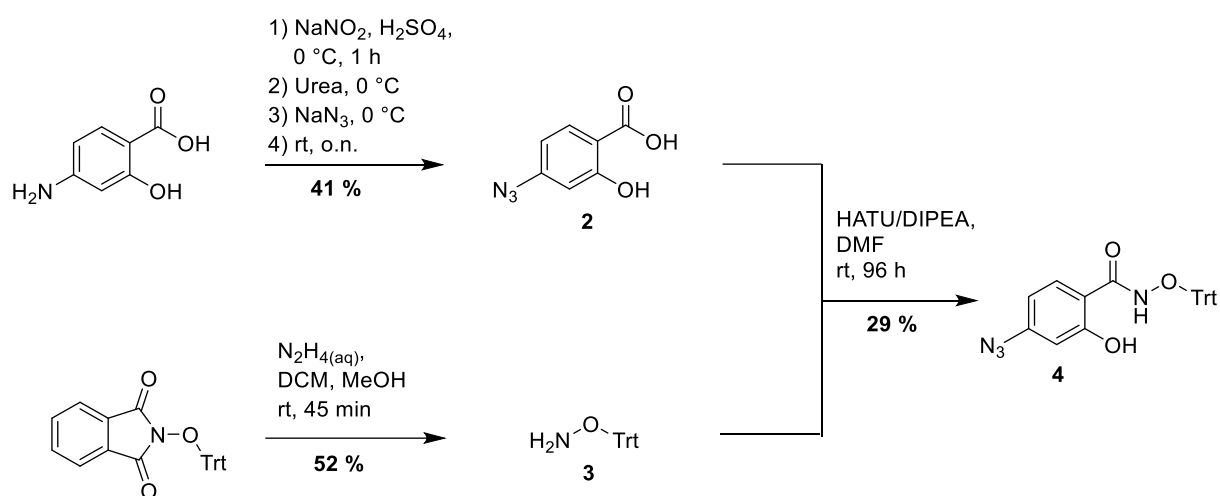
For the synthesis of boronic acid linker the protocol from previous work of Pieszka *et al.* [7,8] was followed. Hereby the hydroxyl moiety of the 4-hydroxymethylphenylboronic acid pinacol ester is activated so that it can react with the N-terminus of the peptides in subsequent peptide modifications.



Scheme 15: Reaction scheme of 4-nitrophenyl (4-(4,4,5,5-tetramethyl-1,3,2-dioxaborolan-2-yl) benzyl) carbonate (**1**) [7].

After purification with column chromatography purity was confirmed with proton nuclear magnetic resonance ($^1\text{H-NMR}$) spectroscopy (**Figure 33**). The yield of 64 % comes close to 70 % as described in literature [7].

The synthesis of 4-Azido-2-hydroxy-*N*-(trityloxy) benzamide (**4**) was conducted as shown in **Scheme 16**. To synthesize **2** the protocol from Ríos-Malvárez *et al.* [32] was adapted. The procedure of Pieszka *et al.* [8] to synthesize **3** was followed and the procedure to synthesize **4** was modified.



Scheme 16: Synthesis scheme of 4-azido-2-hydroxy-*N*-(trityloxy) benzamide (**4**).

At first the synthesis of **2** was conducted as described by Pieszka *et al* [8]. An additional step was described there. Before adding sodium azide, the reaction mixture was run over celite. A very low yield of only 10 % was obtained. Since Ríos-Malvárez *et al.* [32] reported successful synthesis of **2** without running it over celite and even with better yields (Pieszka *et al* [8] 57 % and Ríos-Malvárez *et al.* [32] 86 %), the procedure of Ríos-Malvárez *et al.* [32] was followed yet only 41 % were obtained. It is very likely that product was lost during recrystallization because 2.26 g of the crude product and only 1.00 g of the product were obtained.

Characterization of **2** by $^1\text{H-NMR}$ alone was not sufficient, since the only difference between educt and product is the amino group that should not be seen in the product spectrum. Amino groups, however, cannot always be seen in $^1\text{H-NMR}$ spectra. Therefore $^1\text{H-NMR}$ of educt and product are compared to observe the shifts due to the change from the amine to the azide (**Figure 4**).

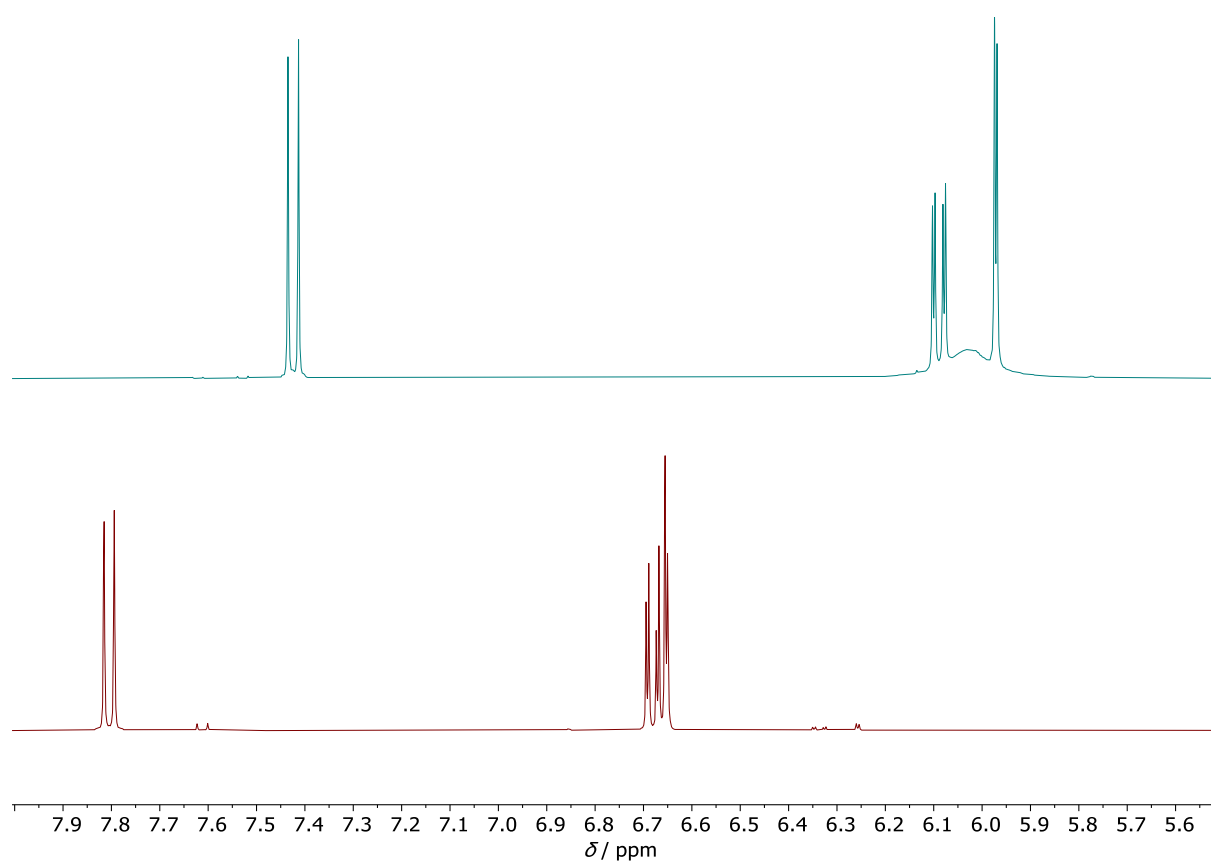


Figure 4: ¹H-NMR spectra of 4-azidosalicylic acid (**2**), in red, and 4-aminosalicylic acid, in turquoise.

To ensure the identity and purity of the product liquid chromatography - mass spectrometry (LC-MS) was measured. As one can see in **Figure 5** the successful conversion could be proven.

LC-MS (ESI-MS, 179 g/mol) m/z 178 [M-H]⁻

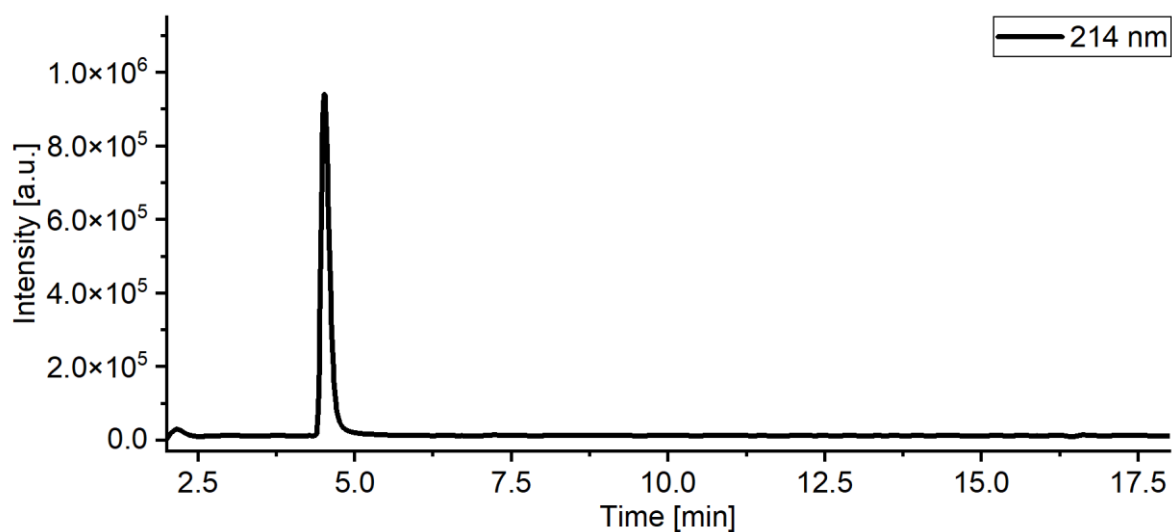


Figure 5: LC-MS chromatogram of 4-azidosalicylic acid (**2**) detected at $\lambda = 214$ nm.

The synthesis of **3** also yielded (52 %) less than expected by literature (86 %) [8]. It is possible that product was lost during recrystallization.

Before conducting the synthesis of **4**, test runs (0.20 mmol scale) with several coupling agents were run because low yields were expected (Pieszka *et al* [8] 39 %). Furthermore, the reaction was conducted without a protection group at the hydroxy moiety of **2**, unlike in literature [8]. Many side reactions are conceivable due to the very reactive active ester intermediate that can be attacked by any other nucleophile. HATU (1.5 eq) / *N,N*-diisopropylethylamine (DIPEA) (4 eq), DIC (1.5 eq) / 4-dimethylaminopyridine (DMAP) (0.5 eq) and 1-ethyl-3-(3-dimethylaminopropyl)carbodiimide (EDC) (1.5 eq) / DMAP (0.5 eq) were tested to run overnight. Thin layer chromatography (TLC) showed that HATU/DIPEA was the most successful coupling agent combination even though conversion was not 100 % (spots of educt could still be seen).

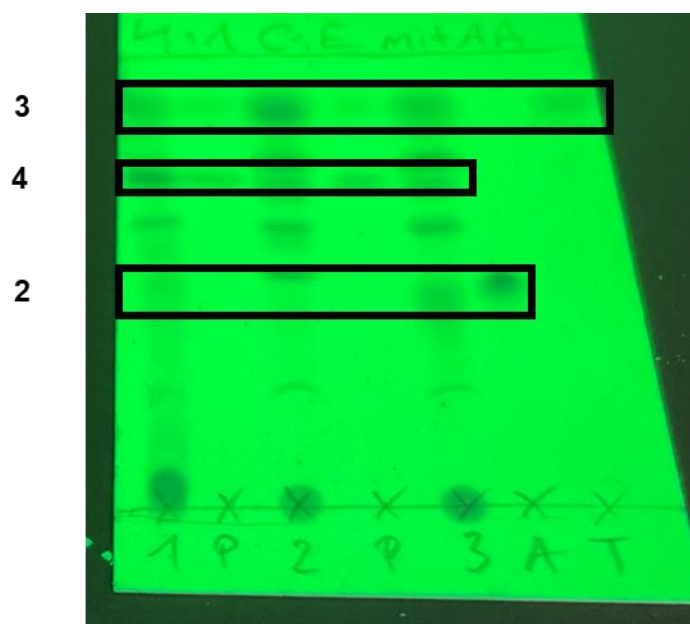


Figure 6: TLC of test reactions for coupling of *N*-trityloxyamine (**3**) with 4-azidosalicylic acid (**2**) to form 4-azido-2-hydroxy-*N*-(trityloxy) benzamide (**4**). Plotted was 1: test reaction with HATU/DIPEA, 2: test reaction with DIC/DMAP, 3: test reaction with EDC/DMAP, P: 4-azido-2-hydroxy-*N*-(trityloxy) benzamide (**4**), A: 4-azidosalicylic acid (**2**), T: *N*-trityloxyamine (**3**). TLC was run for 15 min with 4:1 volume shares of cyclohexane : ethyl acetate with drops of acetic acid.

The reason for more success with HATU as an activator could originate from the different activation mechanism than carbodiimide-based activators have. As a consequence, less side reactions occur.

The reaction was then run with HATU/DIPEA yielding 29 %. Though, the procedure described by Pieszka *et al* [8] using EDC/DMAP yields 39 %. It can be assumed that product was lost during purification.

To prove the before stated assumption that non-carbodiimide-based activators influence the conversion positively further investigations would have been necessary. Unfortunately, this was not possible during the given time frame.

$^1\text{H-NMR}$ of **4** was not distinct enough to characterize the compound because integrals did not coincide with the number of H-atoms, as one can see in **Figure 7**.

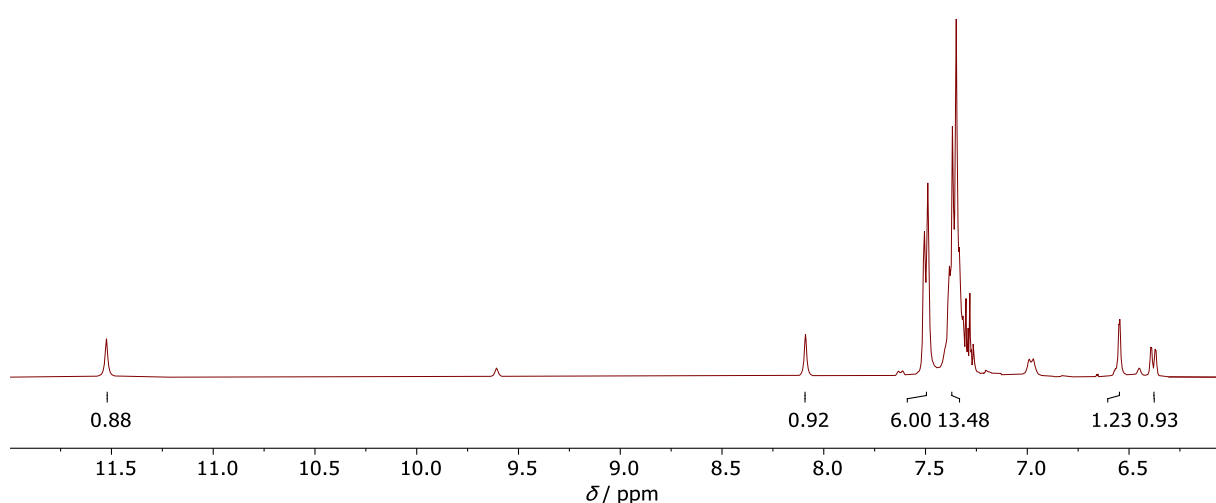


Figure 7: $^1\text{H-NMR}$ spectrum of 4-azido-2-hydroxy-*N*-(trityloxy) benzamide (**4**).

To show the obtained compound was in fact 4-azido salicylic acid LC-MS was measured (**Figure 8**). LC-MS chromatogram displays two peaks. The first, small peak indicates that the compound was not pure. From the mass spectrum of peak 1, it was assumed that *N*-trityloxyamine (**3**) is the impurity. It was presumed that **3** would not interfere in subsequent reactions. Thus, the compound was used without further purification.

Peak 1: **LC-MS** (ESI-MS, 436 g/mol) m/z 895 $[2M+Na]^+$, 459 $[M+Na]^+$

Peak 2: **LC-MS** (ESI-MS, 275 g/mol) m/z 243 $[M-O-NH_2]^+$

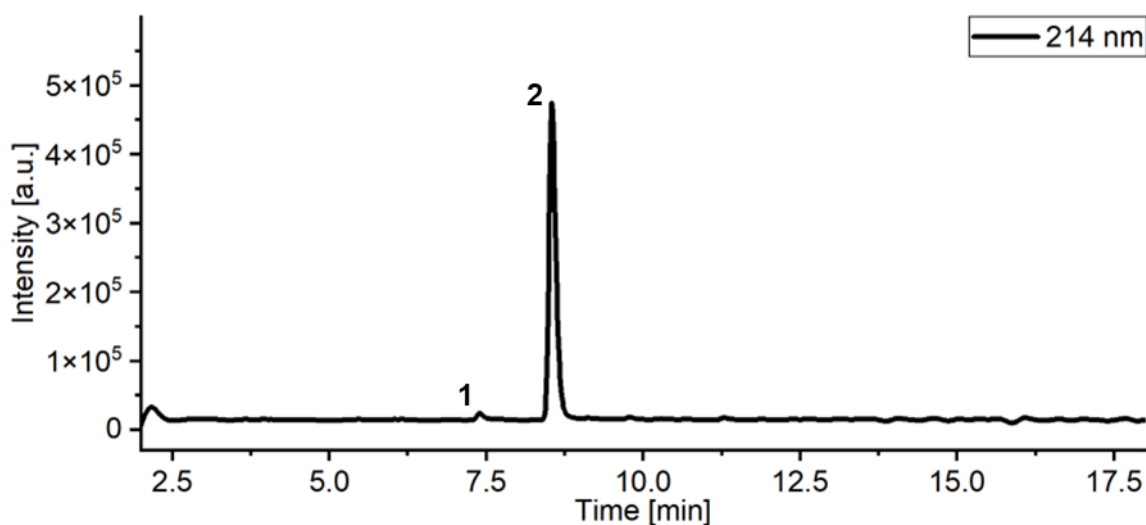
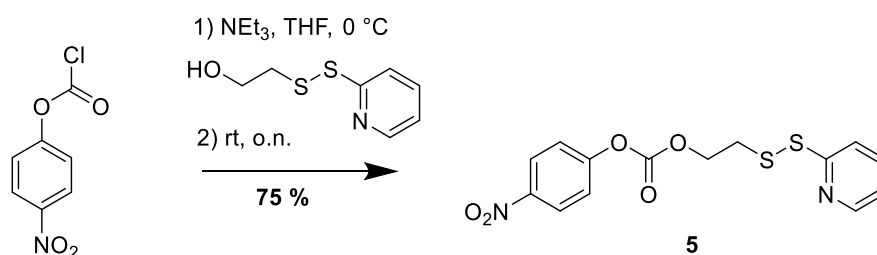


Figure 8: LC-MS chromatogram of 4-azido-2-hydroxy-*N*-(trityloxy) benzamide (**4**) detected at $\lambda = 214$ nm.

H₂O₂ sensitive linkers were successfully synthesized and used for modification of the peptides.

3.1.2 GSH sensitive Linker

To synthesize 4-nitrophenyl(2-(pyridine-2-yl)disulfaneyl) ethyl carbonate (**5**) the procedure from Skakuj *et al.* [9] as shown in **Scheme 17** was performed. Again, the hydroxyl moiety of 2-(pyridin-2-ylsulfaneyl) ethan-1-ol is activated by forming a carbonate diester. This enables further reactions with the N-terminus of the peptides.



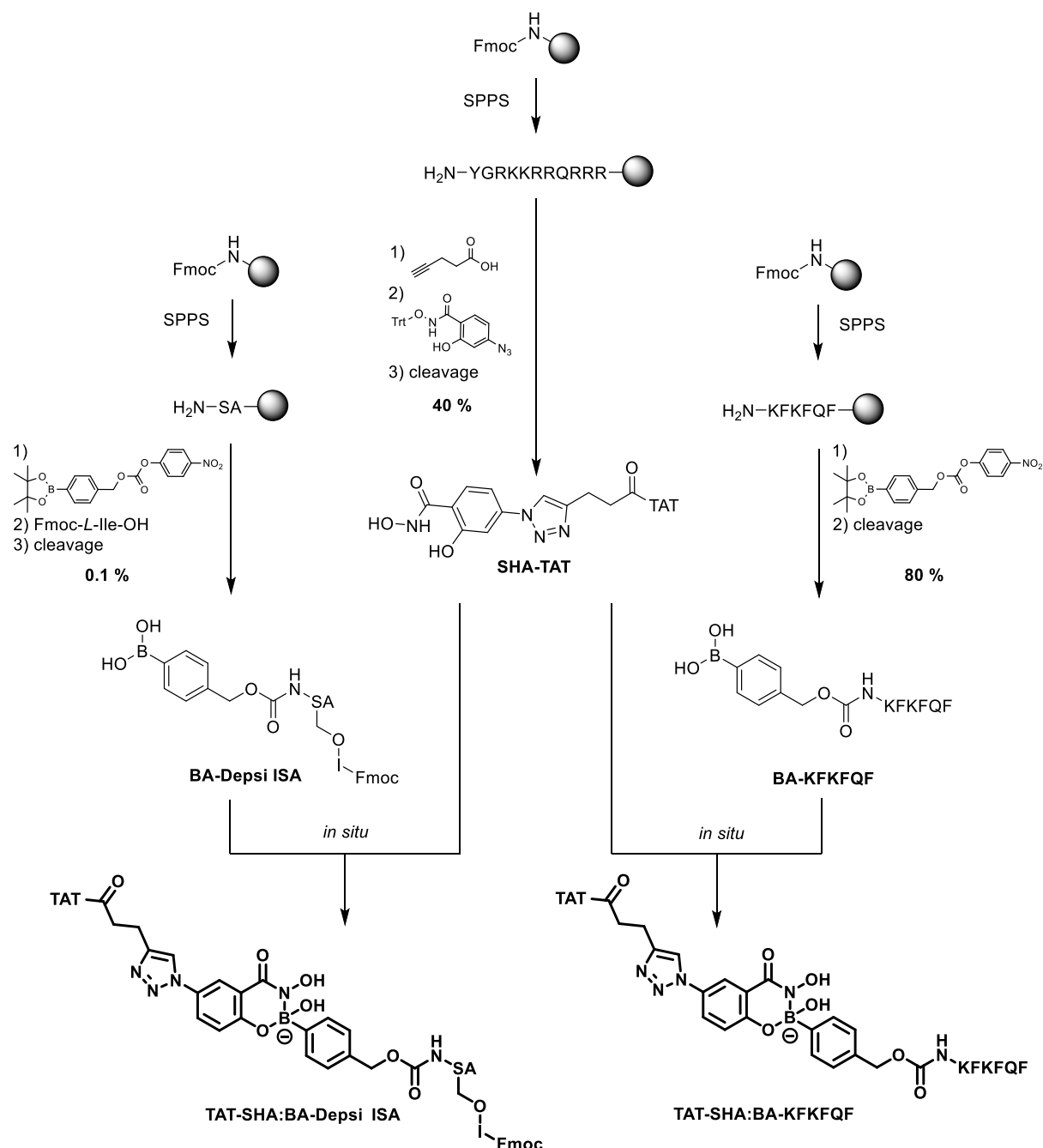
Scheme 17: Reaction scheme of 4-nitrophenyl(2-(pyridine-2-yl)disulfaneyl) ethyl carbonate (**5**).

The GSH sensitive linker was synthesized successfully, and purity of **5** was checked with ¹H-NMR. The compound was used in subsequent peptide modifications.

3.2 Synthesis of Peptides

The peptide sequences used for this project are well known to self-assemble upon cleavage, which was shown by previous work of the Weil group. The optimized procedure for SPPS with DIC/Oxyma as coupling reagents of the Weil group was used. Protocols for peptide modification from Pieszka *et al.* [7,8] and from yet unpublished work of S. Chagri were followed.

3.2.1 H₂O₂ sensitive Peptides



Scheme 18: Synthesis routes for SHA-TAT, BA-Depsi ISA and BA-KFKFQF.

Adjustments of the protocol for click reaction by Pieszka *et al.* [7,8] were made. Instead of DIPEA TBTA was added as a stabilizing agent of the Cu(I) species. To make sure oxidation of Cu(I) was prevented the reaction was performed under nitrogen atmosphere and the reducing agent sodium ascorbate was used. The yield of SHA-TAT with 40 % is higher than expected (Pieszka *et al.* [7,8] 7.1 %). Most certainly factors involved with this improvement in yield are the optimized SPPS procedure and the adjusted conditions for click reaction. But the modified synthesis scale of the click reaction must be considered too. Limiting compound was the SHA (0.05 mmol) unlike in literature where TAT was the limiting compound (0.10 mmol). Thus, resulting in higher yields.

BA-Depsi ISA only led to a yield of 0.1 %. This could be a result of the challenges faced while purifying the peptide. After running preparative high performance liquid chromatography (HPLC) LC-MS still showed two peaks (**Figure 9**). MS of peak 1 indicates that the impurity could be the unesterified BA-SA sequence.

Peak 1: **LC-MS** (ESI-MS, 354 g/mol) m/z 362 $[M-O+Na]^+$

Peak 2: **LC-MS** (ESI-MS, 689 g/mol) m/z 690 $[M+H]^+$

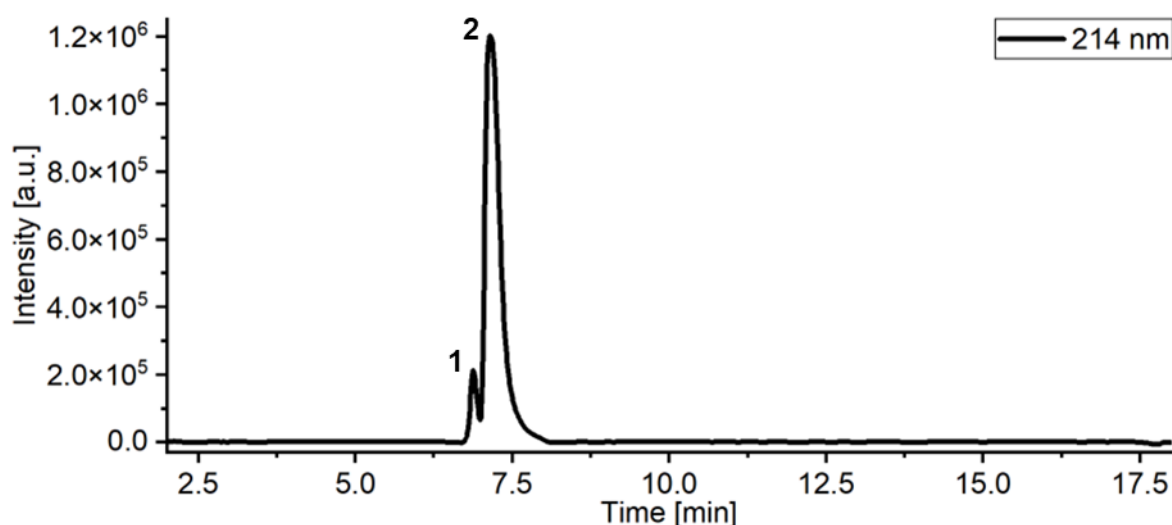


Figure 9: LC-MS chromatogram of BA-Depsi ISA after first purification with preparative HPLC detected at $\lambda = 214$ nm.

Further purification with the semipreparative HPLC led to a pure compound (**Figure 10**). 61 mg of the crude product were obtained but only 1 mg of the pure product were yielded. Due to limited time the crude product could not be purified completely explaining the low yields. By optimizing the method used for preparative HPLC a second purification at semipreparative HPLC could be circumvented.

LC-MS (ESI-MS, 689 g/mol) m/z 690 $[M+H]^+$, 688 $[M-H]^-$

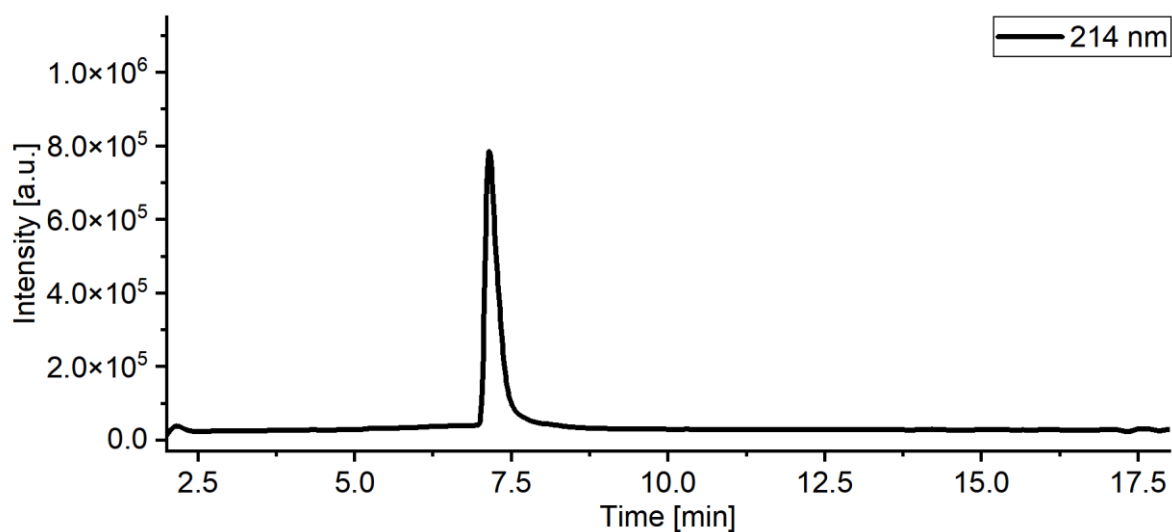


Figure 10: LC-MS chromatogram of BA-Depsi ISA detected at $\lambda = 214$ nm.

Yields for BA-KFKFQF were unexpectedly high, since SPPS procedure typically does not lead to yields above 60 %. Therefore, LC-MS was measured to show BA-KFKFQF was pure.

LC-MS (ESI-MS, 1022 g/mol) m/z 1023 $[M+H]^+$, 1005 $[M-H_2O+H]^+$, 512 $[M+2H]^{2+}$, 1020 $[M-H]^-$

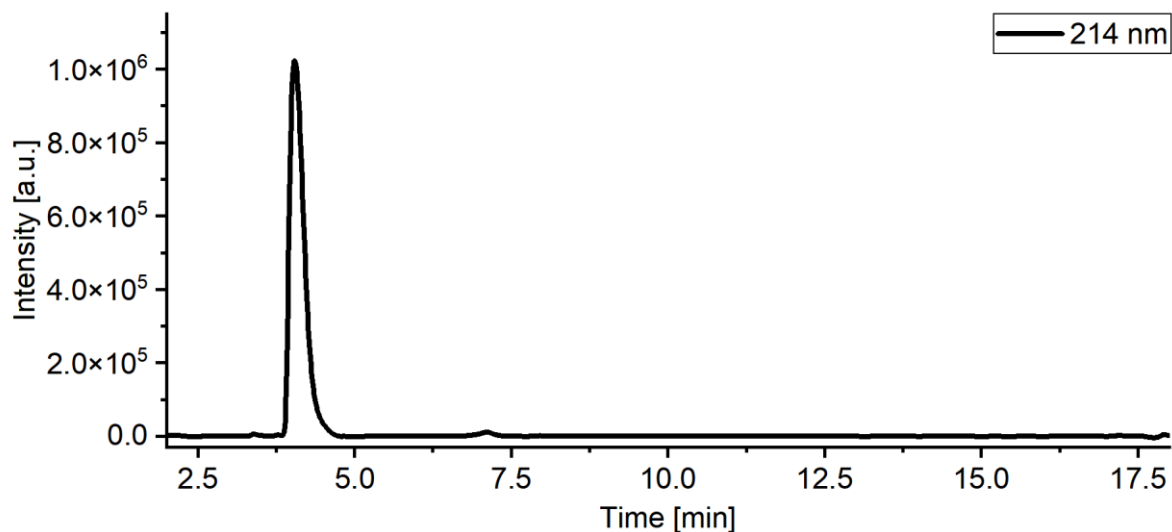
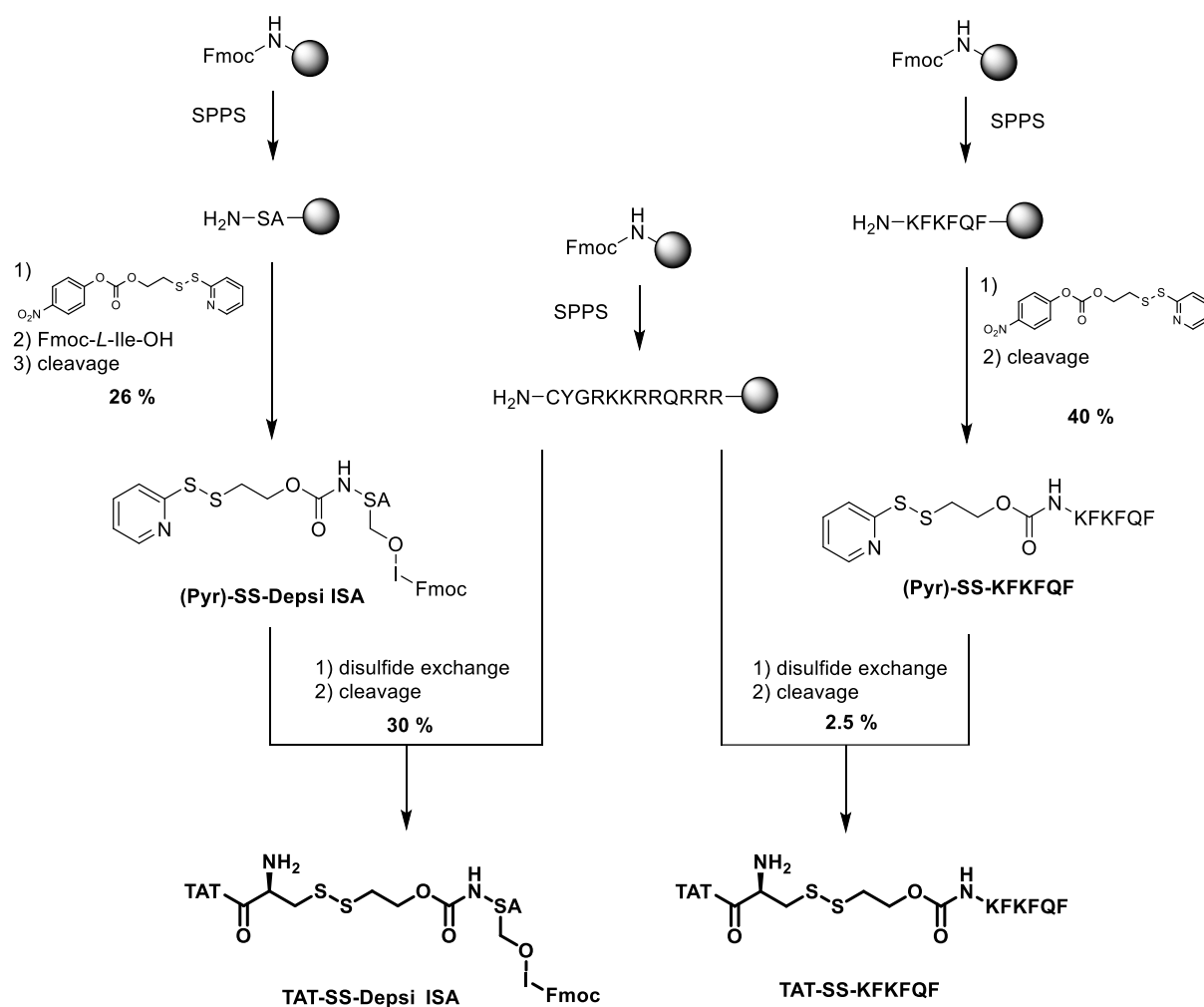


Figure 11: LC-MS chromatogram of BA-KFKFQF detected at $\lambda = 214$ nm.

3.2.2 GSH sensitive Peptides



Scheme 19: Synthesis routes for TAT-SS-Depsi ISA and TAT-SS-KFKFQF.

For (Pyr)-SS-Depsi ISA, (Pyr)-SS-KFKFQF and TAT-SS-Depsi ISA yields between 25 and 40 % were obtained. Whereas the yields for TAT-SS-KFKFQF were lower than expected. Due to the very polar sequence purification with the preparative HPLC was difficult. Initially the product eluted at 3 min with the injection peak. It took several runs to figure out a suitable method, hence lots of product was lost. The synthesis could not be repeated because the peptide synthesizer was out of order.

3.3 Morphology

To examine the morphology of the peptides TEM pictures were recorded by Patrick Roth. 1 mM solutions of the peptides in phosphate buffered saline (PBS) buffer with the respective triggers (H_2O_2 or GSH) were incubated for 24 h at 37 °C. The trigger concentrations were 10 mM imitating intracellular levels of H_2O_2 or GSH. [5] As negative controls, peptides were incubated in PBS for 24 h at 37 °C without addition of the respective triggers.

3.3.1 H_2O_2 sensitive Peptides

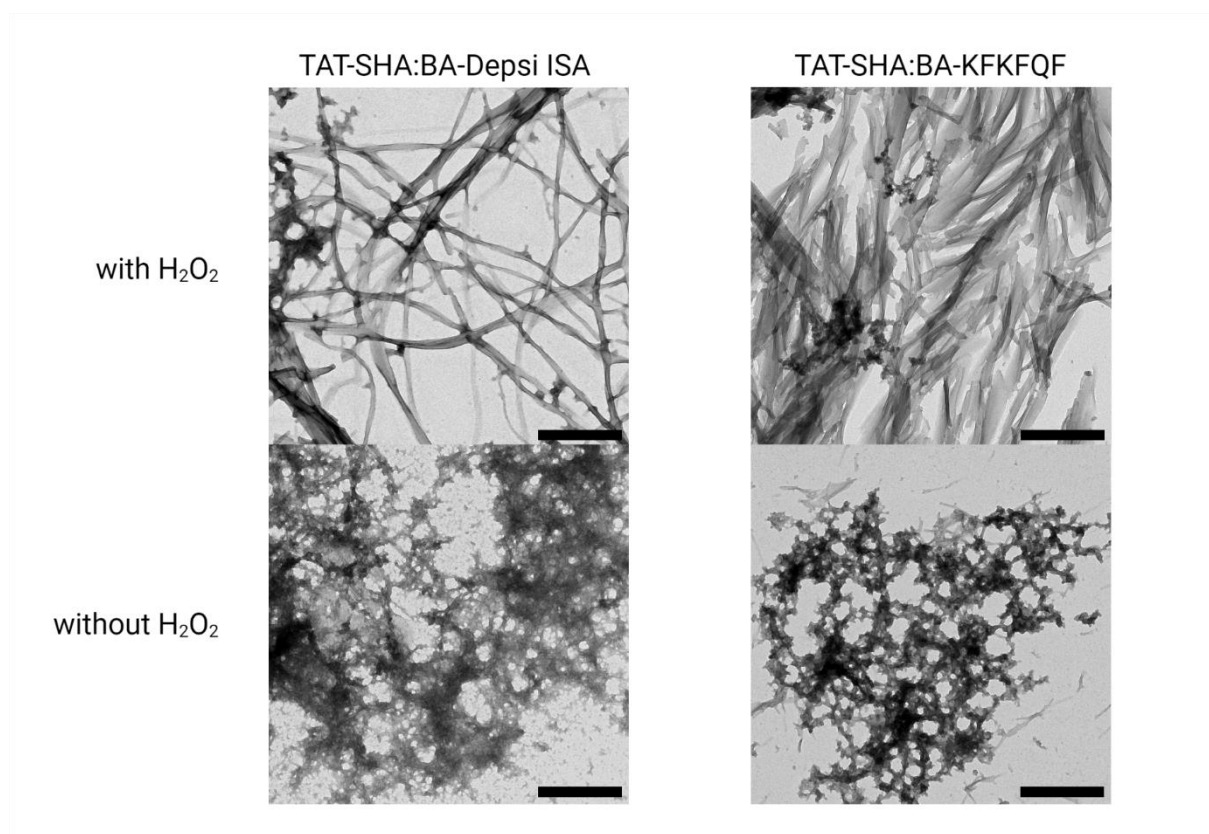


Figure 12: TEM pictures of boronic acid linker peptides with TAT sequence at 1 mM concentration. Scale bar = 500 nm.

For both peptide sequence, Fmoc-ISA and KFKFQF, fibrils can be found after incubation with H_2O_2 , whereas the samples without trigger mainly display aggregates. The negative control of TAT-SHA:BA-KFKFQF exhibits a bit fibril formation too, which can be explained with the high concentrations used.

Figure 12 shows that the peptides fulfill their purposes. For one thing, it could be shown that the cleavage from the boronic acid linker under the desired conditions works and secondly the formation of fibrils of the self-assembling sequences (Fmoc-ISA and KFKFQF) could be shown.

Aggregates could also be found in the samples with trigger (see **Figure 13**). This could occur due to the high concentrations used for this experiment.

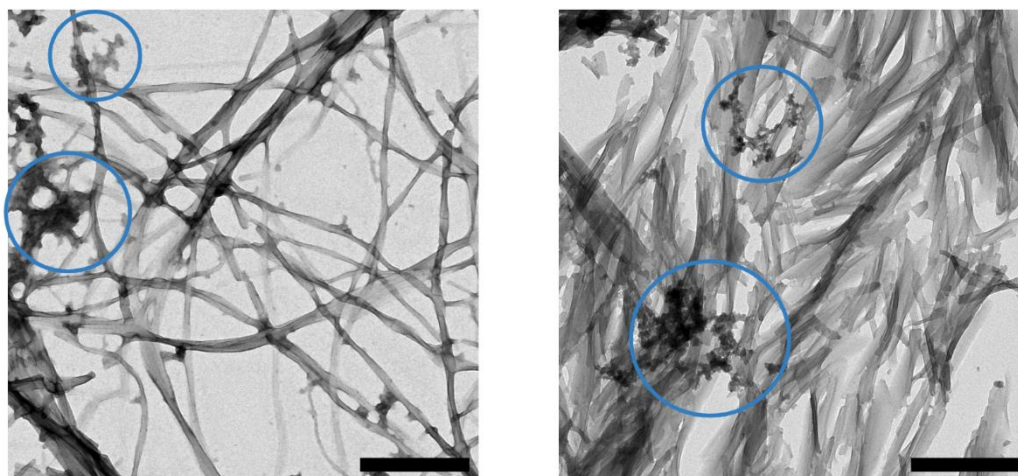


Figure 13: TEM pictures of TAT-SHA:BA-Depsi ISA and TAT-SHA:BA-KFKFQF incubated with H_2O_2 . Aggregates are framed with blue circles. Scale bar = 500 nm.

The fibrils found for the TAT-SHA:BA-Depsi ISA are thin and straight, while TAT-SHA:BA-KFKFQF rather forms thick, plaque-like fibrils. The average thickness of TAT-SHA:BA-Depsi ISA fibrils is 39 nm and of TAT-SHA:BA-KFKFQF fibrils is 78 nm. The average thickness was measured with *ImageJ*.

This difference in the fibril formation probably originates from the different mechanisms of self-assembly. While Fmoc-ISA self-assembles due to π - π interactions, KFKFQF self-assembles due to β -sheet formation. To prove this assumption CD measurements would be necessary. Unfortunately, this was not possible during this thesis.

Fibrils of TAT-SHA:BA-Depsi ISA partly exhibit twists. The arrows in **Figure 14** point to such twists.

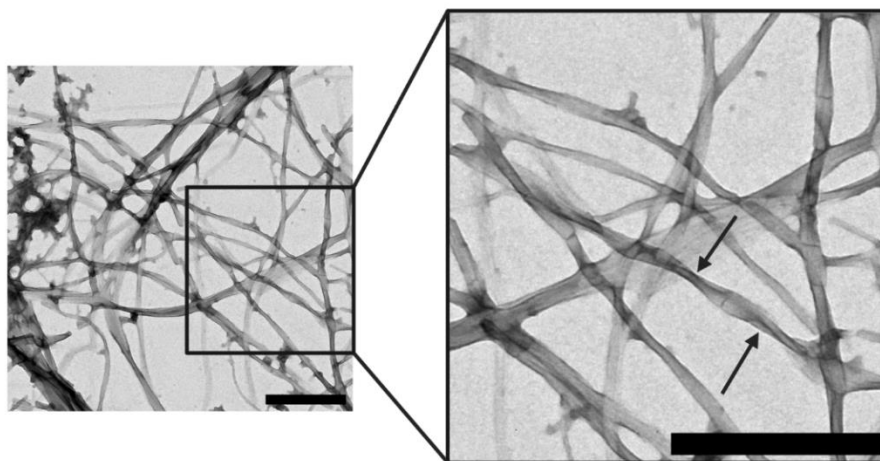


Figure 14: Closeup of TEM picture of TAT-SHA:BA-Depsi ISA incubated with H_2O_2 . Scale bar = 500 nm. Arrows point to twists in the fibril.

To make sure self-assembly was induced after cleavage from boronic acid linker and not already after cleavage from TAT, TEM was recorded for BA-Depsi ISA and BA-KFKFQF without SHA-TAT. The results are depicted in **Figure 15**.

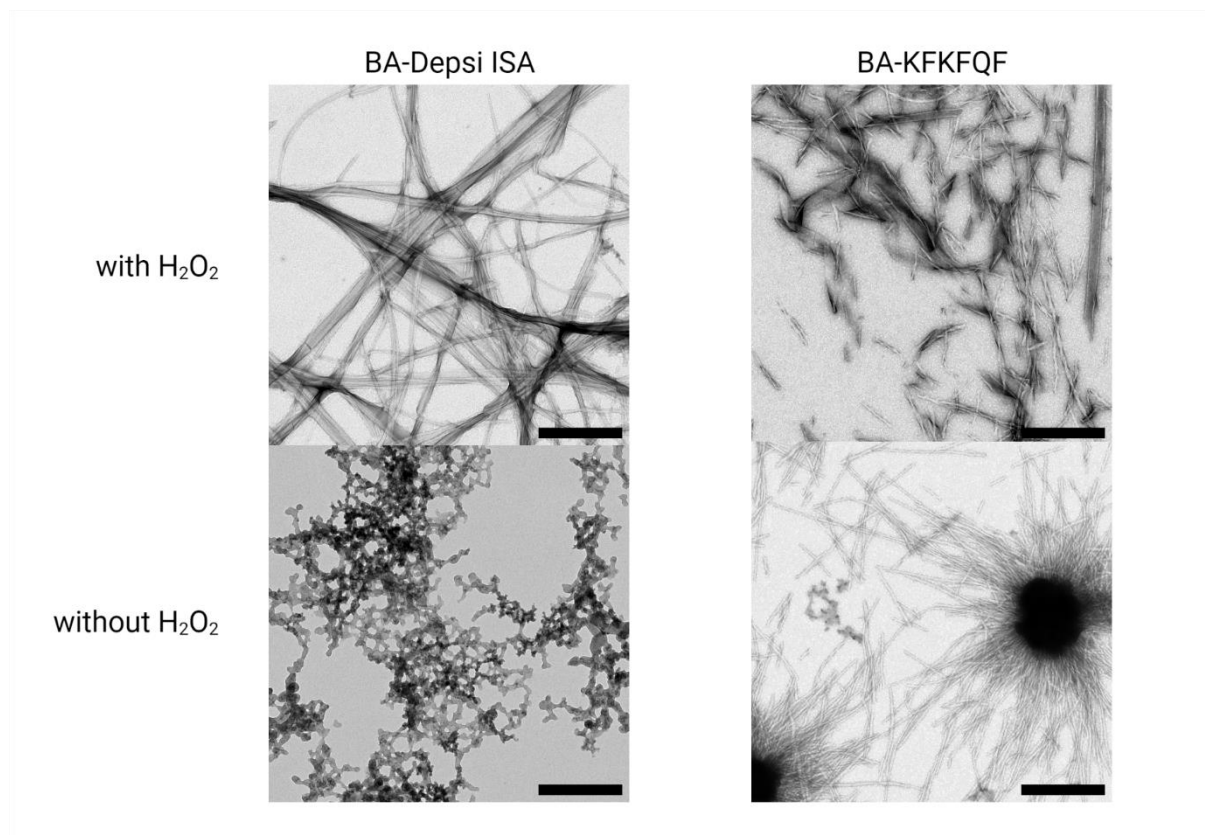


Figure 15: TEM pictures of boronic acid linker peptides without TAT sequence at 10 mM concentration. Scale bar = 500 nm.

BA-Depsi ISA displays fibril formation only when incubated with H_2O_2 , consequently only after cleavage from boronic acid ester. The average thickness of the fibrils amounts to 37 nm similar to fibrils of TAT-SHA:BA-Depsi ISA that are averagely 39 nm thick.

BA-KFKFQF does show fibrils with and without trigger. Thus, fibril formation is independent of cleavage from boronic acid linker. Since KFKFQF is not a depsipeptide linearization is not the main trigger for self-assembly but cleavage from TAT is.

Though the exhibited fibrils vary. The fibrils found for BA-KFKFQF with H_2O_2 (average thickness: 35 nm) are thicker than the fibrils found for BA-KFKFQF without H_2O_2 (average thickness: 13 nm). In addition, fibrils of BA-KFKFQF without H_2O_2 seem to arrange radially.

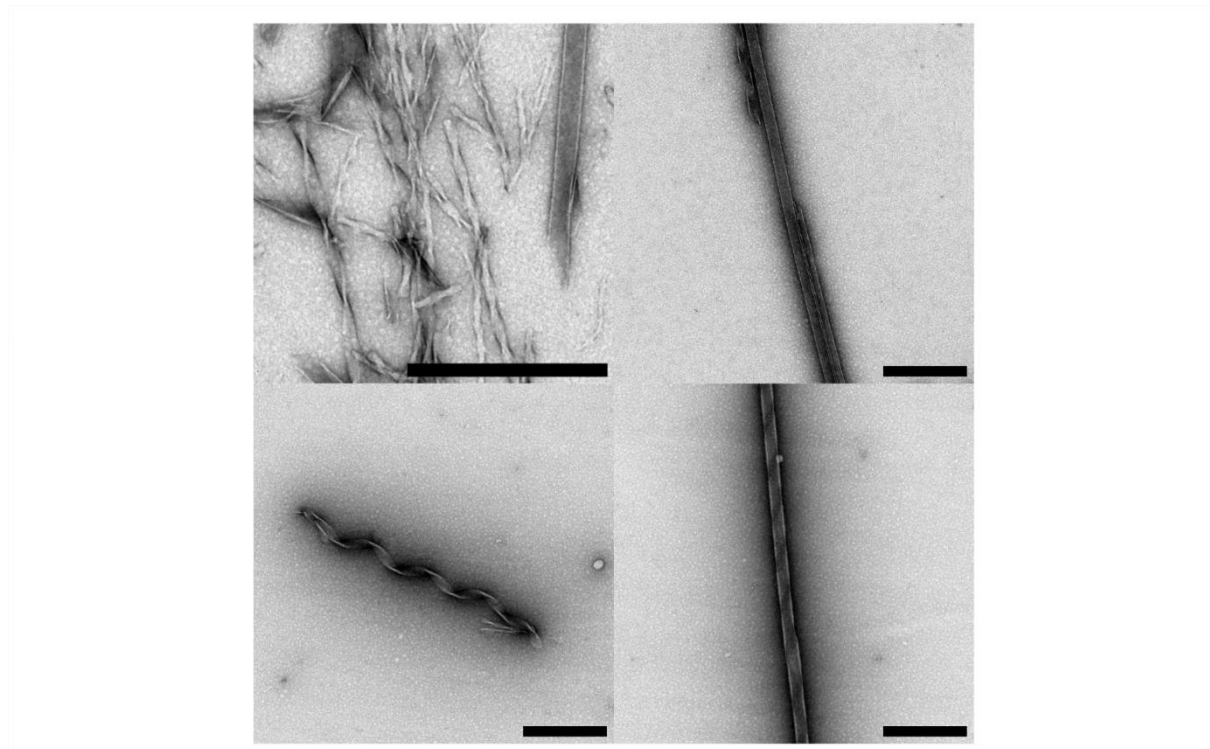


Figure 16: TEM pictures of BA-KFKFQF incubated with H_2O_2 . Scale bar = 500 nm.

The cleaved BA-KFKFQF shows tube-like and twisted fibrils as shown in **Figure 16**. The upper right image depicts a tube, while the lower two depict twisted fibrils with differently sized gaps. The upper left image depicts both.

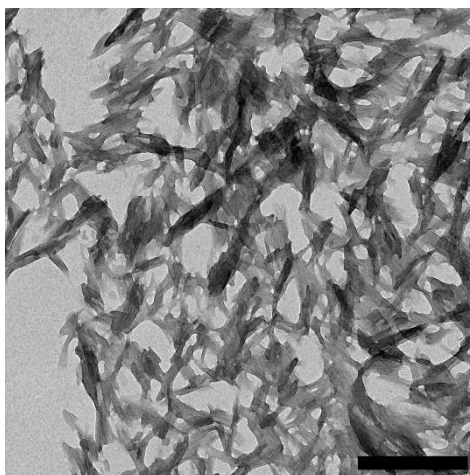


Figure 17: TEM picture of BA-KFKFQF without H₂O₂. Scale bar = 500 nm.

Apart from the tube-like or twisted fibrils also fibrils in the form of plaques (**Figure 17**) were found for the BA-KFKFQF sample without H₂O₂. These structures look very much like the ones found for TAT-SHA:BA-KFKFQF.

Both the TAT-SHA:BA-Depsi ISA and the TAT-SHA:BA-KFKFQF systems exhibited fibrils after incubation with H₂O₂, but their morphology was very different. TEM images of the systems without SHA-TAT revealed that BA-KFKFQF can already self-assemble. Consequently, the importance of TAT to prevent the self-assembly of KFKFQF systems could be demonstrated. Whereas for the depsipeptide system cleavage from boronic acid linker was shown to be crucial for self-assembly.

3.3.2 GSH sensitive Peptides

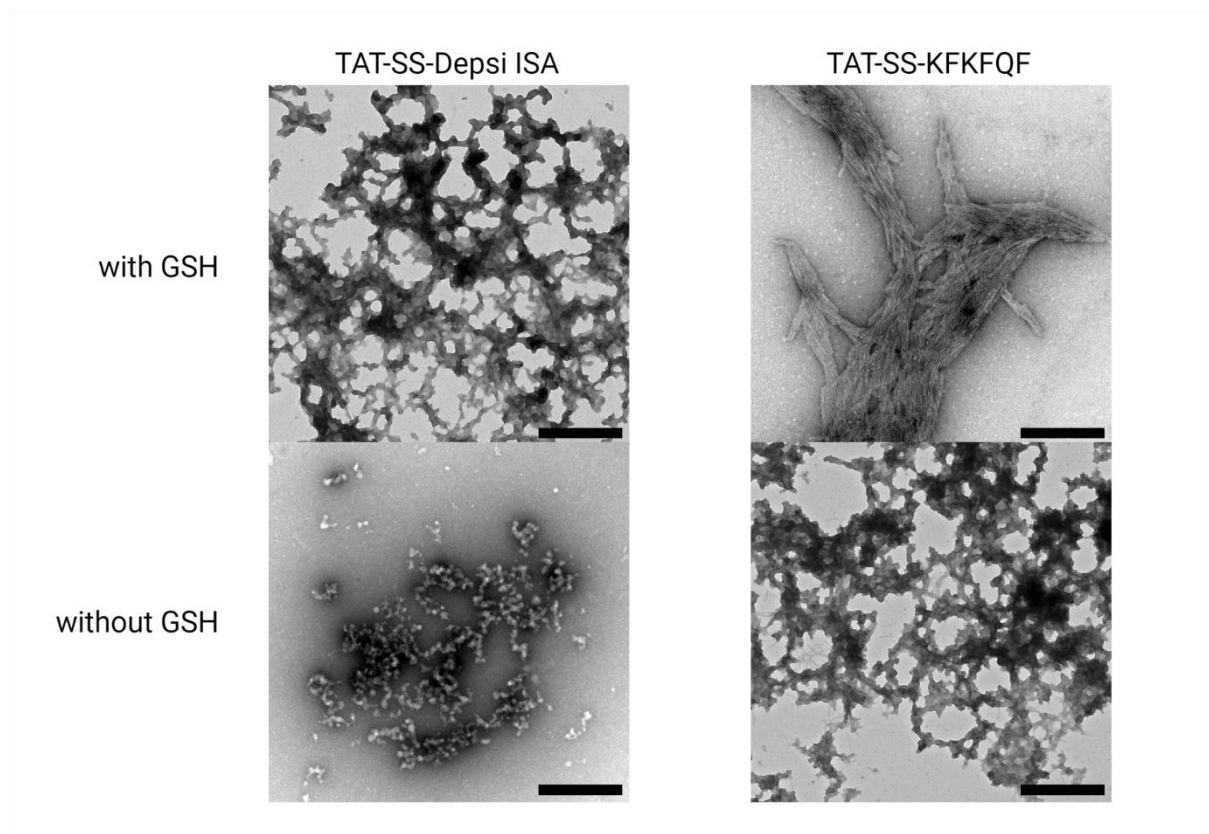


Figure 18: TEM pictures of disulfide linker peptides at 1 mM concentration. Scale bar = 500 nm.

For the disulfide linker peptides only TAT-SS-KFKFQF exhibits fibril development when incubated with trigger. TAT-SS-Depsi ISA does not show fibrillation. To confirm the results a repetition of the experiment is necessary, which was not performed during this thesis due to limitation in time.

Looking closely at the negative control of TAT-SS-KFKFQF fibrils can be seen, like already seen for TAT-SHA:BA-KFKFQF (**Figure 12**). This can be related to the high concentrations used.

It could be shown that TAT-SS-KFKFQF is cleaved and subsequently self-assembles under defined conditions. However, TAT-SS-Depsi ISA did not show any fibrillation behavior which might be due to the high concentrations.

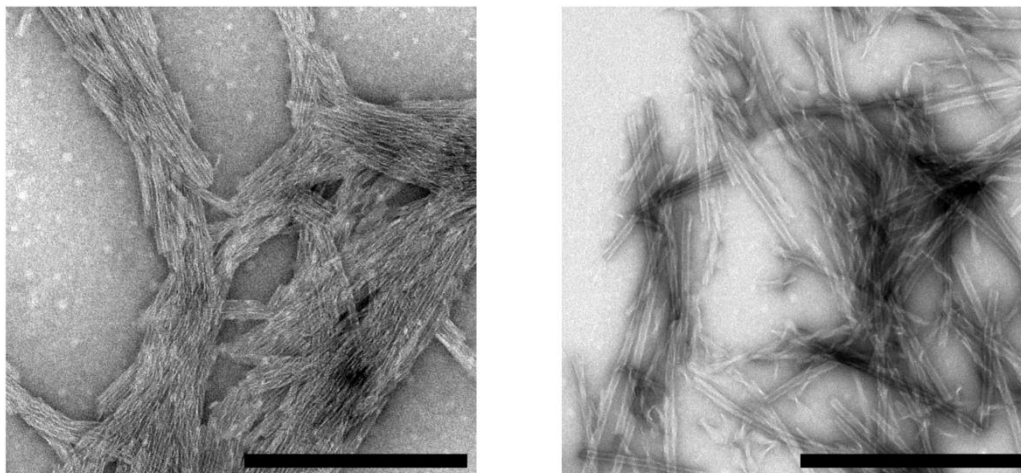


Figure 19: TEM pictures of TAT-SS-KFKFQF with GSH. Scale bar = 500 nm.

In **Figure 19** two different TEM images of TAT-SS-KFKFQF are shown. The fibrils in the left image look more organized and denser than the ones in the right image. The left image shows straight, tube-like fibrils and twisted fibrils that look like they are in a transition state to become tube-like fibrils. A closeup of the right image displaying both kinds of fibrils are shown in **Figure 20**.

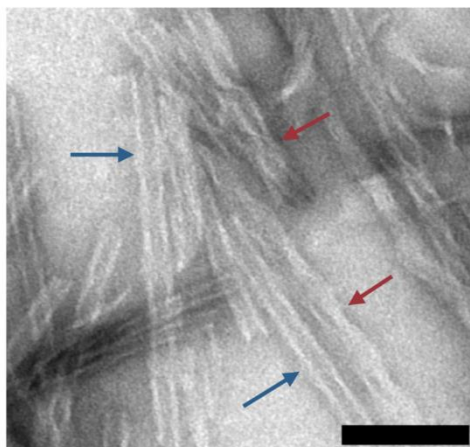


Figure 20: Closeup of TEM picture of TAT-SS-KFKFQF with GSH. Blue arrows point to tube-like fibrils and red arrows to twisted fibrils. Scale bar = 100 nm.

Figure 21 shows a closeup of the denser image of TAT-SS-KFKFQF (left image in **Figure 19**) demonstrating that the left image in **Figure 19** are just the same but more organized and denser fibrils that can be seen on the right image in **Figure 19** too.

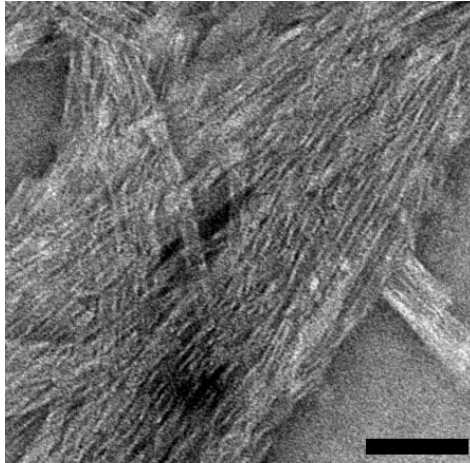


Figure 21: Closeup of TEM picture of TAT-SS-KFKFQF with GSH. Scale bar = 100 nm.

Fibril formation of the TAT-SS-KFKFQF system incubated with GSH could be proven. The fibrils look much alike the fibrils found in the BA-KFKFQF images, especially the ones with H_2O_2 . TAT-SS-Depsi ISA did not show fibril formation.

3.4 Kinetic studies

Further investigations regarding the kinetics of the cleavage were undertaken. Since the peptides with the Depsi ISA sequence were already investigated in previous work of the group only KFKFQF sequences were studied. BA-KFKFQF and TAT-SS-KFKFQF were incubated with H_2O_2 and GSH, respectively, and shaken at room temperature. The trigger concentrations were 10 mM. Semipreparative HPLC was run at different times.

3.4.1 H_2O_2 sensitive Peptides

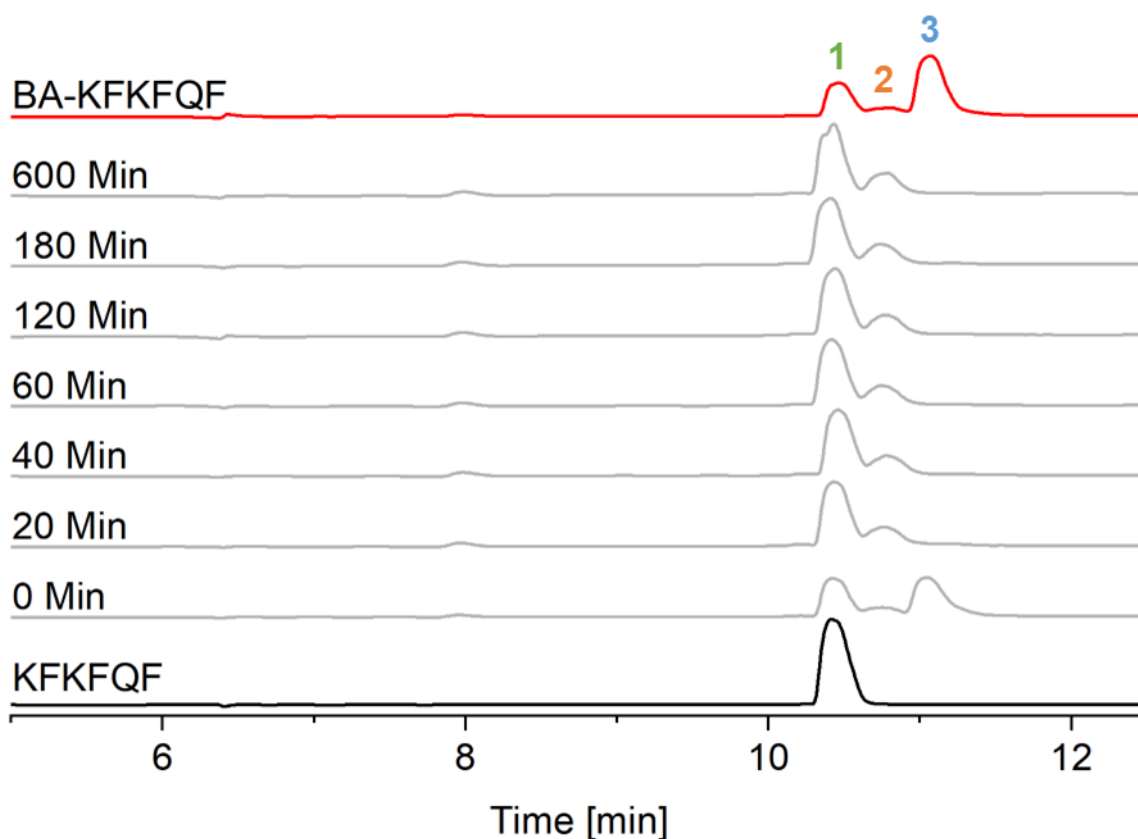


Figure 22: Kinetics of BA-KFKFQF incubated with H_2O_2 (10 mM). Plotted are the chromatograms of semipreparative HPLC measured at 0, 20, 40, 60, 120, 180 and 600 minutes after incubation. Additionally, chromatograms of BA-KFKFQF and KFKFQF are shown.

BA-KFKFQF was incubated without SHA-TAT attached because cleavage of TAT-SHA:BA-KFKFQF is a two-step cleavage and here only the cleavage from the boronic acid linker should be investigated.

To be able to identify the compounds in the different peaks matrix assisted laser desorption ionization - time of flight - mass spectrometry (MALDI-TOF-MS) were measured. According to the spectra shown in **Figure 23** peak 1 is the KFKFQF sequence with a molecular weight of

844 g/mol. This is underlined by the coinciding elution times of peak 1 and the peak in the KFKFQF chromatogram.

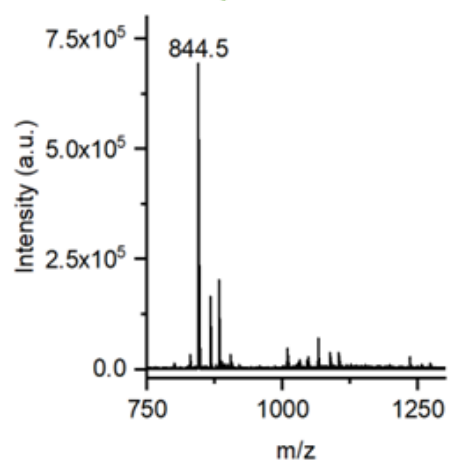
Since cleavage of BA-KFKFQF should only lead to KFKFQF and small molecules, only two peaks were expected: One for BA-KFKFQF that would vanish and one for KFKFQF that would increase. MALDI-TOF-MS spectrum of peak 2 showed an unexpected mass that might reveal a possible side reaction after cleavage. Alongside of the mass of KFKFQF another mass at 950.5 could be observed that corresponds to the mass of KFKFQF-phenol as shown in **Scheme 20**: H₂O₂ induced cleavage of BA-KFKFQF and postulated subsequent side reaction.. A possible explanation for the occurrence of this additional peak could be the reaction of the evolving *p*-quinone methide with an ϵ -amino group of the KFKFQF sequence in a Michael addition. Further characterization would have to be conducted to prove this assumption. Characterization of peak 3 led to the conclusion that it is BA-KFKFQF which makes sense since it vanishes after 20 min.

The chromatogram of BA-KFKFQF already shows the same peaks found in the chromatograms of the cleavage indicating that oxygen in the air is sufficient to induce cleavage.

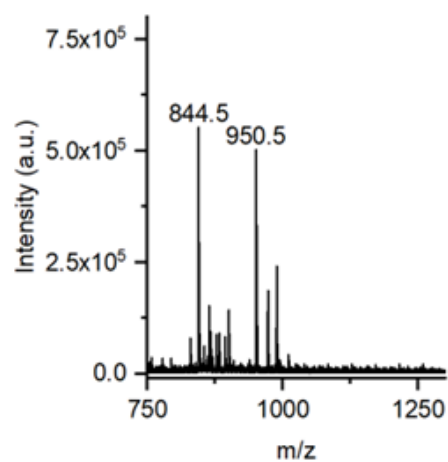
The cleavage of boronic acid linker seems to be very fast, because the peak of BA-KFKFQF disappears already after 20 min. It has to be taken in account though that BA-KFKFQF is obviously not stable at air.

It could be shown that the cleavage from the boronic acid linker works in principle. Yet the system exhibits some disadvantages, like the instability at air and the side reaction upon cleavage.

Peak 1 KFKFQF



Peak 2 KFKFQF and KFKFQF-Phenol



Peak 3 BA-KFKFQF

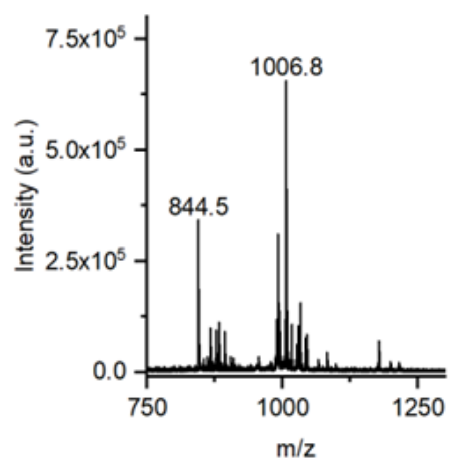
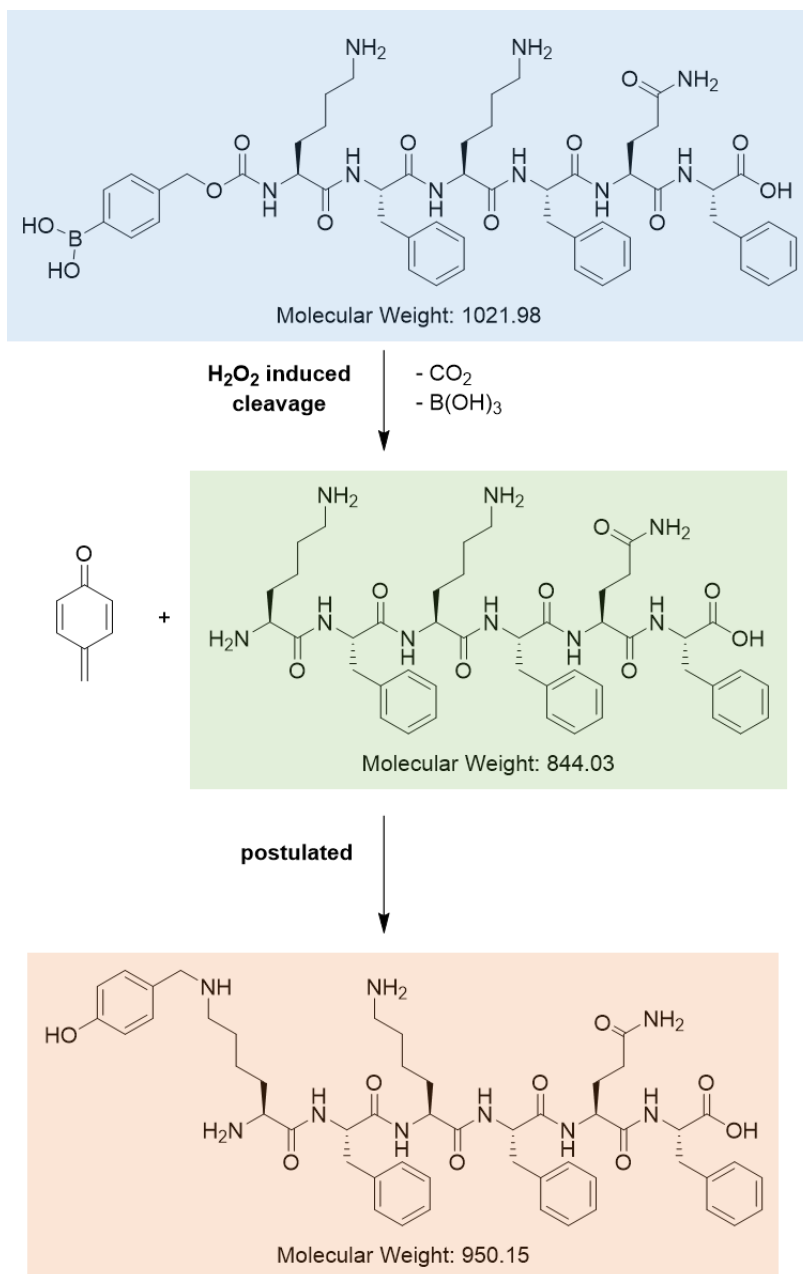


Figure 23: MALDI-TOF spectra of the three peaks found in the kinetic studies of BA-KFKFQF (Figure 22).



Scheme 20: H₂O₂ induced cleavage of BA-KFKFQ and postulated subsequent side reaction. The structures are highlighted matching the peaks in **Figure 22**.

3.4.2 GSH sensitive Peptides

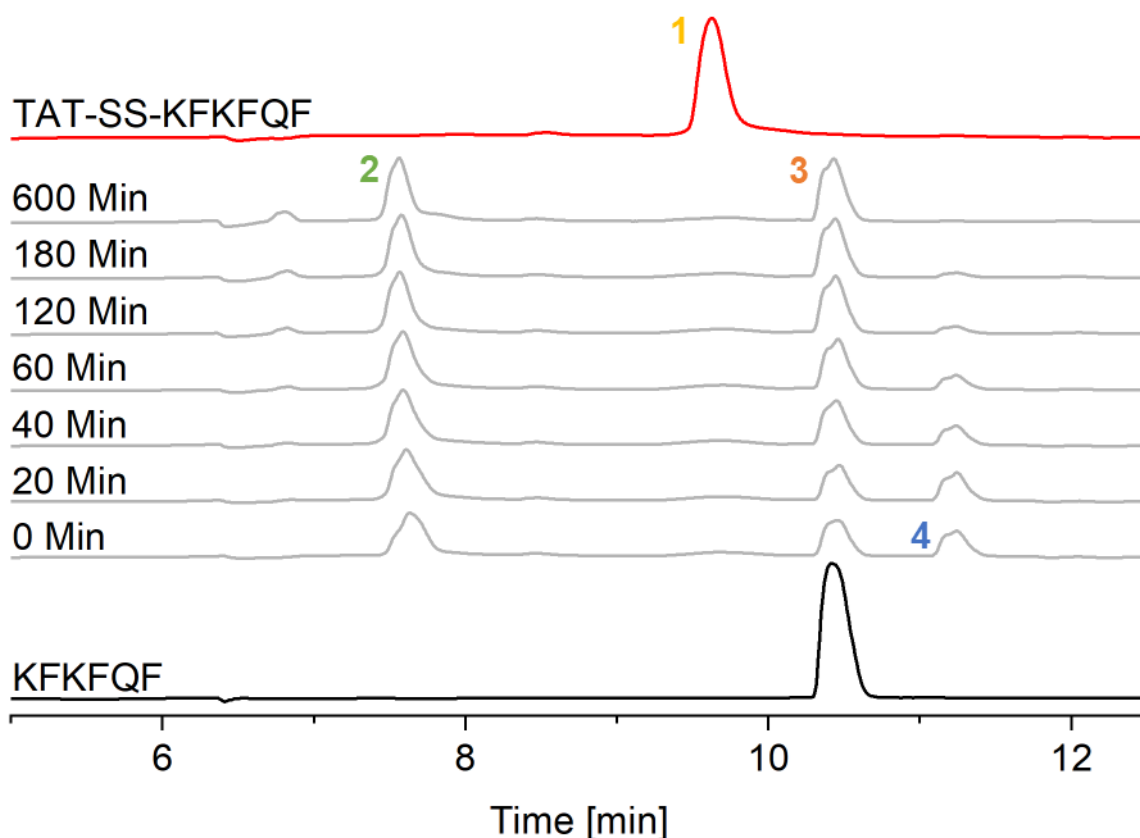


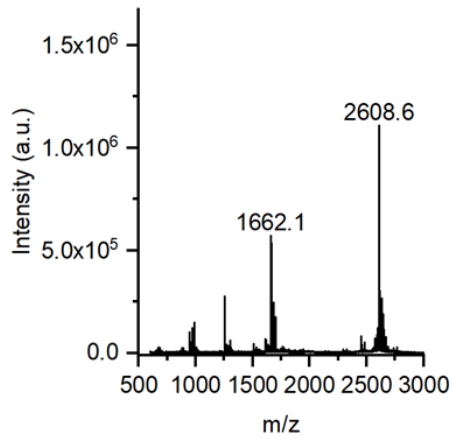
Figure 24: Kinetics of TAT-SS-KFKFQF incubated with GSH (10 mM). Plotted are the chromatograms of semipreparative HPLC measured at 0, 20, 40, 60, 120, 180 and 600 minutes after incubation. Additionally, chromatograms of TAT-SS-KFKFQF and KFKFQF are shown.

Peak 1 is TAT-SS-KFKFQF which was confirmed by the MALDI-TOF-MS spectrum shown in **Figure 25**. The masses found for peak 2 coincide with the masses of Cys-TAT and Cys-TAT GSH. KFKFQF and KFKFQF GSH were found in peak 3. The intermediate KFKFQF with thiol linker as described in **Scheme 21** was found to be peak 4.

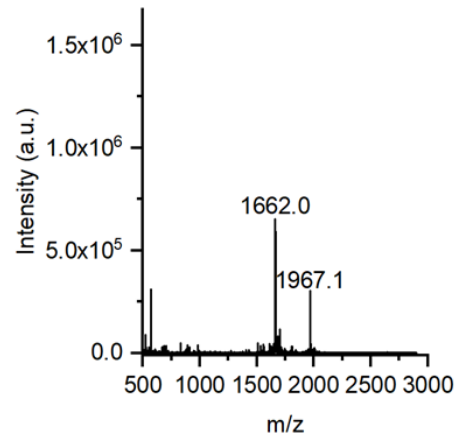
Peak 1 can only be seen in the reference chromatogram of TAT-SS-KFKFQF indicating that cleavage of TAT-SS-KFKFQF starts quickly. Peak 4 however, diminishes slowly and only after 600 min it is completely vanished. Consequently, the conversion from the thiol intermediate to KFKFQF is very slow in comparison to the first step that proceeds nearly immediately.

The successful cleavage of TAT-SS-KFKFQF could be confirmed. Additionally, a fast conversion to the intermediate and a slow conversion to the self-assembling motif, KFKFQF, could be shown.

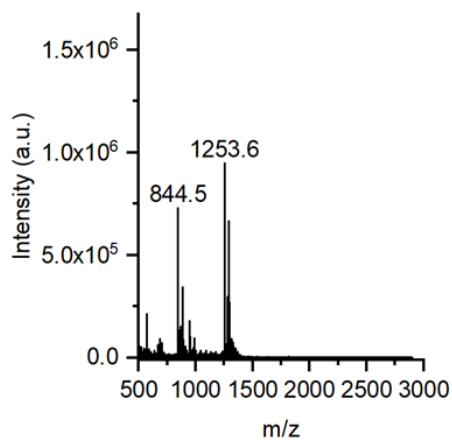
Peak 1 TAT-SS-KFKFQF



Peak 2 Cys-TAT and Cys-TAT GSH



Peak 3 KFKFQF and KFKFQF GSH



Peak 4 KFKFQF with Thiol Linker

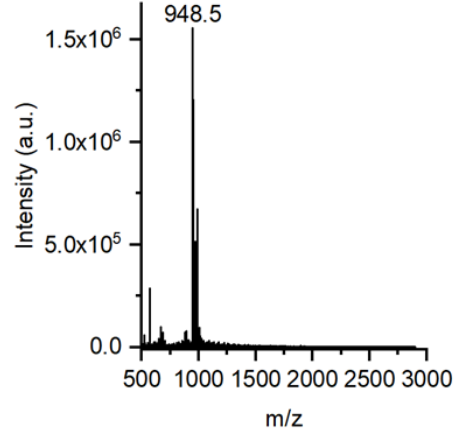
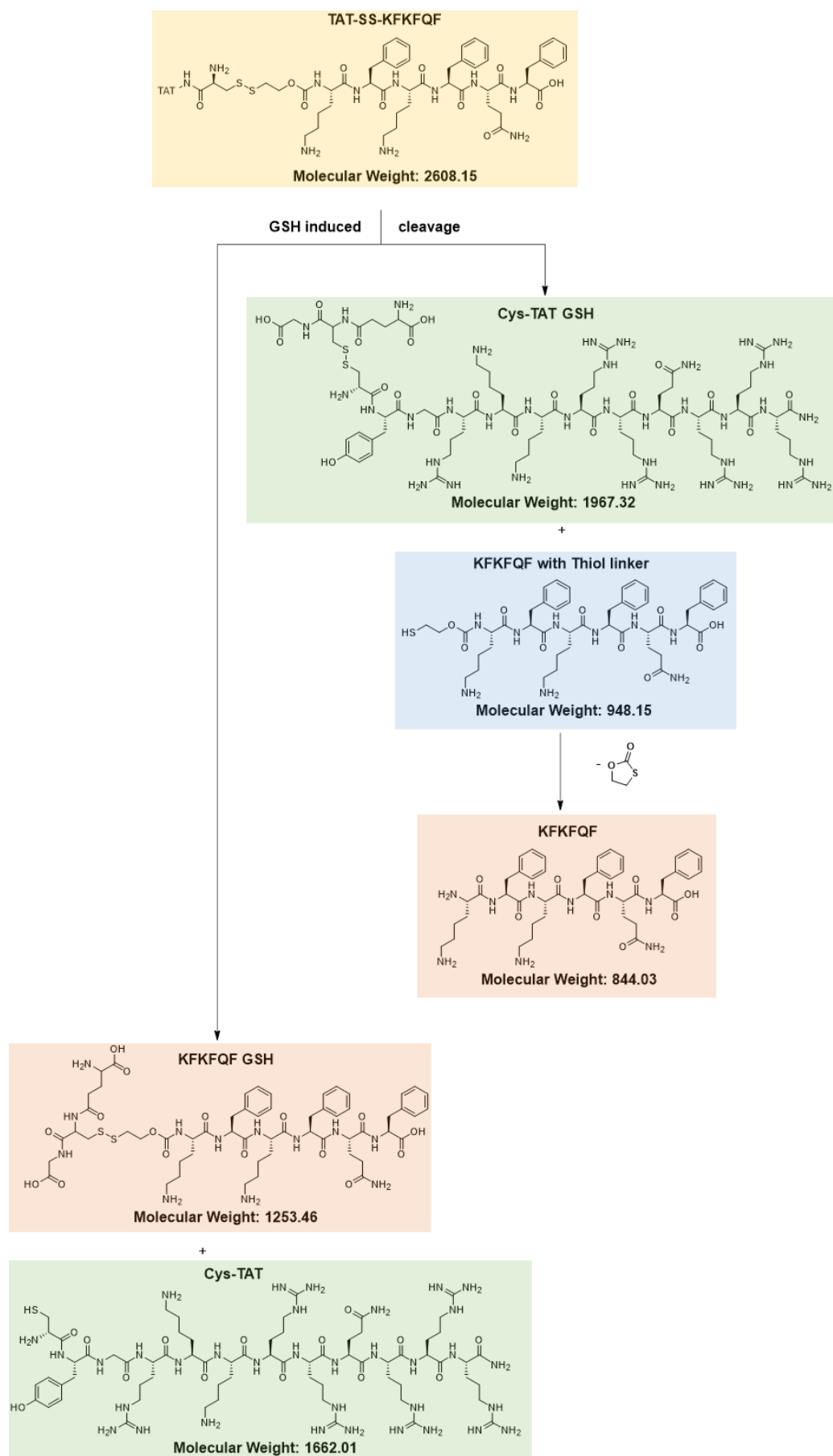


Figure 25: MALDI-TOF spectra of the four peaks found in the kinetic studies of TAT-SS-KFKFQF (Figure 24).



Scheme 21: GSH induced cleavage of TAT-SS-KFKFQF. The structures are highlighted matching the colors of the peaks in **Figure 24**.

4 Experimental Part

4.1 Methods

All chemicals used for synthesis were acquired commercially from *Sigma Aldrich*, *VWR Chemicals*, *Thermo Fisher Scientific*, *Merck*, *Carl Roth*. Before usage no further purification was conducted.

4.1.1 Column Chromatography

For purification via column chromatography Silica 60 M (particle size 0.04 mm to 0.063 mm) from *Macherey-Nagel GmbH & Co. KG* was used as the stationary phase. Cyclohexane and ethyl acetate were used as solvents for the mobile phase. Both were acquired commercially in analytical reagent grade purity. The volume shares (v:v) are stated in chapter 4.2 in the respective paragraphs.

4.1.2 High Performance Liquid Chromatography

The solvents used as mobile phase for HPLC were MQ H₂O and acetonitrile (ACN). HPLC was run under acidic conditions, hence 0.1 vol% TFA were added to the solvents. For sample preparation the peptides were dissolved in these very solvents. The volume shares (v:v) are stated in chapter 4.2 in the respective paragraphs. Before injection the solution was filtered through a syringe filter (CHROMAFIL® Xtra RC-20/13 by *Macherey-Nagel GmbH & Co. KG*, ø 13 mm, 0.2 µm, regenerated cellulose, non-sterile).

Semi-preparative HPLC:

Device by *Shimadzu*: DGU-20A_{5R}, LC-20AP (2x), CBM-20A, SPD-M20A, SIL-10AP, FRC-10A
Column: Agilent ZORBAX Eclipse XDB-C18, 80 Å, 5 µm, 9.4 x 250 mm; Agilent Safety Guard Kit

Flow rate: 4 mL/min

Preparative HPLC:

Device by *Shimadzu*: DGU-20A_{5R}, LC-20AT, CBM-20A, CTO-20AC, SPD-M20A, SIL-20AC, FRC-10A

Column: Phenomenex Gemini® 5 µm NX-C18, 110 Å, 150 x 30 mm; Phenomenex® AJ0-8377 pre-column

Flow rate: 25 mL/min

Table 2: Model gradients for semi-preparative and preparative HPLC.

Semi-preparative HPLC		Preparative HPLC	
<i>t</i> / min	% ACN	<i>t</i> / min	% ACN
0	5	0	0
1	5	5	0
16	100	20	40
18	100	25	100
21	5	27	100
26	5	30	0
		35	0

4.1.3 Kinetic studies

The time dependency of the stimuli (H_2O_2 or GSH) induced cleavage of boronic acid and disulfide linker system was investigated by semipreparative HPLC studies. Peptides were incubated with the designated trigger and HPLC measurements were performed at certain times.

Sample preparation:

A 0.25 mM solution of each peptide was prepared. First, peptides were dissolved in methanol preparing a 0.50 mM solution. Subsequently, the disulfide linker peptides were further diluted (1:1) in 50 mM NH_4HCO_3 buffer containing 10 mM GSH. The boronic acid ester linker peptides were diluted in 10 mM NH_4HCO_3 buffer containing 10 mM H_2O_2 . Samples were shaken at room temperature between injections.

4.1.4 Mass Spectrometry

LC-MS was used to check the reaction progress of peptide synthesis and to analyze the purity of peptides and small molecules. The device used for LC-MS was *Shimadzu LCMS-2020 Single Quadrupole MS* equipped with a *Kinetex® EVO C18* column (2.6 μm , 100 Å) and run with MQ H_2O and ACN each with 0.1 vol% TFA (5 % to 95 % ACN, 20 min).

Reaction progress and characterization, especially of bigger peptides, were performed with MALDI-TOF-MS using a *Waters MALDI SYNAPT G2-Si HDMS*.

4.1.5 Nuclear Magnetic Resonance Spectroscopy

The spectra were measured with *Bruker AvanceNeo 400*. Deuterated solvents (CDCl_3 , CD_2Cl_2 , and DMSO-d_6) were acquired commercially from *Sigma Aldrich* and *Deutero GmbH*. Samples were prepared in a 2 - 5 mg/mL concentration.

4.1.6 Solid Phase Peptide Synthesis

Peptide synthesis was conducted in a microwave equipped *Liberty Blue Automated Peptide Synthesizer* by *CEM*. The peptides were synthesized from C- to N-terminus following the Fmoc SPPS strategy by Merrifield. As activator and activator base DIC and Oxyma were used. A piperidine solution (20 vol% in DMF) was used as deprotection agent and DMF as the general washing agent. Only *L*-amino acids were used. The resins used were Fmoc-Ala-Wang resin (*Novabiochem*®, loading: 0.71 mmol/g, 100 - 200 mesh), Fmoc-Phe-Wang resin (*Novabiochem*®, loading: 0.61 mmol/g, 100 - 200 mesh) and Rink Amide AM resin (*Novabiochem*®, loading: 0.78 mmol/g, 100 - 200 mesh). All concentrations of reagents are shown in **Table 3**.

Table 3: Concentrations of reagents used for automated SPPS.

Reagents	Concentrations in DMF
Fmoc-amino acid	0.2 M
Activator (DIC)	0.5 M
Activator-Base (Oxyma)	1.0 M

General Protocol for SPPS:

Resins were swollen in DMF (3 mL) for 1 h while shaking at room temperature. After the resin was transferred to the reaction vessel of the peptide synthesizer it was swollen in DMF (10 mL) again for 15 s. First, the deprotection of the N-terminal Fmoc-group was conducted by adding a 20 % solution of Piperidine in DMF (3 mL). During the deprotection step the temperature was kept at 75 °C for 15 s and at 90 °C for 50 s. Subsequently, the resin was washed three times with DMF (2 x 2 mL, 1 x 3 mL) each time for 5 s. The following step was the coupling step where the respective amino acid (2.5 mL, 5 eq) and the coupling agents, DIC (1 mL, 5 eq) and Oxyma (0.5 mL, 5 eq), were added. Here the temperature was kept at 75 °C for 15 s and at 90 °C for 110 s. Next was a washing step which is conducted as described before. The last four steps are repeated for every amino acid. Arginine represents an exception because the coupling step was conducted twice. Final deprotection of the Fmoc group was done by adding a 20 % solution of Piperidine in DMF (3mL) once for 5 min and once for 10 min. A final washing step was carried out.

Peptide Modifications on Resin:

For modifications of the peptide on the resin a Merrifield apparatus was used. DMF or dichloromethane (DCM) were used to transfer the resin into the Merrifield apparatus.

Cleavage:

Peptides were cleaved from the resin by adding a cleavage solution (95 % (v:v) TFA, 2.5 % MQ H₂O, 2.5 % TIPS) and shaking the resin for 2 h. Side chain protection groups are cleaved simultaneously.

4.1.7 Thin Layer Chromatography

To check the reaction progress and purity of small molecules TLC was performed. ALUGRAM® Xtra SIL G/UV₂₅₄ plates from *Macherey-Nagel GmbH & Co. KG* were used. Detection at $\lambda = 254$ nm.

4.1.8 Transmission Electron Microscopy

Device: *JEOL 1400*

Sample preparation:

10 mM stocks of all 5 peptides were generated. TAT-SS-Fmoc Depsi ISA, TAT-SS-KFKFQF, BA-Fmoc Depsi ISA and BA-KFKFQF were dissolved in dimethyl sulfoxide (DMSO) and SHA-TAT was dissolved in PBS, pH 7.4.

2 μ L of the disulfide linker peptides were diluted with 18 μ L PBS resulting in a final concentration of 1 mM.

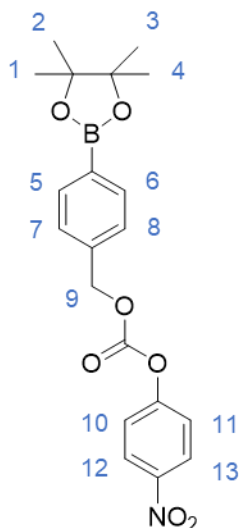
For the boronic acid linker systems 2 μ L of the respective peptide stock were mixed with 2 μ L of the SHA-TAT stock. Further dilution with 16 μ L PBS also led to a final concentration of 1 mM. After addition of the respective trigger (H₂O₂ or GSH). The samples were shaken over night at 37 °C and 400 rpm.

TEM grid preparation:

3 μ L of the sample were pipetted onto the TEM grid (*plano GmbH*, art. No. S162-3, Formvar/coal film on 3.05 mm Cu grids, 300 mesh) and incubated for 5 min. The TEM grid was dried using a lint-free paper towel. Subsequently the grid was placed upside down on a drop of 1 % uranyl acetate. After incubating for 2.5 min the grid was washed three times with water. The TEM grids were dried before measurement.

4.2 Synthesis

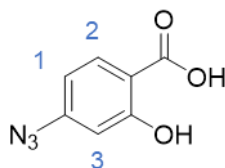
4.2.1 4-Nitrophenyl (4-(4,4,5,5-tetramethyl-1,3,2-dioxaborolan-2-yl)benzyl) carbonate



4-Hydroxymethylphenylboronic acid pinacol ester (1.17 g, 5.00 mmol, 1.00 eq) was dissolved in dry tetrahydrofuran (THF) (15 mL) under nitrogen atmosphere. Triethylamine (TEA) (1.4 mL, 10.1 mmol, 2.02 eq) was added to the solution. The reaction mixture was cooled in an ice-water bath. 4-Nitrophenyl chloroformate (1.14 g, 5.66 mmol, 1.13 eq) was added in portions under nitrogen atmosphere. The reaction mixture was stirred 2.5 h at room temperature. The solvent was removed under reduced pressure. The obtained solid was suspended in ethyl acetate (50 mL). The organic phase was washed with 1 M HCl (50 mL), saturated sodium bicarbonate solution (30 mL) and brine (40 mL). The solvent was removed under reduced pressure. The crude product was purified via column chromatography (4:1 cyclohexane : ethyl acetate) which yielded in 1.27 g (3.18 mmol, 64 %) of colorless crystals.

$^1\text{H NMR}$ (400 MHz, CDCl_3) δ [ppm] = 8.36 – 8.17 (m, 2H; 12, 13), 7.94 – 7.75 (m, 2H; 7, 8), 7.47 – 7.41 (m, 2H; 5, 6), 7.41 – 7.34 (m, 2H; 10, 11), 5.31 (s, 2H; 9), 1.35 (s, 12H; 1, 2, 3, 4).

4.2.2 4-Azidosalicylic acid

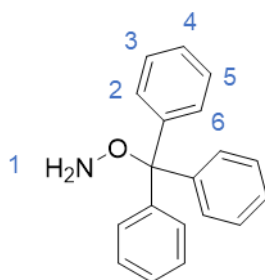


4-Aminosalicylic acid (2.09 g, 13.65 mmol, 1.00 eq) was suspended in a mixture of water (390 mL) and sulfuric acid (65 mL). The grey suspension was cooled in an ice-water bath and

all following steps were performed while cooling, making sure the temperature of the reaction mixture was below 5 °C. A solution of sodium nitrite (1.34 g, 19.42 mmol, 1.42 eq) in water (7.5 mL) was added dropwise and the resulting orange solution was stirred for 1 h. Subsequently, a solution of urea (7.00 g, 116.55 mmol, 8.54 eq) dissolved in water (20 mL) was added dropwise to the reaction mixture. Sodium azide (2.01 g, 30.92 mmol, 2.27 eq) was dissolved in water (10 mL) and added dropwise to the reaction mixture. A yellow suspension was obtained and formation of foam was observed. After complete addition of the sodium azide solution the ice bath was removed and all following steps were performed at room temperature. The reaction mixture was stirred overnight under nitrogen atmosphere. After filtration the crude product was purified by recrystallization from ethanol. Brown crystals with a yield of 1.00 g (5.59 mmol, 41 %) were obtained.

$^1\text{H NMR}$ (400 MHz, DMSO) δ [ppm] = 7.80 (d, J = 8.4 Hz, 1H; 2), 6.76 – 6.59 (m, 2H; 1, 3).

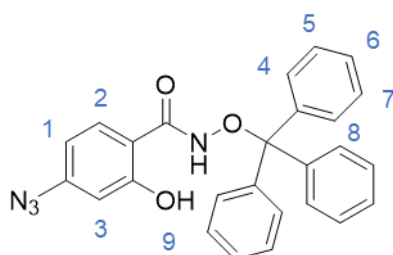
4.2.3 *N*-trityloxyamine



N-trityloxyphthalimide (22.07 g, 54.43 mmol, 1.00 eq) was dissolved in DCM (145 mL). A 64 vol% solution of hydrazine in water (12 mL, 239.49 mmol, 4.40 eq) was diluted with methanol (50 mL). The hydrazine solution was added dropwise while stirring. The reaction mixture was stirred for 45 min. The precipitate was dissolved by adding 5M ammonium hydroxide solution (185 mL). After separating the aqueous and the organic phase the aqueous phase was extracted with DCM (3 x 30 mL). The organic phases were united, washed with brine and dried over sodium sulfate. The solvent was removed under reduced pressure. After recrystallization from methanol 7.86 g (28.55 mmol, 52 %) of colorless crystals were obtained.

$^1\text{H NMR}$ (400 MHz, CD_2Cl_2) δ [ppm] = 7.48 – 7.35 (m, 6H; 3, 5), 7.35 – 7.22 (m, 9H; 2, 6, 4), 4.94 (s, 2H; 1).

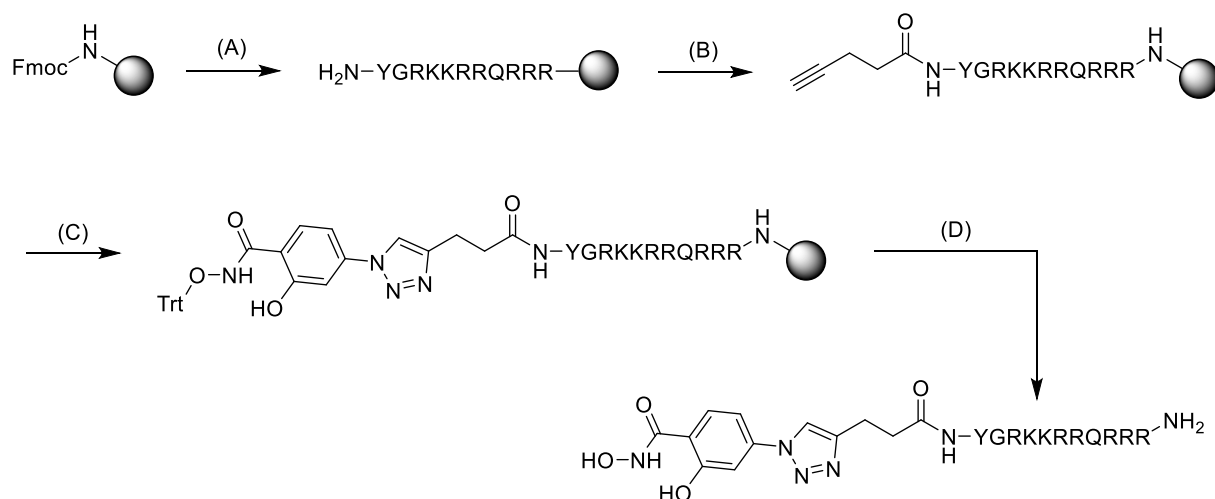
4.2.4 4-Azido-2-hydroxy-*N*-(trityloxy)benzamide



4-Azidosalicylic acid (429 mg, 2.39 mmol, 1.00 eq), trityloxyamine (817 mg, 2.96 mmol, 1.24 eq), HATU (1387 mg, 3.65 mmol, 1.53 eq) and DIPEA (1.6 mL, 9.4 mmol, 4 eq) were dissolved in dry DMF (40 mL). The orange solution was stirred for 96 h under exclusion of light and inert gas atmosphere. The solvent was removed under reduced pressure. The crude product, a brown oil, was purified by column chromatography (8:1 cyclohexane : ethyl acetate). 301 mg (0.69 mmol, 29 %) of a brown oil were yielded.

$^1\text{H NMR}$ (400 MHz, CD_2Cl_2) δ [ppm] = 11.52 (s, 1H; 9), 8.09 (s, 1H; 2), 7.55 – 7.44 (m, 6H; 5, 7), 7.43 – 7.31 (m, 13H; 4, 6, 8), 6.60 – 6.49 (m, 1H; 1), 6.42 – 6.34 (m, 1H; 3).

4.2.5 SHA-TAT



Scheme 22: Synthesis of SHA-TAT: (A) SPPS of TAT sequence, (B) modification of N-terminus with 4-pentynoic acid, (C) CuAAC with SHA, (D) cleavage from resin and deprotection.

(A) SPPS of YGRKKRRQRRR Sequence

The synthesis of YGRKKRRQRRR sequence (0.10 mmol scale), also referred to as TAT, was performed automatically using a peptide synthesizer, as described in 4.1.6. The used reagents are listed in **Table 4**.

Table 4: Reagent usage for SPPS of YGRKKRRQRRR sequence (0.10 mmol scale).

	Mass / g	Volume / mL	DMF / mL
Rink Amide AM resin	0.13	-	-
Fmoc-L-Arg(Pbf)-OH	4.70	-	36
Fmoc-L-Gln(Trt)-OH	0.40	-	3
Fmoc-L-Gly-OH	0.21	-	3
Fmoc-L-Lys(Boc)-OH	0.61	-	6
Fmoc-L-Tyr(<i>t</i> Bu)-OH	0.31	-	3
DIC	1.47	1.80	23
Oxyma	1.88	-	13

(B) Modification of N-Terminus with 4-Pentynoic acid

The resin with the TAT sequence (calculated as 0.10 mmol, 1.00 eq) was transferred into a Merrifield apparatus and washed with dry DMF (3 x 2 mL). A solution of PyBOP (271 mg, 0.52 mmol, 5.20 eq) in dry DMF (2 mL), DIPEA (0.17 mL, 1.00 mol, 10.00 eq) and a solution of 4-pentynoic acid (50 mg, 0.51 mmol, 5.10 eq) in dry DMF (1 mL) were added to the resin. The reaction mixture was shaken for 24 h under nitrogen atmosphere. Subsequently, the fluid components were removed by filtration and the resin was washed with DMF (3 x 5 mL).

(C) CuAAC with SHA

The resin (calculated as 0.10 mmol, 2.00 eq) was washed with DMF (5 mL). SHA (22 mg, 0.05 mmol, 1.00 eq) dissolved in DMF (2 mL), TBTA (103 mg, 0.19 mmol, 3.80 eq) dissolved in DMF (2 mL), sodium ascorbate (40 mg, 0.20 mmol, 4.00 eq) suspended in DMF (2.5 mL) and copper iodide (21 mg, 0.11 mmol, 0.22 eq) suspended in DMF (1.5 mL) were added to the resin. It was shaken overnight under nitrogen atmosphere. Fluid components were removed by filtration. The resin was washed with DMF (2 x 5 mL) and DCM (3 x 5 mL).

(D) Cleavage from Resin and Deprotection

A cleavage solution (95 vol% TFA) was prepared using 99.5 vol% TFA (9.50 mL) and diluting it with MQ H₂O (2.50 % (v:v); 0.25 mL) and TIPS (2.50 % (v:v); 0.25 mL). The cleavage solution was added to the resin (8 mL) and shaken for 2.5 h. The fluid components were removed by filtration and the resin was washed with the cleavage solution (2 mL). To precipitate the peptide the filtrate was added dropwise to ice-cold ether (40 mL). After centrifugation for 15 min at 4000 rpm and 0 °C the ether was removed by decantation and subsequent evaporation. The peptide was purified at HPLC. A colorless powder with a yield of 28 mg (0.02 mmol, 40 %) was obtained.

HRMS (MALDI-TOF-MS, 1833 g/mol) m/z 1833 $[M+H]^+$

LC-MS (ESI-MS, 1833 g/mol) m/z 459 $[M+4H]^{4+}$

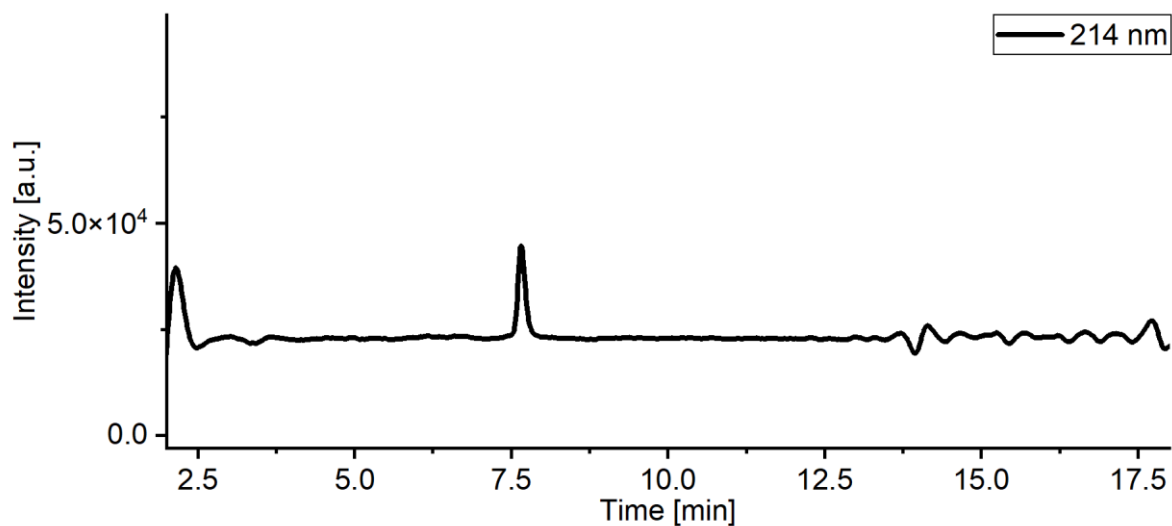
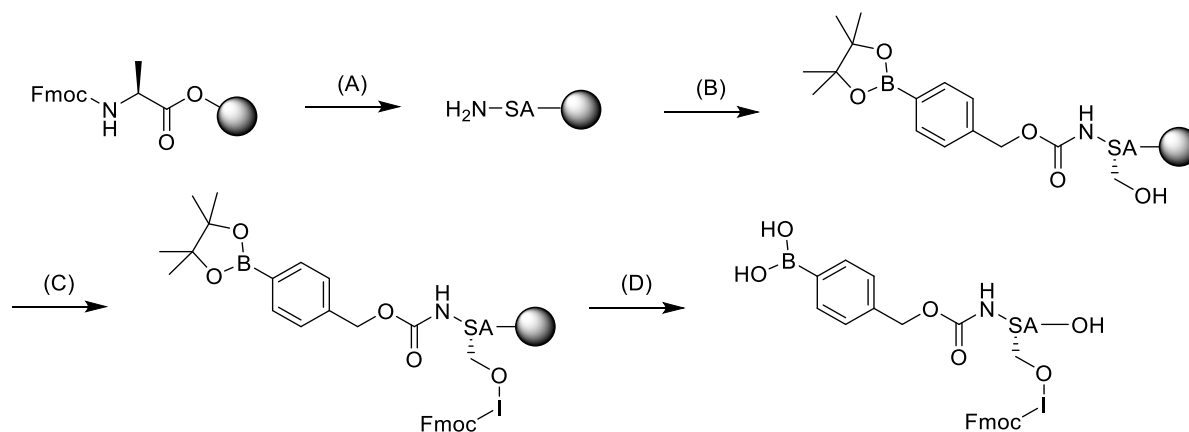


Figure 26: LC-MS chromatogram of SHA-TAT detected at $\lambda = 214$ nm.

4.2.6 BA-Depsi-ISA



Scheme 23: Synthesis of BA-Depsi-ISA: (A) SPPS of SA sequence, (B) modification of N-terminus with boronic acid ester, (C) esterification of serine with isoleucine, (D) cleavage from resin and deprotection.

(A) SPPS of SA Sequence

The synthesis (1.00 mmol scale) was performed automatically using a peptide synthesizer, as described in 4.1.6. The used reagents are listed in **Table 5**.

Table 5: Reagent usage for SPPS of SA sequence (1.00 mmol scale).

	Mass / g	Volume / mL	DMF / mL
Fmoc- <i>L</i> -Ala-Wang resin	1.40	-	-
Fmoc- <i>L</i> -Ser-OH	1.16	-	24
DIC	0.89	1.10	14
Oxyma	1.11	-	8

(B) Modification of N-Terminus with Boronic acid ester

The resin with SA sequence (calculated as 1.00 mmol, 1.00 eq) was transferred into a Merrifield apparatus. 4-Nitrophenyl (4-(4,4,5,5-tetramethyl-1,3,2-dioxaborolan-2-yl) benzyl) carbonate (500 mg, 1.25 mmol, 1.25 eq) was dissolved in dry DMF (5 mL) and added to the resin as well as DIPEA (0.85 mL, 5.00 mmol, 5.00 eq), which was also dissolved in dry DMF (6 mL). The resin was shaken overnight under nitrogen atmosphere. The fluid components were removed by filtration and the resin was washed with DMF (3 x 5 mL).

(C) Esterification of Serine with Isoleucine

Fmoc-*L*-Ile-OH (3.54 g, 10.00 mmol, 10.00 eq) dissolved in dry DMF (5 mL), DMAP (0.13 g, 1.06 mmol, 1.06 eq) dissolved in dry DMF (5 mL) and DIC (0.80 mL, 5.17 mmol, 5.17 eq) were added to the resin (calculated as 1.00 mmol, 1.00 eq) and shaken for 2 h. The fluid components were removed by filtration and fresh coupling reagents were added to the resin. Fmoc-*L*-Ile-OH (3.56 g, 10.07 mmol, 10.07 eq), dissolved in dry DMF (5 mL), DMAP (0.12 g, 0.98 mmol, 0.98 eq), dissolved in dry DMF (5 mL) and DIC (0.80 mL, 5.17 mmol, 5.17 eq) were added. The resin was shaken overnight. The fluid components were removed by filtration. The resin was washed with DMF (3x5 mL) and DCM (3 x 5 mL).

(D) Cleavage from Resin and Deprotection

The cleavage solution (8 mL, see 4.2.5) was added to the resin and shaken for 2 h. The fluid components were removed by filtration into a fresh flask. Remnants of peptides were washed from the resin with the cleavage solution (2 mL) and added to the filtrate. The solvents were removed under reduced pressure. The peptide was purified at HPLC. 1 mg (0.001 mmol, 0.1 %) of a colorless powder were obtained.

HRMS (MALDI-TOF-MS, 689 g/mol) m/z 728 [M+K]⁺, 700 [M-BH₂+Na]⁺

LC-MS (ESI-MS, 689 g/mol) m/z 690 $[M+H]^+$, 688 $[M-H]^-$

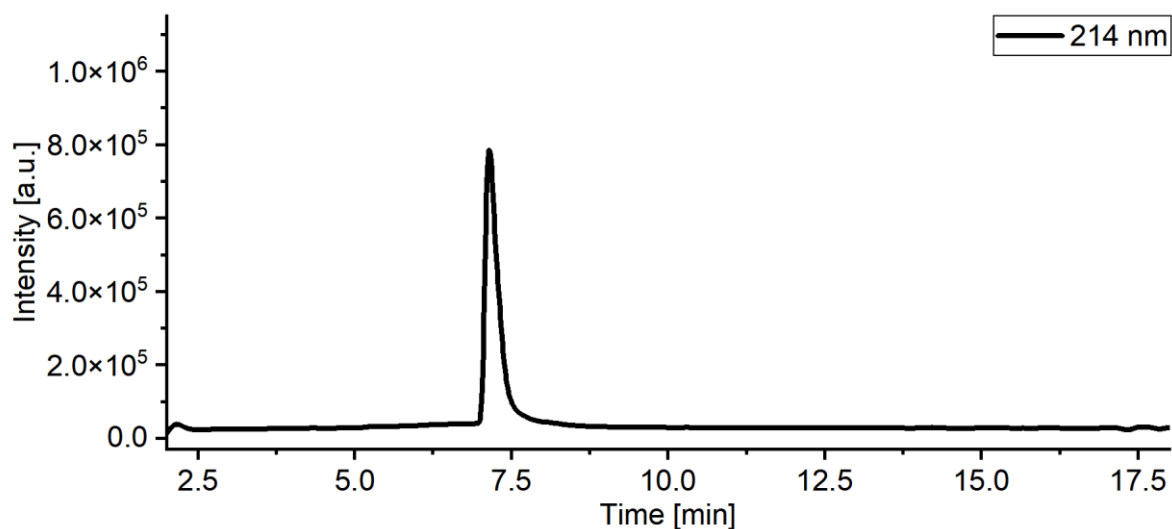
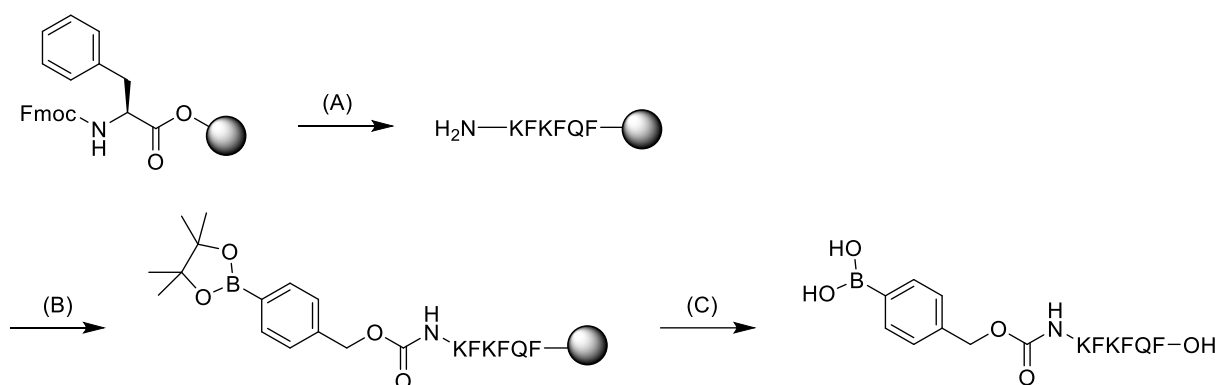


Figure 27: LC-MS chromatogram of BA-Depsi ISA detected at $\lambda = 214$ nm.

4.2.7 BA-KFKFQF



Scheme 24: Synthesis of BA-KFKFQF: (A) SPPS of KFKFQF sequence, (B) modification of N-terminus with boronic acid ester, (C) cleavage from resin and deprotection.

(A) SPPS of KFKFQF Sequence

The peptide synthesis (0.10 mmol scale) was conducted in an automated peptide synthesizer, as described in 4.1.6. The reagent usage is listed in **Table 6**.

Table 6: Reagent usage for SPPS of KFKFQF sequence (0.10 mmol scale).

	Mass / g	Volume / mL	DMF / mL
Fmoc-L-Phe-Wang resin	0.17	-	-
Fmoc-L-Phe-OH	0.48	-	6
Fmoc-L-Lys(Boc)-OH	0.59	-	6
Fmoc-L-Gln(Trt)-OH	0.39	-	3
DIC	0.90	1.10	8
Oxyrna	0.72	-	5

(B) Modification of N-Terminus with Boronic acid ester

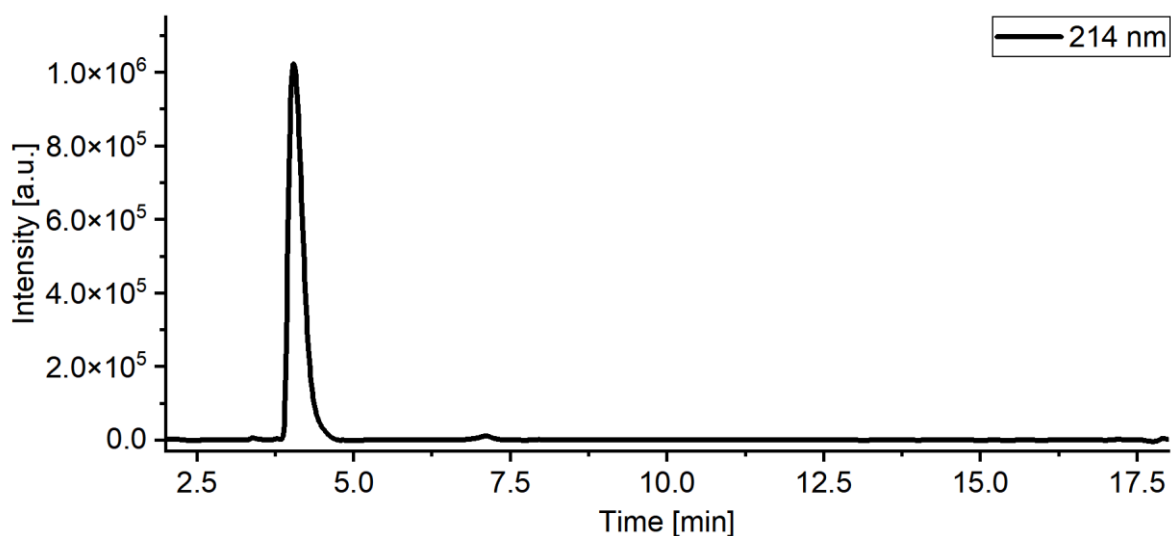
This modification step was conducted like described in 4.2.6 in a 0.10 mmol scale.

(C) Cleavage from Resin and Deprotection

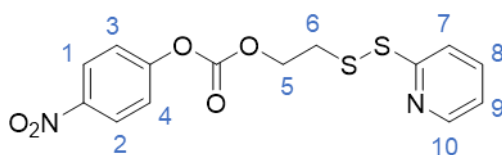
The cleavage was conducted as described before in 4.2.5, but only shaken for 2 h. 86 mg (0.08 mmol, 80 %) of a colorless powder were obtained after purification at HPLC.

HRMS (MALDI-TOF-MS, 1022 g/mol): m/z 1033 [M-BOH+K]⁺, 1017 [M-BOH+Na]⁺, 994 [M-BOH+H]⁺, 845 [M-Boronic acid linker+H]⁺

LC-MS (ESI-MS, 1022 g/mol) m/z 1023 [M+H]⁺, 1005 [M-H₂O+H]⁺, 512 [M+2H]²⁺, 1020 [M-H]⁻

**Figure 28:** LC-MS chromatogram of BA-KFKFQF detected at $\lambda = 214$ nm.

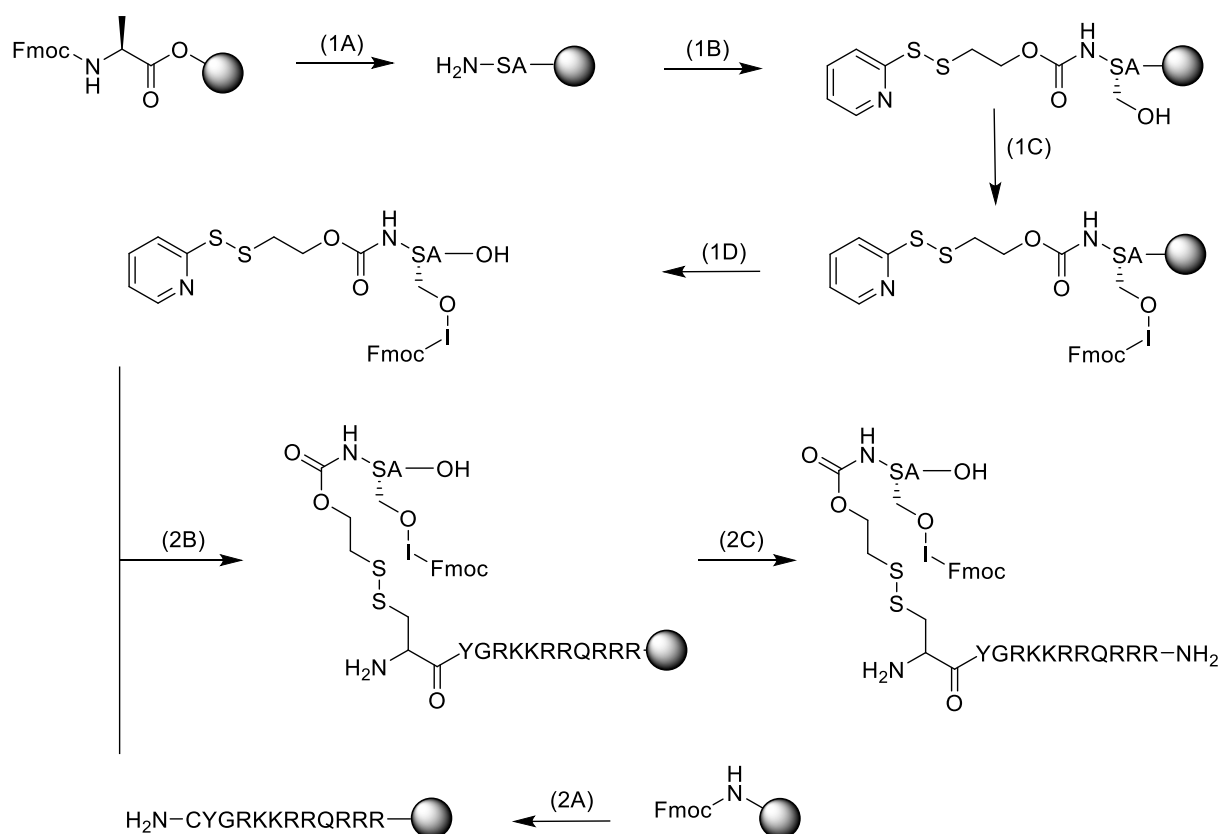
4.2.8 4-Nitrophenyl(2-(pyridine-2-ylsulfaneyl) ethyl) carbonate



4-Nitrochloroformate (5.47 g, 27.14 mmol, 1.50 eq) was dissolved in dry THF (18 mL). The solution was cooled in an ice bath. 2-(Pyridin-2-ylsulfaneyl) ethan-1-ol (3.34 g, 17.83 mmol, 1.00 eq) was dissolved in dry THF (12 mL). TEA (4.5 mL, 32.46 mmol, 1.82 eq) was added to the solution of 2-(pyridine-2-ylsulfaneyl) ethan-1-ol. The mixture was added dropwise to the solution of 4-nitrochloroformate while cooling and stirring. The yellow mixture was stirred over night at room temperature. Ethyl acetate (140 mL) was added. The solution was washed with water (2 x 120 mL) and brine (2 x 100 mL). Each aqueous phase was extracted with ethyl acetate (80 mL). The united organic phases were dried over sodium sulfate, filtrated and the solvent was removed under reduced pressure. The crude product was purified via column chromatography (4:1 cyclohexane : ethyl acetate). A yellow oil was obtained with a yield of 4.74 g (13.45 mmol, 75 %).

¹H NMR (400 MHz, CD₂Cl₂) δ [ppm] = 8.45 (m, *J* = 4.8, 1.8, 1.0 Hz, 1H; 10), 8.27 (m, *J* = 9.2 Hz, 2H; 1, 2), 7.69 (m, *J* = 9.8 Hz, 2H; 8, 9), 7.42 – 7.35 (m, 2H; 3, 4), 7.17 – 7.09 (m, 1H; 7), 4.55 (t, *J* = 6.4 Hz, 2H; 5), 3.16 (t, *J* = 6.4 Hz, 2H; 6)

4.2.9 TAT-SS-Depsi-ISA



Scheme 25: Synthesis of TAT-SS-Depsi-ISA: (1A) SPPS of SA sequence, (1B) modification of N-terminus with 4-nitrophenyl(2-(pyridine-2-yl)disulfaneyl) ethyl carbonate, (1C) esterification of serine with isoleucine, (1D) cleavage from resin and deprotection, (2A) SPPS of Cys-TAT, (2B) disulfide exchange, (2C) cleavage from resin and deprotection.

(1A) SPPS of SA Sequence

The synthesis (0.50 mmol scale) was performed automatically using a peptide synthesizer, as described in 4.1.6. The used reagents are listed in **Table 7**.

Table 7: Reagent usage for SPPS of SA sequence (0.50 mmol scale).

	Mass / g	Volume / mL	DMF / mL
Fmoc- <i>L</i> -Ala-Wang resin	0.71	-	-
Fmoc- <i>L</i> -Ser-OH	0.96	-	12
DIC	0.41	0.50	5
Oxyma	0.79	-	7

(1B) Modification of N-Terminus with 4-Nitrophenyl(2-(pyridine-2-yl)disulfaneyl) ethyl carbonate)

The resin with the SA sequence (calculated as 0.50 mmol, 1.00 eq) was transferred into a Merrifield apparatus and washed with dry DMF (4 mL). 4-Nitrophenyl(2-(pyridine-2-yl)disulfaneyl) ethyl carbonate) (221 mg, 0.63 mmol, 1.26 eq) was dissolved in dry DMF (5 mL). The carbonate and DIPEA (0.45 mL, 2.60 mmol, 5.20 eq) were added to the resin and shaken overnight. The fluid components were separated by filtration. The resin was washed first with DMF (3 x 5 mL).

(1C) Esterification of Serine with Isoleucine

This step was performed like described in 4.2.6 in a 0.50 mmol scale.

(1D) Cleavage from Resin and Deprotection

The cleavage was conducted as described before (see 4.2.6). A yield of 97 mg (0.13 mmol, 26 %) was received after purification at HPLC.

LC-MS (ESI-MS, 724 g/mol) m/z 725 $[M+H]^+$, 1448 $[M-2H]^{2-}$, 723 $[M-H]^-$

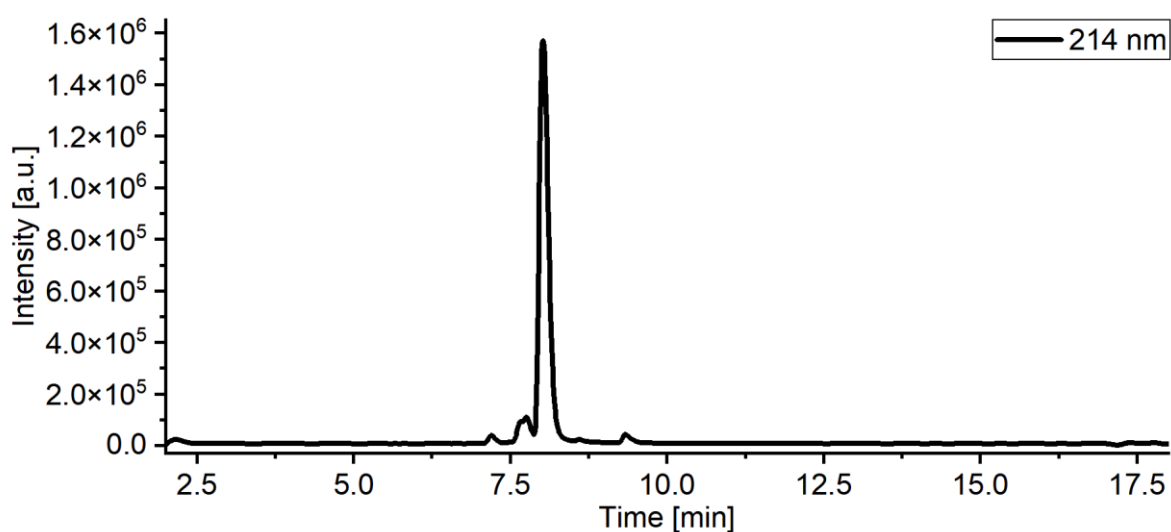


Figure 29: LC-MS chromatogram of (Pyr)-SS-Depsi ISA detected at $\lambda = 214$ nm.

(2A) SPPS of CYGRKKRRQRRR Sequence

The synthesis of CYGRKKRRQRRR sequence (0.10 mmol scale), also referred to as Cys-TAT, was performed automatically using a peptide synthesizer, as described in 4.1.6. The used reagents are listed in **Table 8**.

Table 8: Reagent usage for SPPS of CYGRKKRRQRRR sequence (0.10 mmol scale).

	Mass / g	Volume / mL	DMF / mL
Rink Amide AM resin	0.13	-	-
Fmoc-L-Arg(Pbf)-OH	4.70	-	36
Fmoc-L-Gln(Trt)-OH	0.41	-	3
Fmoc-L-Gly-OH	0.22	-	3
Fmoc-L-Lys(Boc)-OH	0.62	-	6
Fmoc-L-Tyr(<i>t</i> Bu)-OH	0.30	-	3
Fmoc-L-Cys(MMT)-OH	0.37	-	3
DIC	1.55	1.90	24
Oxyrna	1.92	-	13

(2B) Disulfide Exchange

The resin with the Cys-TAT (calculated as 0.10 mmol, 1.00 eq) was transferred into a Merrifield apparatus. The resin was washed with DCM (3 x 5 mL).

First, the MMT protecting group of the cysteine was removed with a MMT deprotection solution (2 % (v:v) TFA, 5 % TIPS, 93 % DCM). The MMT deprotection solution (6 x 5 mL) was added and shaken for 8 min each time. The fluid components were removed by filtration and the resin was washed with DCM (3 x 5 mL) and dry DMF (3 x 2 mL).

(Pyr)-SS-Depsi ISA (97 mg, 0.13 mmol, 1.30 eq) dissolved in dry DMF (4 mL) was added to the resin and shaken for 2 h. The fluid components were separated by filtration and the resin was washed with DMF (3 x 5 mL) and DCM (3 x 5 mL).

(2C) Cleavage from Resin and Deprotection

The cleavage was conducted as described earlier in 4.2.5. A yield of 74 mg (0.03 mmol, 30 %) of a colorless powder was obtained after purification at HPLC.

HRMS (MALDI-TOF-MS, 2276 g/mol): m/z 2298 [M+Na]⁺, 2276 [M+H]⁺

LC-MS (ESI-MS, 2276 g/mol) m/z 1139 $[M+2H]^{2+}$, 759 $[M+3H]^{3+}$

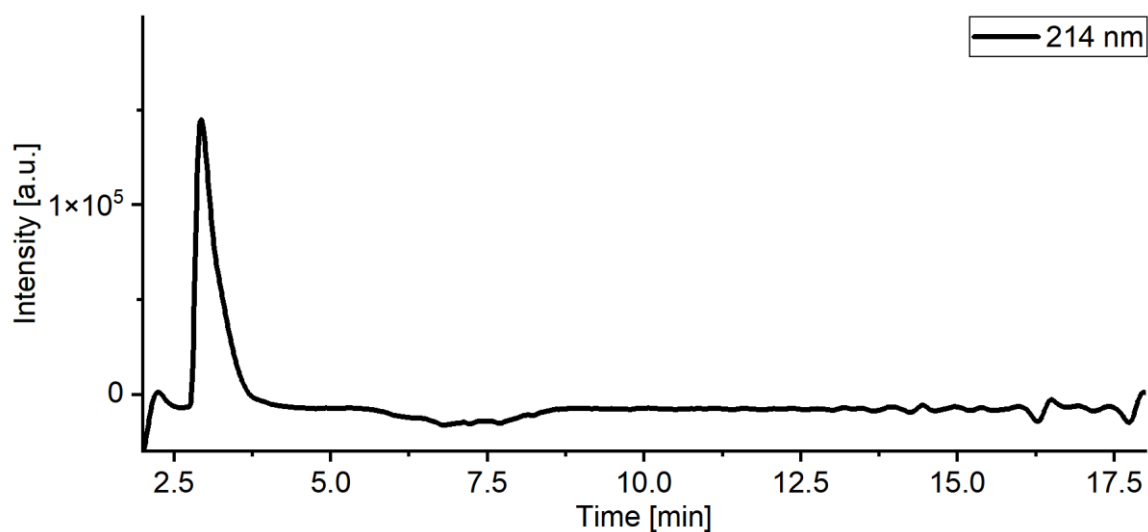
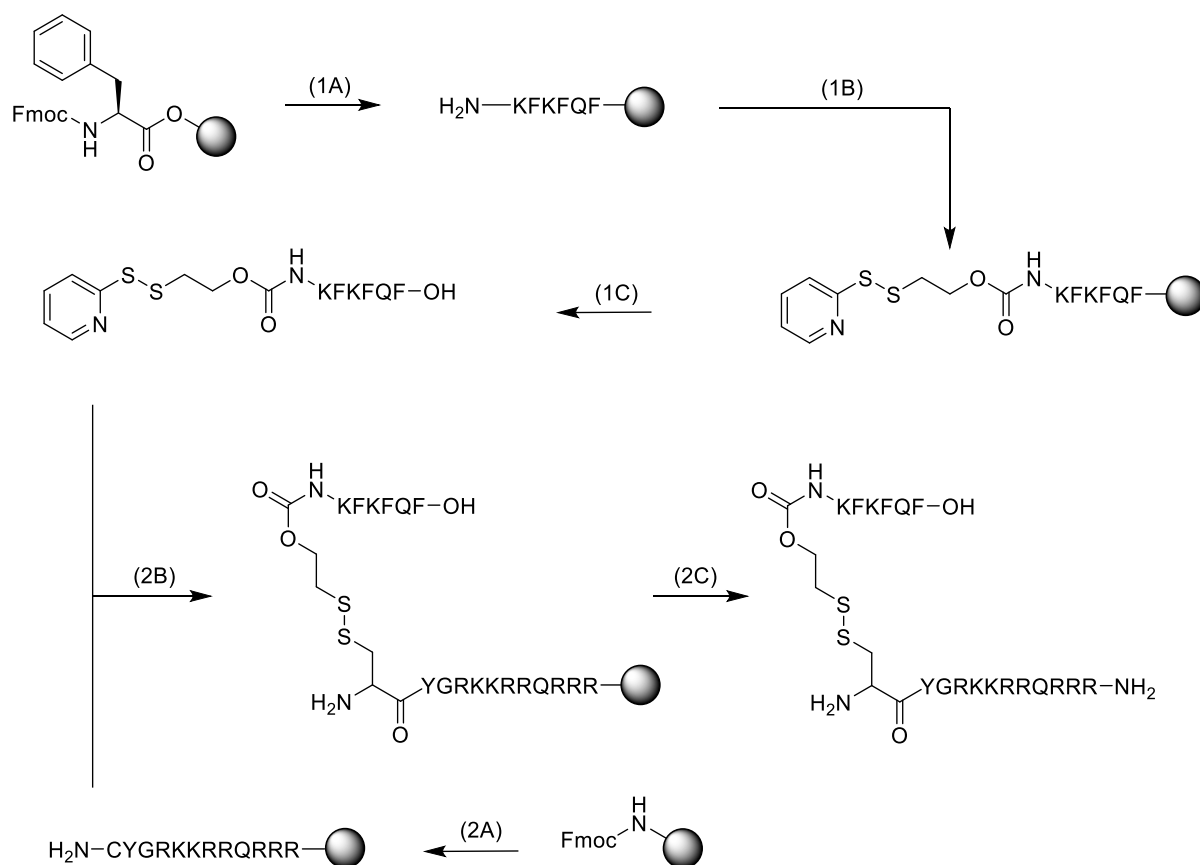


Figure 30: LC-MS chromatogram of TAT-SS-Depsi ISA detected at $\lambda = 214$ nm.

4.2.10 TAT-SS-KFKFQF



Scheme 26: Synthesis of TAT-SS-KFKFQF: (1A) SPPS of KFKFQF sequence, (1B) modification of N-terminus with 4-nitrophenyl(2-(pyridine-2-yl)disulfanyl) ethyl carbonate, (1C) cleavage from resin and deprotection, (2A) SPPS of Cys-TAT, (2B) disulfide exchange, (2C) cleavage from resin and deprotection.

(1A) SPPS of KFKFQF Sequence

The peptide synthesis (0.10 mmol scale) was conducted in an automated peptide synthesizer, as described in 4.1.6. The reagent usage is listed in **Table 9**.

Table 9: Reagent usage for SPPS of KFKFQF sequence (0.10 mmol scale).

	Mass / g	Volume / mL	DMF / mL
Fmoc-L-Phe-Wang resin	0.17	-	-
Fmoc-L-Phe-OH	0.48	-	6
Fmoc-L-Lys(Boc)-OH	0.59	-	6
Fmoc-L-Gln(Trt)-OH	0.39	-	3
DIC	0.90	1.10	8
Oxyma	0.72	-	5

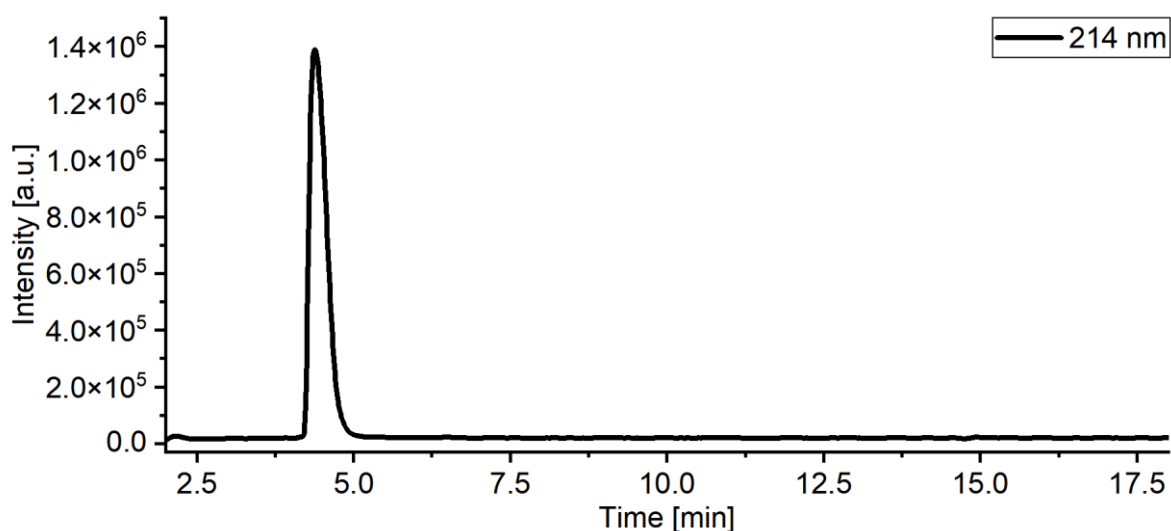
(1B) Modification of N-Terminus with 4-Nitrophenyl(2-(pyridine-2-yl)disulfaneyl) ethyl carbonate)

After the resin with the KFKFQF sequence was transferred into a Merrifield apparatus, the synthesis protocol from 4.2.9 was followed in a 0.10 mmol scale.

(1C) Cleavage from Resin and Deprotection

The cleavage process as described in 4.2.5 was followed, but only shaken for 2 h. A yield of 39 mg (0.04 mmol, 40 %) was received after purification at HPLC.

LC-MS (ESI-MS, 1056 g/mol) m/z 1057 $[M+H]^+$, 529 $[M+2H]^{2+}$, 1055 $[M-H]^-$

**Figure 31:** LC-MS chromatogram of (Pyr)-SS-KFKFQF detected at $\lambda = 214$ nm.

(2A) SPPS of CYGRKKRRQRRR Sequence

The synthesis of CYGRKKRRQRRR sequence (0.10 mmol scale), also referred to as Cys-TAT, was performed automatically using a peptide synthesizer, as described in 4.1.6. The used reagents are listed in **Table 10**.

Table 10: Reagent usage for SPPS of CYGRKKRRQRRR sequence (0.10 mmol scale).

	Mass / g	Volume / mL	DMF / mL
Rink Amide AM resin	0.13	-	-
Fmoc-L-Arg(Pbf)-OH	4.70	-	36
Fmoc-L-Gln(Trt)-OH	0.41	-	3
Fmoc-L-Gly-OH	0.22	-	3
Fmoc-L-Lys(Boc)-OH	0.62	-	6
Fmoc-L-Tyr(<i>t</i> Bu)-OH	0.30	-	3
Fmoc-L-Cys(MMT)-OH	0.37	-	3
DIC	1.55	1.90	24
Oxyma	1.92	-	13

(2B) Disulfide Exchange

The reaction was conducted according to the protocol in 4.2.9. Since only 0.04 mmol of the (Pyr)-SS-KFKFQF were obtained in (1C), the limiting factor in this reaction was not the Cys-TAT (calculated as 0.10 mmol, 2.5 eq) but the (Pyr)-SS-KFKFQF (39 mg, 0.04 mmol, 1.00 eq).

(2C) Cleavage from Resin and Deprotection

The reaction protocol from 4.2.5 was followed. The peptide was obtained as a colorless powder in a yield of 3 mg (0.001 mmol, 2.5 %) after purification at HPLC.

HRMS (MALDI-TOF-MS, 2608 g/mol): m/z 2631 [M+Na]⁺, 2609 [M+H]⁺

LC-MS (ESI-MS, 2608 g/mol) m/z 870 [M+3H]³⁺, 653 [M+4H]⁴⁺, 523 [M+5H]⁵⁺, 436 [M+6H]⁶⁺

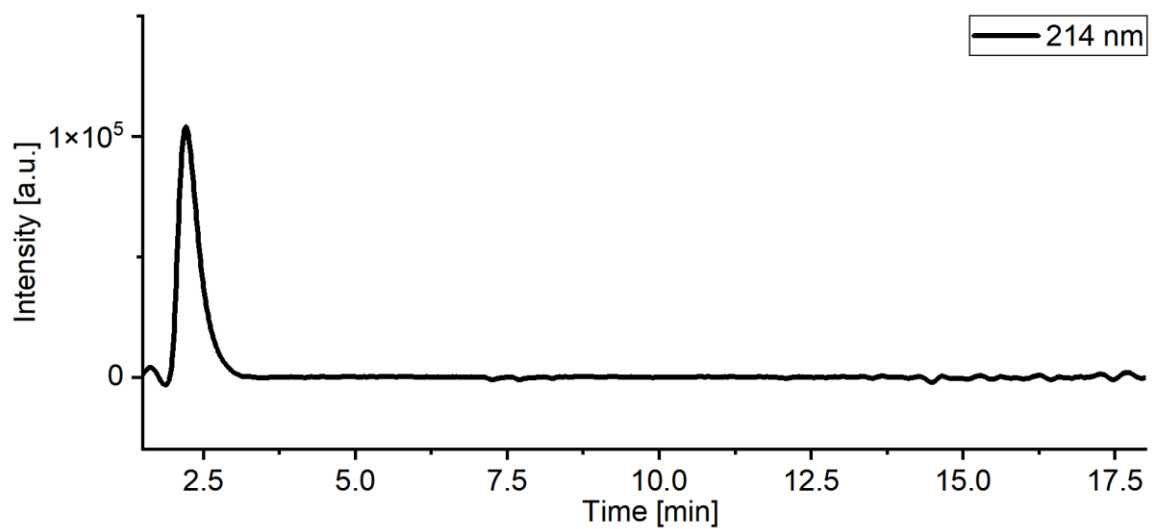


Figure 32: LC-MS chromatogram of TAT-SS-KFKFQF detected at $\lambda = 214$ nm.

5 Summary

The aim of the project was to synthesize different peptides and analyze their ability to self-assemble in a controllable manner induced by conditions found inside cancer cells. These four peptides consist of three domains: A cell penetrating TAT sequence, a responsive linker and a self-assembling motif. Two different linkers were used: The boronic acid linker adapted from Pieszka *et al.* [7,8] that is cleaved by H₂O₂ and the disulfide linker adapted from S. Chagri that is responsive to GSH. As self-assembling sequences Fmoc ISA and KFKFQF were used. After a pH-dependent *O,N*-acyl shift of the cleaved pro-assembling motif Depsi-Fmoc ISA the linear Fmoc ISA can self-assemble due to π - π -stacking of the Fmoc-moiety. KFKFQF can form amyloids after cleavage. The impact of the linker and the self-assembling sequence on the formation of fibrils was investigated by taking TEM pictures and measuring the kinetics of the cleavage.

First the linkers were synthesized. For the boronic acid linker systems two small molecules had to be synthesized: The boronic acid linker itself and SHA to connect the linker and the self-assembling group with the TAT sequence. The synthesis of the boronic acid linker was a one-step synthesis that led to a yield (64 %) comparable to those in literature [7]. The synthesis of SHA involved three steps. After changing the followed protocol from Pieszka *et al.* [7,8] to Ríos-Malvárez *et al.* [32] 4-azidosalicylic acid was obtained in an acceptable yield. Synthesis of *N*-trityloxyamine was successful. For synthesis of 4-azido-2-hydroxy-*N*-(trityloxy) benzamide different coupling agent combinations were tested. HATU/DIPEA was found to be the best one. The disulfide linker was successfully prepared in a one-step synthesis yielding 75 %.

The peptides were synthesized in an automated peptide synthesizer. The TAT sequences and the respective self-assembling sequences were synthesized separately. Modification of the peptides was conducted outside of the peptide synthesizer in a Merrifield apparatus. The TAT sequence and the self-assembling sequence of the boronic acid linker peptide systems were purified separately because of the dynamic bonds of the boronic acid ester. Overall, the peptide synthesis was successful, only purification of TAT-SS-KFKFQF via HPLC led to bigger challenges probably leading to lower yields. The yield of BA-Depsi ISA does not permit evaluation because not all crude product could be purified within the given time frame.

The morphology of the peptides was studied by recording TEM images of 1 mM samples of TAT-SHA:BA-Depsi ISA, TAT-SHA:BA-KFKFQF, TAT-SS-Depsi ISA and TAT-SS-KFKFQF incubated with and without the respective triggers, H₂O₂ and GSH, for 24 h at 37 °C. Except for TAT-SS-Depsi ISA all samples with trigger exhibited fibrils. The cleavage of boronic acid

esters includes two steps. To investigate if the cleavage from the boronic acid linker and not from TAT is the reason to induce self-assembly TEM images of BA-Depsi ISA and BA-KFKFQF under the same conditions as before were taken. It could be shown that BA-Depsi ISA only fibrillates after cleavage from boronic acid linker. BA-KFKFQF, however, showed fibrils in the samples with and without trigger. Thus, fibrillation of KFKFQF is not triggered upon cleavage of boronic acid linker supporting the assumption that TAT is the reason for inhibition of self-assembly in case of the KFKFQF motifs.

Kinetic studies were conducted only for the KFKFQF sequences since Depsi-ISA sequences were previously studied by Pieszka *et al.* [7,8] and S. Chagri. In case of the boronic acid linker system only BA-KFKFQF without the TAT sequence was used to be able to investigate the cleavage from the boronic acid linker. Results showed that the cleavage proceeded very fast. Though it must be mentioned that BA-KFKFQF was not stable at air. Therefore, it was already partly being cleaved. Furthermore, an unwanted side reaction occurs upon cleavage. Kinetic studies of TAT-SS-KFKFQF showed that the first step of this cleavage mechanism is very fast and the second one is very slow.

All in all, TAT-SHA:BA-Depsi ISA and TAT-SS-KFKFQF proved to work well since only desired fibril formation was observed. TAT-SHA:BA-KFKFQF and TAT-SS-Depsi ISA, however, resulted to be deficient. TAT-SHA:BA-KFKFQF showed fibril formation that was independent of the trigger. Furthermore, kinetic studies showed that the BA-KFKFQF was not stable at air and a side reaction upon cleavage that might interfere with the self-assembly mechanism occurred. TAT-SS-Depsi ISA showed no fibrillation at all.

Since TAT-SS-KFKFQF seems to be a very promising system that is not yet as explored as TAT-SHA:BA-Depsi ISA further measurements could lead to a deeper understanding of the underlying mechanism of self-assembly. Structural analyses with circular dichroism measurements or experiments regarding the critical fibrillation concentration by recording TEM at different concentrations would provide further information about the self-assembly behavior of the system. To investigate the efficacy of the system for therapeutical applications cell studies testing the cytotoxicity or the impact on the cell metabolism could be conducted.

6 Zusammenfassung

Das Ziel des Projekts war es verschiedene Peptide zu synthetisieren und ihre Fähigkeit unter bestimmten Bedingungen, die in Krebszellen vorgefunden werden können, zu analysieren. Diese vier Peptide sind aus drei Domänen aufgebaut: Eine zellpenetrierende TAT Sequenz, ein responsiver Linker und eine selbst-assemblierende Motiv. Zwei verschiedene Linker wurden verwendet: Der Boronsäure Linker von Pieszka *et al.* [7,8], der durch H_2O_2 gespalten wird und der Disulfid Linker von S. Chagri, der durch GSH gespalten wird. Als selbst-assemblierende Sequenzen wurden Fmoc ISA und KFKFQF verwendet. Nach einem pH-abhängigen *O,N*-acyl shift des abgespaltenen Depsi-Fmoc ISA kann das lineare Fmoc-ISA durch π - π -stacking des Fmoc Rests selbst-assemblieren. KFKFQF kann nach der Abspaltung des Boronsäure Linkers Amyloid Strukturen ausbilden. Die Auswirkungen des Linkers und der selbst-assemblierenden Sequenz auf die Bildung von Fibrillen wurde durch die Aufnahme von TEM Bildern und durch die Messung der Kinetik der Spaltung untersucht.

Zuerst wurden die Linker synthetisiert. Für die Boronsäure Linker Systeme mussten zwei kleine Moleküle hergestellt werden: Der Boronsäure Linker selbst und SHA um den Linker und die selbst-assemblierende Gruppe mit der TAT Sequenz zu verbinden. Die einstufige Synthese des Boronsäure Linkers führte zu einer Ausbeute (64 %), die vergleichbar zu der in der Literatur [7] ist. Die SHA Synthese besteht aus drei Stufen. Nachdem die Vorschrift geändert wurde, wurde 4-Azidosalicylsäure in einer akzeptablen Ausbeute erhalten. *N*-Trityloxyamin konnte erfolgreich synthetisiert werden. Für die Synthese von 4-Azido-2-hydroxy-*N*-trityloxybenzamid wurden verschiedene Kupplungsreagenzien getestet. Dabei hat sic HATU/DIPEA als beste Kombination erwiesen. Der Disulfid Linker wurde in einer einstufigen Synthese mit 75 % Ausbeute erfolgreich hergestellt.

Die Peptide wurden in einem automatischen Peptid-Synthesizer synthetisiert. Die TAT Sequenzen und die jeweiligen selbst-assemblierenden Sequenzen wurden separat hergestellt. Modifikationen der Peptide wurden außerhalb des Peptid-Synthesizers in einer Merrifield Apparatur durchgeführt. Die TAT Sequenz und die selbst-assemblierenden Sequenzen mit dem Boronsäure Linker wurden, wegen der dynamischen Bindungen des Boronsäureesters, separat aufgereinigt. Insgesamt war die Peptidsynthese erfolgreich, nur bei der Aufreinigung von TAT-SS-KFKFQF kam es zu Schwierigkeiten, was zu niedrigen Ausbeuten führte. Die Ausbeuten von BA-Depsi ISA können nicht bewertet werden, da die Aufreinigung sehr zeitaufwändig war und im Rahmen dieser Arbeit nicht das gesamte Rohprodukt aufgereinigt werden konnte.

Die Morphologie der Peptide wurde durch die Aufnahme von TEM Bildern von 1 mM Proben von TAT-SHA:BA-Depsi ISA, TAT-SHA:BA-KFKFQF, TAT-SS-Depsi ISA und TAT-SS-KFKFQF inkubiert mit und ohne die jeweiligen Trigger, H₂O₂ und GSH, für 24 h bei 37 °C. Alle Proben außer TAT-SS-Depsi ISA wiesen Fibrillen Bildung auf. Die Spaltung der Boronsäure Systeme beinhaltet zwei Stufen. Um zu untersuchen, ob die Abspaltung des Boronsäure Linkers und nicht die Abspaltung von TAT der Grund für die Selbstassemblierung ist, wurden TEM-Bilder von BA-Depsi ISA und BA-KFKFQF unter denselben Bedingungen wie zuvor beschrieben aufgenommen. Es konnte gezeigt werden, dass BA-Depsi ISA nur nach der Abspaltung des Boronsäure Linkers fibrilliert. BA-KFKFQF jedoch wies Fibrillen in den Proben mit und ohne Trigger auf. Demnach wird die Fibrillen Bildung nicht durch die Abspaltung des Boronsäure Linkers ausgelöst. Dies unterstützt die Annahme, dass in den Fällen der KFKFQF Sequenzen TAT die Selbstassemblierung inhibiert.

Untersuchungen zur Kinetik wurden nur für die KFKFQF Sequenzen durchgeführt, da diese für die Depsi-ISA Sequenzen von Pieszka *et al.* [7,8] und S. Chagri schon durchgeführt wurden. Im Fall des Boronsäure Linker Systems wurde die BA-KFKFQF Sequenz ohne TAT untersucht, um nur die Abspaltung des Boronsäure Linkers untersuchen zu können. Die Ergebnisse zeigten, dass die Abspaltung sehr schnell verläuft. Allerdings muss erwähnt werden, dass BA-KFKFQF an der Luft nicht stabil ist und deshalb zum Teil schon gespalten war. Außerdem tritt eine ungewünschte Nebenreaktion nach der Abspaltung auf. Die kinetischen Untersuchungen von TAT-SS-KFKFQF zeigten, dass der erste Schritt dieses Abspaltungsmechanismus sehr schnell verläuft, der zweite allerdings nur sehr langsam.

Alles in Allem erwiesen sich TAT-SHA:BA-Depsi ISA und TAT-SS-KFKFQF als gut, da nur gewünschte Fibrillen Bildung auftrat. TAT-SHA:BA-KFKFQF und TAT-SS-Depsi ISA jedoch waren mangelhaft. TAT-SHA:BA-KFKFQF wies Fibrillen Bildung unabhängig vom Trigger auf. Außerdem zeigten die kinetischen Untersuchungen, das BA-KFKFQF an der Luft nicht stabil ist und eine Nebenreaktion nach der Spaltung auftritt. TAT-SS-Depsi ISA zeigte überhaupt keine Fibrillen.

Da die Ergebnisse des TAT-SS-KFKFQF Systems sehr vielversprechend aussahen, könnten weitere Messungen zu einem tieferen Verständnis des zugrundeliegenden Mechanismus der Selbst-Assemblierung führen. Strukturelle Analysen durch Circular dichroismus Messungen oder Experimente zur kritischen Fibrillierungskonzentration durch Aufnahmen von TEM Bildern von Proben mit verschiedenen Konzentrationen geben Aufschluss über das Verhalten der Selbstassemblierung. Um die Effizienz des Systems für therapeutische Zwecke zu

untersuchen, könnten Zellversuche, die die Zytotoxizität oder die Auswirkungen auf den Zellmetabolismus testen, durchgeführt werden.



Acknowledgements

First of all, I would like to thank Prof. Dr. Tanja Weil for the opportunity to write this thesis in her group Synthesis of Macromolecules at the Max Planck Institute for Polymer Research. Great thanks to Dr. David Ng for giving me the chance to work in his wonderful subgroup Synthetic Life-like Systems. Furthermore, I would like to thank Prof. Dr. Andreas Walther for doing the second revision of this thesis.

Special thanks go out to my supervisor Konrad Maxeiner who made sure I had a pleasant and enlightening time. Thank you for the intensive supervision, advice and help, the answers to all my questions and for showing me all those new techniques.

I would like to thank Dr. Zhixuan Zhou for advice and all the LC-MS measurements he did on my behalf. I would also like to thank Patrick Roth for measuring TEM.

Thanks to everyone for welcoming me so kindly at the Max Planck Institute for Polymer Research. I am particularly thankful to the subgroup of Dr. David Ng for making this time so enjoyable and memorable.

Finally, I want to thank my family and friends for their support and love.

References

- [1] Berg JM, Tymoczko JL, Gatto GJ, Stryer L. Stryer Biochemie. 8th ed. Berlin, Heidelberg: Springer Berlin Heidelberg; 2018.
- [2] Makin OS, Serpell LC. Structures for amyloid fibrils. *The FEBS journal* 2005;272(23):5950–61.
- [3] Assemblies of Peptides in a Complex Environment and their Applications.
- [4] Bershadsky A, Vasiliev J. Cytoskeleton. New York, NY: Springer; 1988.
- [5] Chagri S, Ng DYW, Weil T. Designing bioresponsive nanomaterials for intracellular self-assembly. *Nature reviews. Chemistry* 2022;6(5):320–38.
- [6] Ulijn RV, Smith AM. Designing peptide based nanomaterials. *Chemical Society reviews* 2008;37(4):664–75.
- [7] Pieszka M, Sobota AM, Gačanin J, Weil T, Ng DYW. Orthogonally Stimulated Assembly/Disassembly of Depsipeptides by Rational Chemical Design. *Chembiochem a European journal of chemical biology* 2019;20(11):1376–81.
- [8] Pieszka M, Han S, Volkmann C, Graf R, Lieberwirth I, Landfester K et al. Controlled Supramolecular Assembly Inside Living Cells by Sequential Multistaged Chemical Reactions. *Journal of the American Chemical Society* 2020;142(37):15780–9.
- [9] Skakuj K, Wang S, Qin L, Lee A, Zhang B, Mirkin CA. Conjugation Chemistry-Dependent T-Cell Activation with Spherical Nucleic Acids. *Journal of the American Chemical Society* 2018;140(4):1227–30.
- [10] Sieste S, Mack T, Lump E, Hayn M, Schütz D, Röcker A et al. Supramolecular Peptide Nanofibrils with Optimized Sequences and Molecular Structures for Efficient Retroviral Transduction. *Adv. Funct. Mater.* 2021;31(17):2009382.
- [11] Frankel AD, Pabo CO. Cellular uptake of the tat protein from human immunodeficiency virus. *Cell* 1988;55(6):1189–93.
- [12] Aliashkevich A, Alvarez L, Cava F. New Insights Into the Mechanisms and Biological Roles of D-Amino Acids in Complex Eco-Systems. *Frontiers in microbiology* 2018;9:683.
- [13] Voet D, Voet JG, Pratt CW. Principles of biochemistry: International student version. 4th ed. Hoboken, N.J.: Wiley; 2012.
- [14] Woolfson DN. The Design of Coiled-Coil Structures and Assemblies. In: Parry DAD, Squire J, editors. *Fibrous proteins: Coiled-coils, collagen and elastomers*. Amsterdam, Boston: Elsevier; 2005, p. 79–112.
- [15] Jakubke HD:JH. Aminosäuren, Peptide, Proteine. Weinheim: Verlag Chemie; 1982.
- [16] Jensen KJ, Tofteng Shelton P, Pedersen SL. Peptide Synthesis and Applications. Totowa, NJ: Humana Press; 2013.

- [17] Hegarty AF, McCormack MT, Brady K, Ferguson G, Roberts PJ. Competing acyl transfer and intramolecular O → N acyl group migration from an isolable O-acylisourea. *J. Chem. Soc., Perkin Trans. 2* 1980(6):867.
- [18] Subirós-Funosas R, Prohens R, Barbas R, El-Faham A, Albericio F. Oxyma: an efficient additive for peptide synthesis to replace the benzotriazole-based HOBt and HOAt with a lower risk of explosion. *Chemistry (Weinheim an der Bergstrasse, Germany)* 2009;15(37):9394–403.
- [19] NobelPrize.org. The Nobel Prize in Chemistry 2022. [November 04, 2022]; Available from: <https://www.nobelprize.org/prizes/chemistry/2022/press-release/>.
- [20] Tang W, Becker ML. "Click" reactions: a versatile toolbox for the synthesis of peptide-conjugates. *Chemical Society reviews* 2014;43(20):7013–39.
- [21] Prescher JA, Bertozzi CR. Chemistry in living systems. *Nature chemical biology* 2005;1(1):13–21.
- [22] Rostovtsev VV, Green LG, Fokin VV, Sharpless KB. A Stepwise Huisgen Cycloaddition Process: Copper(I)-Catalyzed Regioselective "Ligation" of Azides and Terminal Alkynes. *Angew. Chem. Int. Ed.* 2002;41(14):2596–9.
- [23] Brse S, Banert K. *Organic azides: Syntheses and applications*. Chichester, West Sussex, U.K.: John Wiley; 2010.
- [24] Worrell BT, Malik JA, Fokin VV. Direct evidence of a dinuclear copper intermediate in Cu(I)-catalyzed azide-alkyne cycloadditions. *Science (New York, N.Y.)* 2013;340(6131):457–60.
- [25] Click Chemistry. [November 01, 2022]; Available from: <https://www.organic-chemistry.org/namedreactions/click-chemistry.shtm>.
- [26] Vivès E, Brodin P, Lebleu B. A truncated HIV-1 Tat protein basic domain rapidly translocates through the plasma membrane and accumulates in the cell nucleus. *The Journal of biological chemistry* 1997;272(25):16010–7.
- [27] Subrizi A, Tuominen E, Bunker A, Róg T, Antopolsky M, Urtti A. Tat(48-60) peptide amino acid sequence is not unique in its cell penetrating properties and cell-surface glycosaminoglycans inhibit its cellular uptake. *Journal of controlled release official journal of the Controlled Release Society* 2012;158(2):277–85.
- [28] Le Zou, Peng Q, Wang P, Zhou B. Progress in Research and Application of HIV-1 TAT-Derived Cell-Penetrating Peptide. *The Journal of membrane biology* 2017;250(2):115–22.
- [29] Stubelius A, Lee S, Almutairi A. The Chemistry of Boronic Acids in Nanomaterials for Drug Delivery. *Accounts of chemical research* 2019;52(11):3108–19.

- [30] Sohma Y, Hayashi Y, Skwarczynski M, Hamada Y, Sasaki M, Kimura T et al. O-N intramolecular acyl migration reaction in the development of prodrugs and the synthesis of difficult sequence-containing bioactive peptides. *Biopolymers* 2004;76(4):344–56.
- [31] Steed J. Core concepts in supermolecular chemistry. Hoboken, NJ: John Wiley & Sons; 2007.
- [32] Ríos-Malvárez ZG, Cano-Herrera M-A, Dávila-Becerril JC, Mondragón-Solórzano G, Ramírez-Apan MT, Morales-Morales D et al. Synthesis, characterization and cytotoxic activity evaluation of 4-(1,2,3-triazol-1-yl) salicylic acid derivatives. *Journal of Molecular Structure* 2021;1225:129149.

Appendix

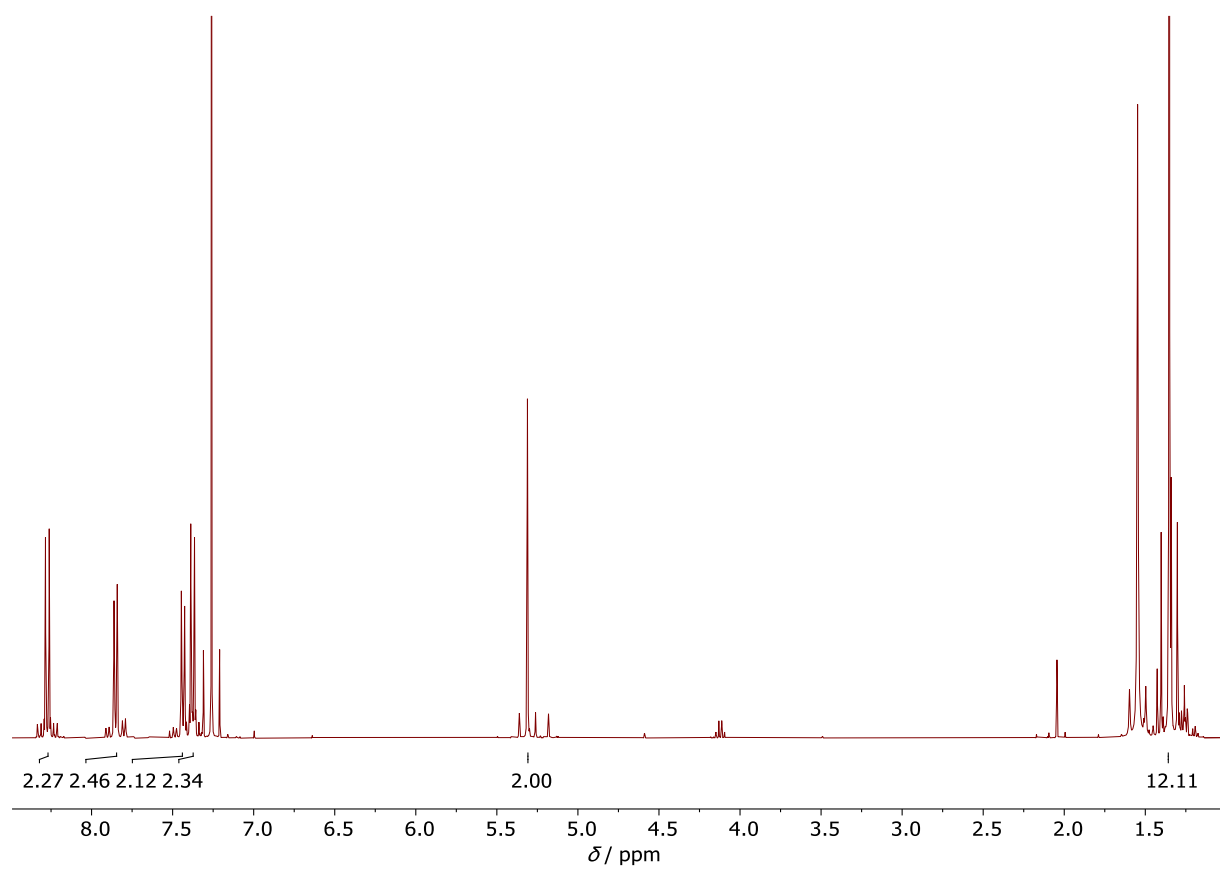


Figure 33: $^1\text{H-NMR}$ spectrum of 4-nitrophenyl (4-(4,4,5,5-tetramethyl-1,3,2-dioxaborolan-2-yl)benzyl) carbonate.

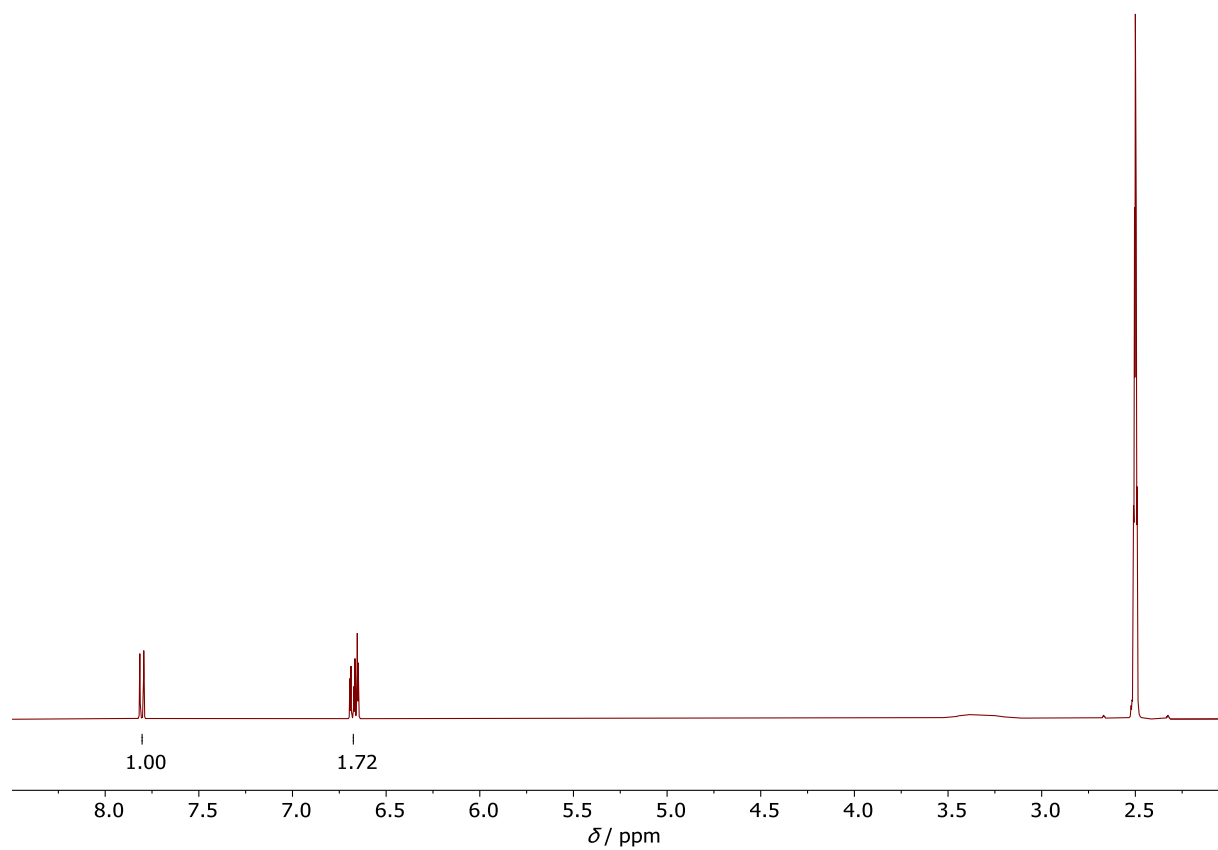


Figure 34: $^1\text{H-NMR}$ spectrum of 4-azidosalicylic acid.

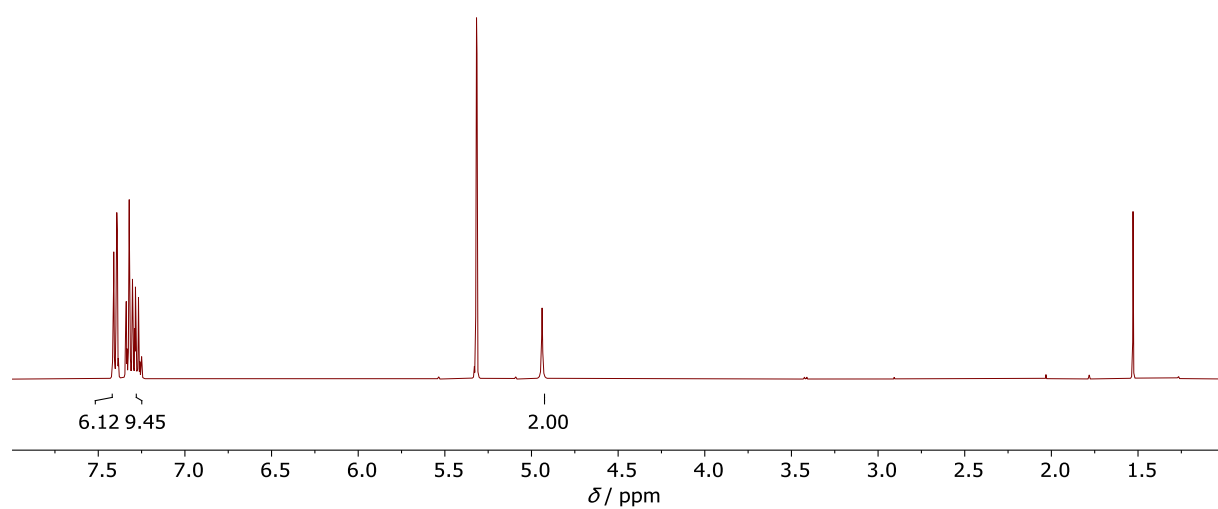


Figure 35: $^1\text{H-NMR}$ spectrum of *N*-trityloxyamine.

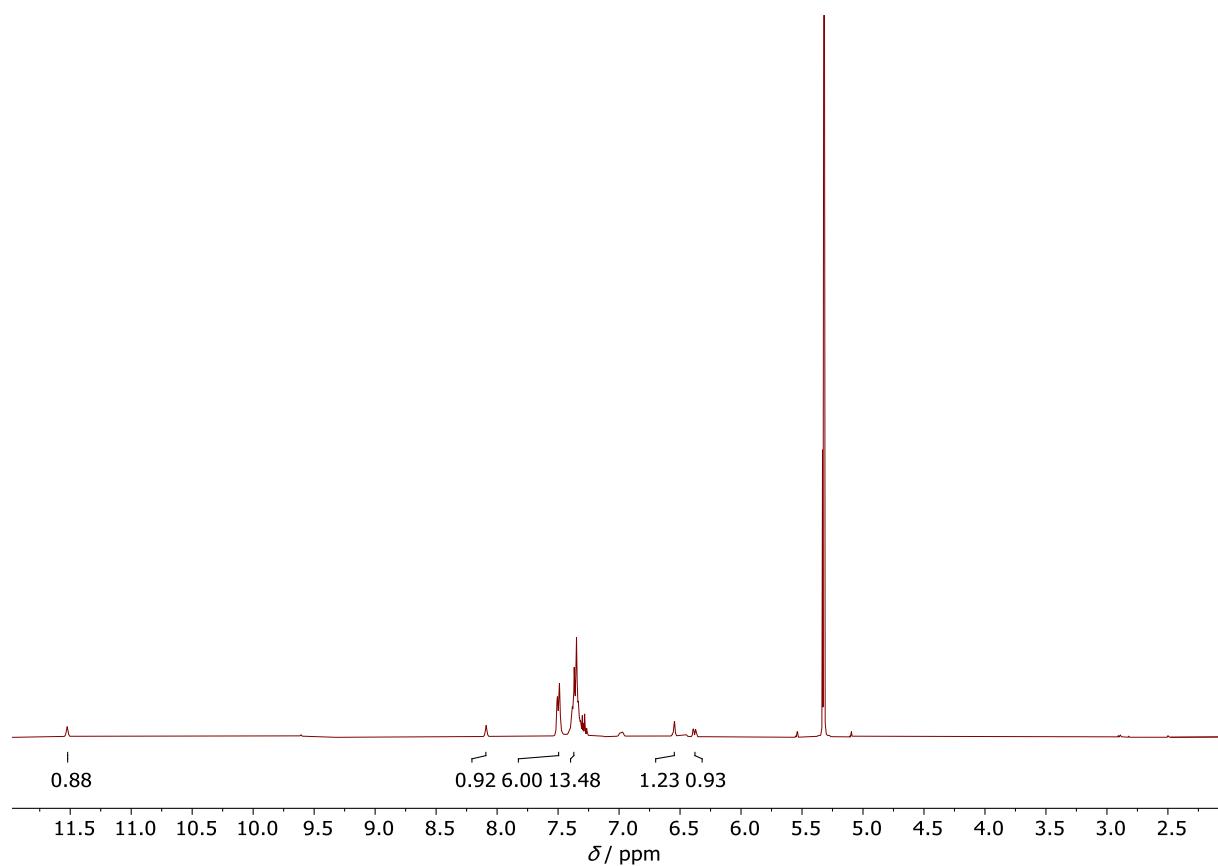


Figure 36: ¹H-NMR spectrum of 4-azido-2-hydroxy-N-(trityloxy)benzamide.

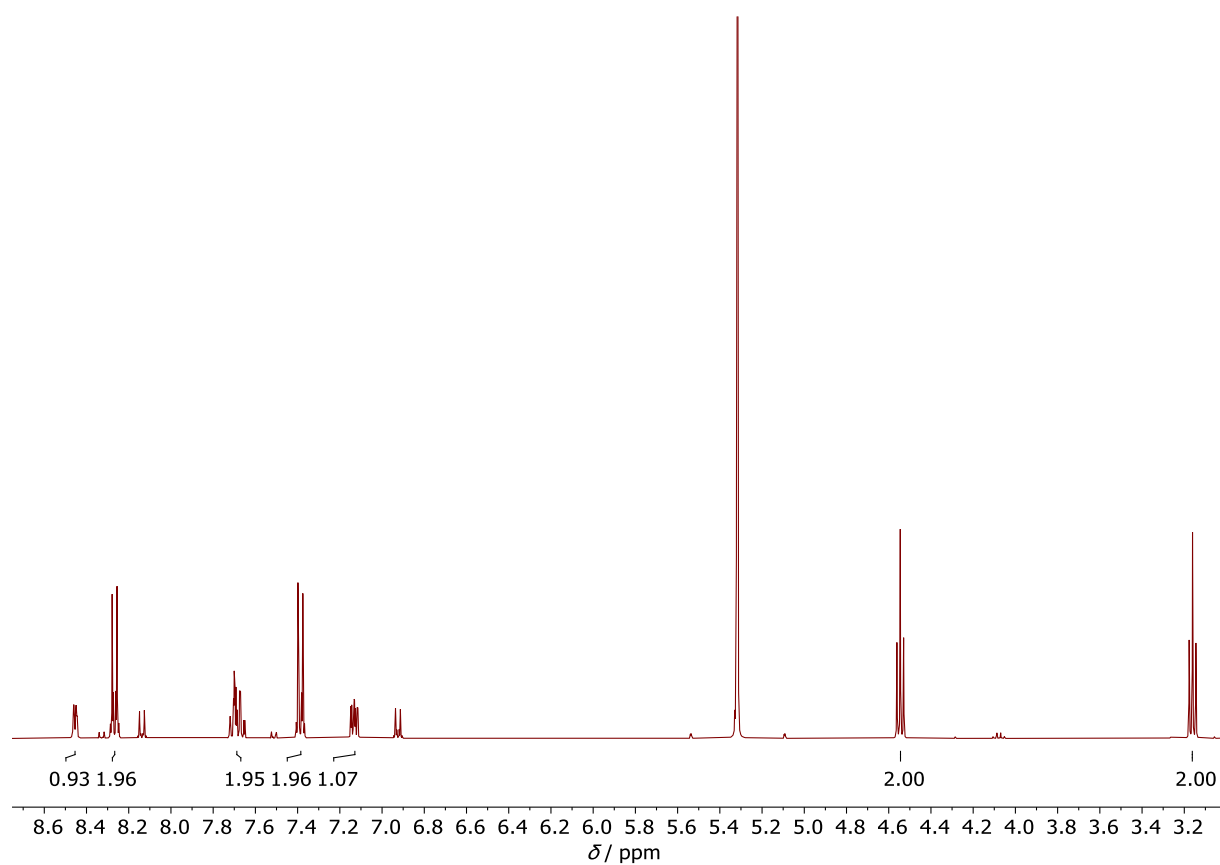


Figure 37: ¹H-NMR spectrum of 4-nitrophenyl(2-(pyridine-2-yl)disulfaneyl) ethyl carbonate.

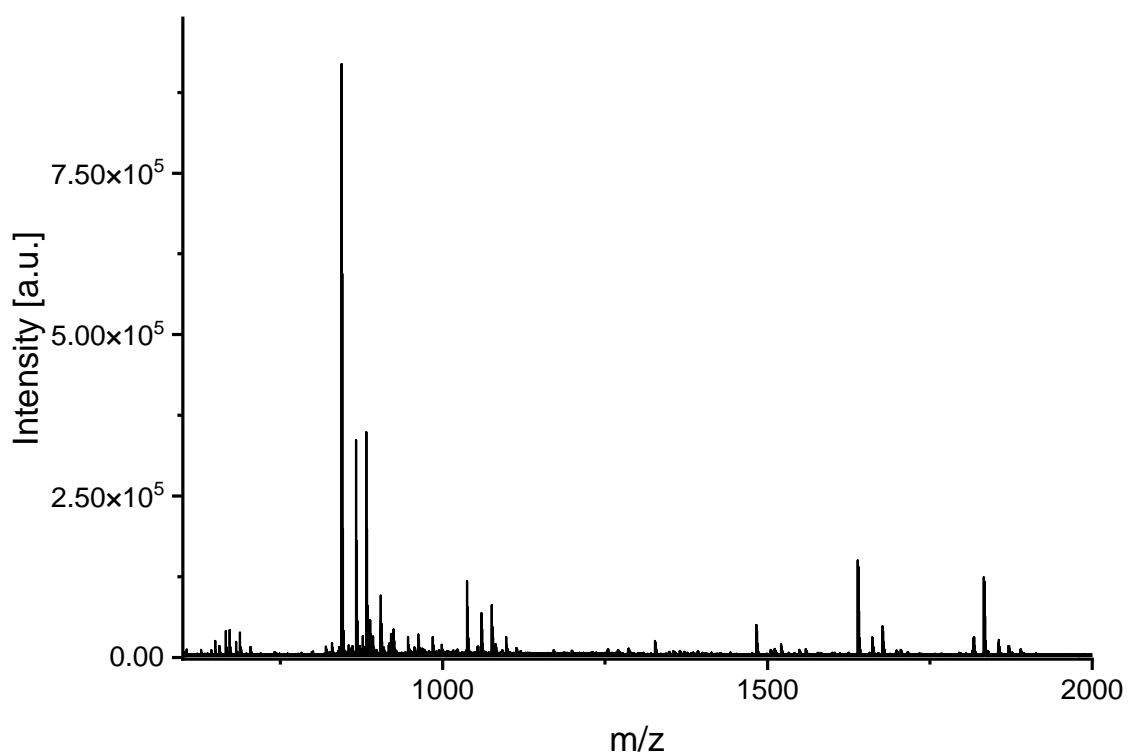


Figure 38: MALDI-TOF spectrum of SHA-TAT.

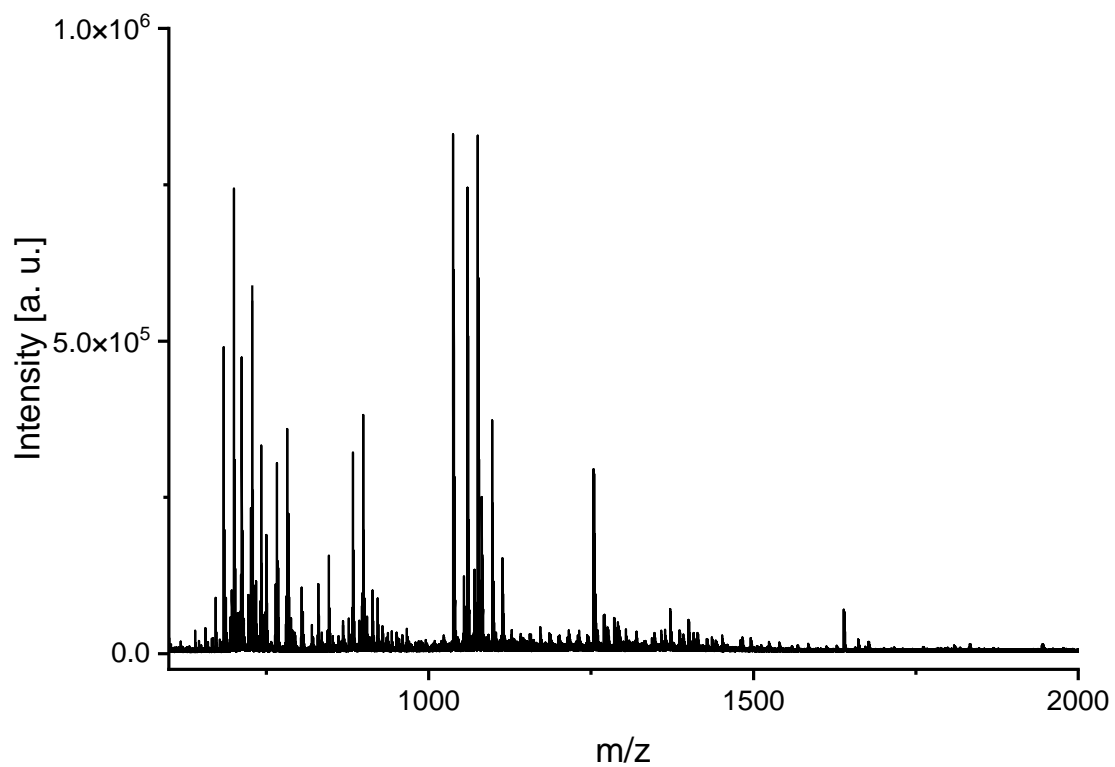


Figure 39: MALDI-TOF spectrum of BA-Depsi ISA.

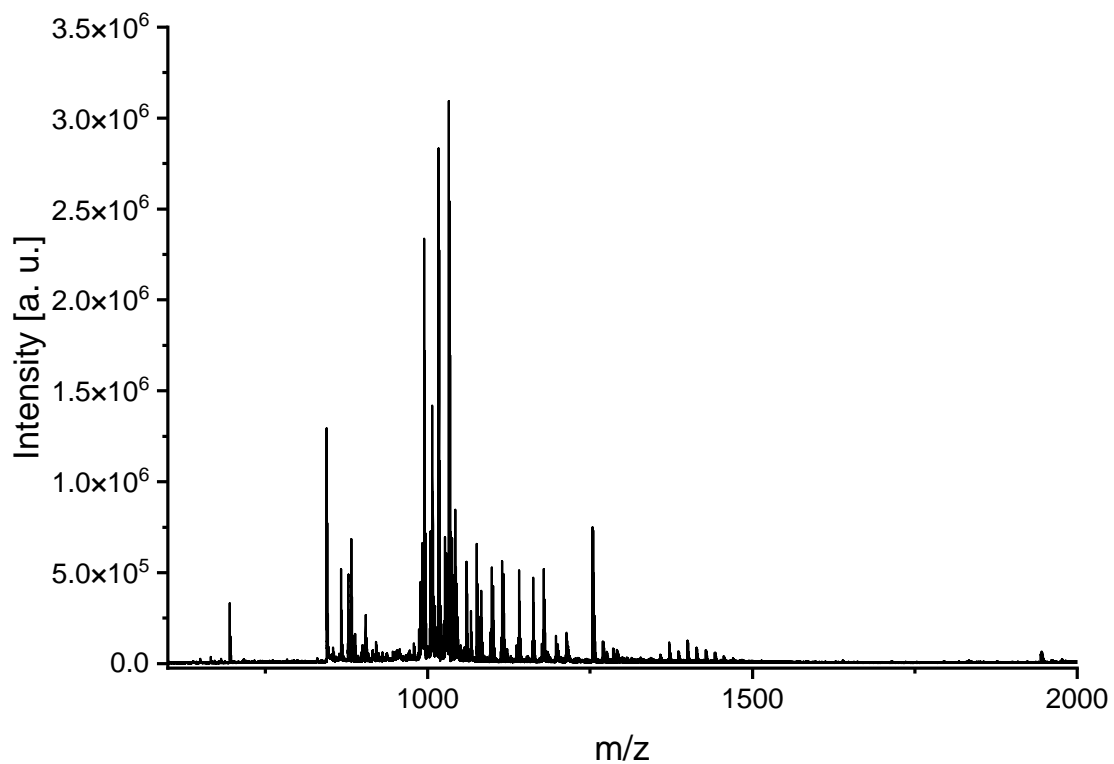


Figure 40: MALDI-TOF spectrum of BA-KFKFQF.

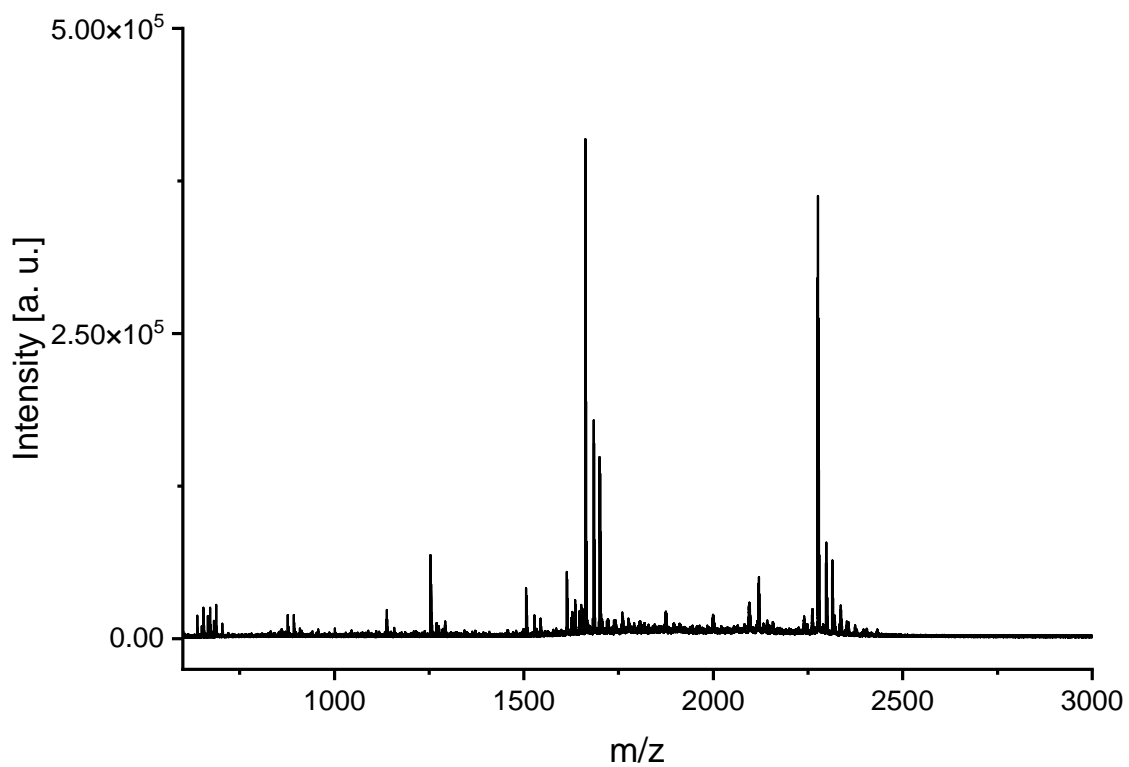


Figure 41: MALDI-TOF spectrum of TAT-SS-Depsi ISA.

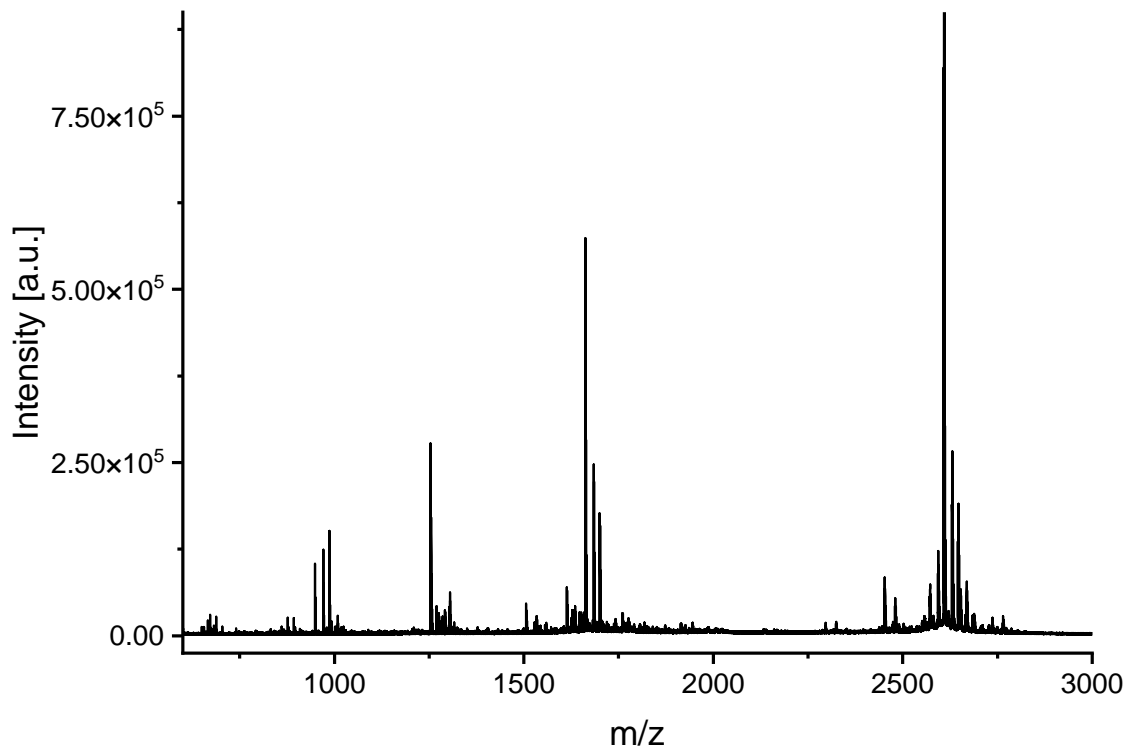


Figure 42: MALDI-TOF spectrum of TAT-SS-KFKFQF.